

DOCTOR OF PHILOSOPHY

Modelling and Design of Electrostatic Based Wind Energy Harvester

Aljadiri, Rita Tareq

Award date:
2014

Awarding institution:
Coventry University

[Link to publication](#)

General rights

Copyright and moral rights for the publications made accessible in the public portal are retained by the authors and/or other copyright owners and it is a condition of accessing publications that users recognise and abide by the legal requirements associated with these rights.

- Users may download and print one copy of this thesis for personal non-commercial research or study
- This thesis cannot be reproduced or quoted extensively from without first obtaining permission from the copyright holder(s)
- You may not further distribute the material or use it for any profit-making activity or commercial gain
- You may freely distribute the URL identifying the publication in the public portal

Take down policy

If you believe that this document breaches copyright please contact us providing details, and we will remove access to the work immediately and investigate your claim.

Modelling and Design of Electrostatic Based Wind Energy Harvester

By

Rita Tareq Aljadiri

September 2014

***A thesis submitted in partial fulfilment of the University's
requirements for the Degree of Doctor of Philosophy***

Coventry University

Emirates Aviation University

DECLARATION

I hereby declare that the work in this thesis is my own except for quotations and summaries which have been duly acknowledged.

September 2014

Rita Tareq Aljadiri

ABSTRACT

Wireless sensor networks and portable electronic devices, such as mobile phones, media players, digital cameras and iPods, require local electric power supplies. Although these devices are operational all the time, they consume just a few milli-or micro-watts. This means energy harvesting from the environment is an attractive option for powering these devices. Mechanical energy harvesters can use electromagnet, electrostatic or piezoelectric approaches. Of these, electrostatic devices are found to be the most suitable approach for harvesting mechanical energy since they are compact, sensitive to low level mechanical energy, easier to integrate in small scale systems, not requiring smart materials, simple to fabricate, inexpensive and simply structured using less circuitry. Most of electrostatic harvesters proposed in previous studies use mechanical vibration. However, only a few studies have investigated harvesting rotational mechanical energy. The objective of this thesis is to investigate the possibility of harvesting rotational mechanical energy from wind using the electrostatic approach. The proposal involves capturing wind energy using a micro wind turbine then converting it into usable electrical energy. This work first considers general design considerations and the design procedure that must be followed to construct a suitable electrostatic based wind energy harvester. Second, it describes the operating principles of various parts needed to design a novel efficient electrostatic harvesting system. The new harvester consists of a micro wind turbine, a gearbox, a multi-pole variable capacitor or capacitor array, an LC to LC energy transfer circuit, a capacitance sensing system and a microcontroller. The harvesting process has three main steps. First, wind energy is captured and converted into mechanical power using the micro wind turbine. Second, mechanical power is converted into electrical power using the variable capacitor in three phases: pre-charge, harvest and reset. Third, the electrical energy is processed and stored in a Lithium ion battery. The proposed harvester was simulated using Matlab/Simulink to study energy transfer throughout the three energy harvesting phases. Energy analysis was then carried out to study the effect of varying the structure of the multi-pole capacitor on the amount of harvested energy. Results from the simulation for capacitance variation from 2.5 nF to 0.6 nF indicated that an eight-pole variable capacitor can produce 29.43 $\mu\text{J}/\text{sec}$ at a wind speed of 10 m/sec, while a capacitor array of the same capacitance variation with 10 capacitors in the array can produce 295 $\mu\text{J}/\text{sec}$ at a wind speed of 10 m/sec. The results of experiments were carried out to test wind harvesting using a two-pole capacitor proved that the proposed harvester is capable of powering an RF transmitter to transmit wind speed information wirelessly.

TABLE OF CONTENTS

DECLARATION.....	II
ABSTRACT	III
LIST OF FIGURES	VIII
LIST OF TABLES.....	XII
LIST OF ABBREVIATIONS	XIII
LIST OF SYMBOLS.....	XV
ACKNOWLEDGEMENTS	XIX
1. INTRODUCTION	1
1.1 MOTIVATION	1
1.2 ENERGY HARVESTING	2
1.3 AMBIENT ENERGY SOURCES.....	3
1.4 MECHANICAL ENERGY CONVERTERS.....	5
1.4.1 Piezoelectric Converters	6
1.4.2 Electromagnetic converters.....	9
1.4.3 Electrostatic converters.....	11
1.4.4 Assessment of mechanical energy converters.....	13
1.5 PROBLEM STATEMENT	14
1.6 RESEARCH SCOPE	15
1.7 RESEARCH OBJECTIVES	15
1.8 RESEARCH METHODOLOGY	16
1.9 RESEARCH QUESTIONS.....	17
1.10 THESIS ORGANISATION	18
2. LITERATURE REVIEW.....	19
2.1 INTRODUCTION	19
2.2 ELECTROSTATIC ENERGY HARVESTERS.....	19
2.3 VARIABLE CAPACITORS FOR ENERGY HARVESTING	19

2.3.1	Variable area capacitors.....	20
2.3.2	Variable gap capacitors.....	22
2.3.3	Variable dielectric constant capacitors	24
2.4	ELECTROSTATIC HARVESTERCONVERSION MECHANISMS	25
2.4.1	Switched constant voltage systems	25
2.4.2	Switched constant charge systems	26
2.4.3	Continuous electret based systems	27
2.5	COMPARATIVE STUDIES OF CONVERSION MECHANISMS	29
2.6	COMPARATIVE STUDIES OF CAPACITOR STRUCTURES	30
2.7	SUMMARY	33
3.	DESIGN CONSIDERATIONS FOR ELECTROSTATIC HARVESTERS.....	34
3.1	INTRODUCTION.....	34
3.2	DESIGN CONSIDERATIONS.....	34
3.2.1	Types of mechanical energy	35
3.2.2	Variable capacitor structures.....	36
3.2.3	Variable capacitor materials.....	38
3.2.4	Energy transfer strategies.....	39
3.2.5	Types of storage devices.....	41
3.3	DESIGN PROCEDURE	42
3.4	SUMMARY	44
4.	ELECTROSTATIC WIND ENERGY HARVESTING PRINCIPLES	46
4.1	INTRODUCTION.....	46
4.2	ELECTROSTATIC BASED WIND ENERGY HARVESTERS.....	46
4.3	WIND ENERGY HARVESTING	47
4.3.1	The Wind	47
4.3.2	Historical development of wind turbines.....	48
4.3.3	Types of wind turbines	49

4.3.4	Micro wind turbine	51
4.3.5	Power from wind	52
4.4	ELECTROSTATIC ENERGY CONVERTER.....	56
4.4.1	Variable capacitor.....	57
4.4.2	Energy transfer circuits.....	62
4.4.3	Capacitance sensing systems	75
4.4.4	Controller mechanism.....	79
4.5	SUMMARY	82
5	ELECTROSTATIC-BASED WIND ENERGY HARVESTER.....	84
5.1	INTRODUCTION	84
5.2	PROPOSED HARVESTER SYSTEM.....	84
5.3	MICRO WIND TURBINE	86
5.4	ELECTROSTATIC CONVERTER FOR WIND ENERGY HARVESTING	91
5.4.1	Multi-pole variable capacitor	91
5.4.2	Capacitance optimisation.....	94
5.4.3	Multi-pole capacitor array (MPCA)	97
5.4.4	LC to LC inductive energy transfer circuit.....	99
5.4.5	Harvester controller	101
5.5	RF TRANSMITTER	104
5.6	SCHEMATIC DIAGRAM OF THE ELECTROSTATIC BASED WIND HARVESTER.....	106
5.7	SUMMARY	107
6	SIMULATION MODELLING, PROTOTYPE TESTING AND RESULTS	108
6.1	INTRODUCTION	108
6.2	SIMULATION OF THE ELECTROSTATIC HARVESTER	108
6.2.1	Simulation of the pre-charge phase	110
6.2.2	Simulation of the harvesting phase	112

6.2.3	Simulation of the reset phase	115
6.2.4	Energy harvesting of the multi-pole capacitor	116
6.2.5	Capacitance and volume optimisation of the multi-pole capacitor	120
6.2.6	Simulation testing of the multi-pole capacitor array (MPCA).....	122
6.2.7	Energy optimisation.....	125
6.2.8	Charging time of selected battery power systems.....	126
6.3	EXPERIMENTAL TESTING OF THE ELECTROSTATIC HARVESTER.....	127
6.3.1	Variable capacitor prototype	127
6.3.2	Experimental setup	130
6.3.3	Test setup of electrostatic harvester with the RF transmitter.....	133
6.4	SUMMARY	139
7	CONCLUSION AND FURTHER WORK	140
7.1	CONCLUSION	140
7.2	SUGGESTIONS FOR FURTHER WORK	142
7.3	PUBLICATIONS ARISING FROM THIS WORK.....	144
7.3.1	Peer reviewed Journals	144
7.3.2	Conferences.....	144
	APPENDIX A	145
	APPENDIX B	158
	APPENDIX C	163
	APPENDIX D	167
	APPENDIX E.....	170
	APPENDIX F	173
	REFERENCES.....	178

LIST OF FIGURES

Figure 1-1: Schematic diagram illustrating a basic harvester system	2
Figure 1-2 Power densities of different energy sources	3
Figure 1-3: Piezoelectric harvester in operation	6
Figure 1-4: Piezoelectric device placed in a shoe	7
Figure 1-5: Piezoelectric harvesting device in a total knee replacement.....	7
Figure 1-6: Piezoelectric-based wind energy harvester system	8
Figure 1-7: (a) Piezoelectric windmill	8
Figure 1-8: Electromagnetic harvesters using direct wind flow.	10
Figure 1-9: Aero-elastic flutter-based electromagnetic energy harvester.....	10
Figure 1-10: Micro wind turbine by Hymini.com.....	11
Figure 1-11: Micro wind mill compared to a Penny	11
Figure 1-12: Two methods of obtaining energy using a variable capacitor	12
Figure 1-13: Electret based electrostatic converters.....	12
Figure 3-1: Vibration-based electrostatic harvesting devices	12
Figure 4-1: Basic block diagram of electrostatic based wind energy harvester.....	47
Figure 4-2: Typical wind speed distribution curve.....	48
Figure 4-3: Global wind power cumulative capacities	49
Figure 4-4: Types of wind turbines	49
Figure 4-5: Two-blade versus three-blade turbines.....	50
Figure 4-6: Micro wind turbines	51
Figure 4-7: Cost-effective wind turbine	52
Figure 4-8: Wind power distribution curve.....	53
Figure 4-9: Stream tube	54
Figure 4-10: Typical efficiencies for various rotor types	56
Figure 4-11: Block diagram of an electrostatic converter	56
Figure 4-12: The resistor – capacitor circuit.....	57
Figure 4-13: The electric field between the plates of a fixed or variable capacitor	58
Figure 4-14: Constant voltage approach.....	60
Figure 4-15: Constant charge approach.....	61
Figure 4-16: Inductive energy transfer circuits.....	62
Figure 4-17: Energy harvesting cycle.....	63

Figure 4-18: LC to LC circuit	64
Figure 4-19: Inductor current and C_{var} voltage waveforms during the pre-charge phase.....	68
Figure 4-20: Currents and energy waveforms during the harvesting phase	68
Figure 4-21: Capacitor voltage waveform as C_{var} increases during the reset phase.....	68
Figure 4-22: L to LC circuit.....	69
Figure 4-23: Voltage, current and energy during the three phases of energy harvesting.....	71
Figure 4-24: Charge pump with flyback circuit (a) block diagram and (b) circuit diagram	72
Figure 4-25: Operation of the charge pump harvester.....	74
Figure 4-26: Variable-reluctance sensor	76
Figure 4-27: Inductive proximity switch	77
Figure 4-28: AC capacitive bridge detector.....	78
Figure 4-29 RC comparator oscillator for capacitance measurement	79
Figure 4-30: Microcontroller current consumption during various modes of operation	80
Figure 4-31: Electrostatic energy harvester with state and slope detectors.....	81
Figure 4-32: Self tuning controller circuit	82
Figure 5-1: Block diagram of the proposed electrostatic-based wind energy harvester.....	84
Figure 5-2: Wind energy generation system concepts.....	85
Figure 5-3: AutoCAD model of the micro wind turbine linked to a gear box.....	86
Figure 5-4: Maximal angular velocity versus wind speed	87
Figure 5-5: Mechanical power versus angular velocity at wind speed of 7 m/sec.....	88
Figure 5-6: Power coefficients of micro wind turbine with different number of blades.....	88
Figure 5-7: Torques applied to the electrostatic-based wind energy harvester system	90
Figure 5-8: Multi-pole capacitor plates equivalent to three capacitors in parallel.....	92
Figure 5-9: Multi-pole capacitors.....	92
Figure 5-10: Capacitance variation.....	93
Figure 5-11: Capacitance variation.....	94
Figure 5-12: AutoCAD model of the eight-pole variable capacitor	95
Figure 5-13: Stator and rotor of the eight-pole variable capacitor	96
Figure 5-14: Theoretical capacitance variations with angular position.....	97
Figure 5-15: Types of multi-pole capacitor	98
Figure 5-16: Capacitance variations with angular position of the MPCA.....	98
Figure 5-17: LC to LC inductive energy transfer circuit.....	99
Figure 5-18: LC to LC energy transfer circuit with S1, S2 and S3 control signals	102
Figure 5-19: Operation cycle of the harvester with S1, S2 and S3 control signals.....	102

Figure 5-20: Flow chart of the controller operation	103
Figure 5-21: Wireless sensor node	104
Figure 5-22: RF transmitter.....	105
Figure 5-23: Schematic diagram of the electrostatic-based wind harvester	107
Figure 6-1: Simulink model of the electrostatic converter	109
Figure 6-2: Average daily minimum (red), maximum (green) and average (black) wind speed	110
Figure 6-3: LC to LC pre-charger Simulink model.....	111
Figure 6-4: Pre-charge phase	111
Figure 6-5: Energy invested in the resistors, inductor and capacitor	112
Figure 6-6: Harvesting phase of the LC to LC electrostatic converter.....	113
Figure 6-7: Current during the harvesting phase.....	114
Figure 6-8: Harvested energy during the harvesting phase	114
Figure 6-9: Comparison between simulated and calculated values of current and energy gain	115
Figure 6-10: Reset phase of the LC to LC electrostatic converter	116
Figure 6-11: Capacitor voltage during the reset phase	116
Figure 6-12: Harvested energy of a single pole capacitor $N_{\text{Pole}} = 1$	117
Figure 6-13: Harvested energy of two-pole capacitor $N_{\text{Pole}} = 2$	117
Figure 6-14: Harvested energy of four-pole capacitor $N_{\text{Pole}} = 4$	118
Figure 6-15: Harvested energy of eight-pole capacitor $N_{\text{Pole}} = 8$	118
Figure 6-16: Harvested Energy of multi-pole capacitors.....	119
Figure 6-17: Maximum number of poles in a multi-pole capacitor	120
Figure 6-18: Capacitance optimisation of the multi-pole capacitor	121
Figure 6-19: Cylindrical shape variable capacitor.....	121
Figure 6-20: Volume optimisation of the multi-pole capacitor	122
Figure 6-21: Pre-charge phase of the MPCA.....	123
Figure 6-22: MPCA: (a) Harvesting phase and (b) Reset phase	124
Figure 6-23: Harvested energy using the MPCA	124
Figure 6-24: Energy optimisation for various battery voltages and capacitor arrays at 10m/sec	125
Figure 6-25: Energy optimisation for various harvesting time periods and capacitor arrays	125

Figure 6-26: Energy optimisation for various numbers of poles in the capacitor and numbers of capacitors in the array at 10 m/sec	126
Figure 6-27: First Prototype of a multi pole capacitor	128
Figure 6-28: Arrow shaped capacitor plate dimensions.	129
Figure 6-29: Sample of AutoCAD process at an angle of 5 °.....	129
Figure 6-30: Experimental setup for capacitance measurement	130
Figure 6-31: Results for the prototype capacitance variations	131
Figure 6-32: Experimental result of the transient response when C is at C_{\max}	132
Figure 6-33: Experimental result of the transient response when C is at C_{\min}	132
Figure 6-34: Experimental setup of the electrical part of the harvester	134
Figure 6-35: Photograph of the electrostatic based wind energy harvester	135
Figure 6-36: LCR meter and the variable capacitor prototype	136
Figure 6-37: Capacitance variation with angular position for the prototype device	136
Figure 6-38: Waveform of the capacitor voltage	137
Figure 6-39: Waveform collected at the RF transmitter output	138

LIST OF TABLES

Table 1-1: Various types of energy sources and conversion approaches	4
Table 1-2: Mechanical to electrical conversion devices.....	6
Table 1-3: Advantage and disadvantages of mechanical energy converters	13
Table 1-4: Research questions and methodology to answer them	17
Table 2-1: Comparison of variable capacitors used in electrostatic harvesters	31-32
Table 3-1: Environmental kinetic energy sources.....	35
Table 3-2: Mechanical energy sources in industrial environments.....	36
Table 3-3: Dielectric materials.....	38
Table 3-4: Advantages and disadvantages of power conditioning circuits	40
Table 3-5: Characteristics of Li- ion batteries and super capacitors	42
Table 3-6: Design specifications for electrostatic-based wind energy harvester	45
Table 4-1: Comparison of electrostatic conversion mechanisms.....	61
Table 4-2: Extreme low power XLP microcontrollers	80
Table 5-1: Parameters of capacitance variation with angular position.....	96
Table 5-2: RF transmitter electrical characteristic	106
Table 6-1: Parameters used to verify the Simulink model of the electrostatic converter....	109
Table 6-2: Capacitance function and harvesting time period.....	113
Table 6-3: Harvested energy of multi-pole capacitors	119
Table 6-4: Selected battery power systems.....	126
Table 6-5: Charging times of selected battery power systems.....	127
Table 6-6: Comparison of various types of variable capacitor used in electrostatic harvesters	133

LIST OF ABBREVIATIONS

AC	Alternating current
AM	Amplitude modulation
CAD	Computer aided design
CMOS	Complementary metal oxide semiconductor
DC	Direct current
DRIE	Deep reactive ion etching
EMF	Electro-motive force
FET	Field effect transistor
HAWT	Horizontal axis wind turbine
HVDC	High voltage direct current
IC	Integrated circuit
LC	Inductor - capacitor
LED	Light emitting diode
LV	Low voltage
MCU	Microcontroller unit
MEMS	Micro electro-mechanical system
MEMES	Micro electro-mechanical energy system
MIT	Massachusetts institute of technology
MOSFET	Metal oxide semiconductor field effect transistor
MPCA	Multi pole capacitor array
MPW	Multi project wafer

PIC	Programmable integrated circuit
QV	Charge –Voltage
RF	Radio frequency
TE	Thermo electric
TPV	Thermo photo voltaic
USB	Universal serial bus
VAWT	Vertical axis wind turbine
WSN	Wireless sensor network
XLP	Extreme low power

LIST OF SYMBOLS

A	Area visible to the wind
A_{eff}	Effective area of the capacitor plate
$A_{eff\,max}$	Maximum effective area
$A_{eff\,min}$	Minimum effective area
A_v	Voltage gain
C	Capacitance
C_{max}	Maximum capacitance
C_{min}	Minimum capacitance
C_P	Power coefficient
C_{res}	Reservoir capacitor
C_{store}	Storage capacitor
C_x	RC oscillator capacitor
C_{var}	Variable capacitance
D	Rotor diameter
d	Distance
dt	Rate of change in time
E	Energy
e	Electrons
E_{harv}	Harvested energy
E_{inv}	Invested energy
E_L	Inductor energy
E_{LC}	Energy at resonant

E_{net}	Net energy gain
E_R	Resistor energy
E_{rem}	Remnant energy
i	Current
I_C	Moment of inertia of the capacitor
I_{harv}	Harvested current
I_{net}	Net inertia
I_i	Moment of inertia
I_T	Moment of inertia of the turbine
L	Inductance
m	Mass
N	North pole
n_1	Number of teeth of the high speed gear
n_2	Number of teeth of the low speed gear
N_C	Number of capacitors in the array
N_{Pole}	Number of poles in the capacitor
N_{SR}	Number of rotor-stator sets
P	Power
P_{elec}	Electrical power
P_{mech}	Mechanical power
P_{wind}	Wind power
Q	Charge
Q_{const}	Constant charge
R	Resistance

r	Radius
R_{Bat}	Battery resistance
rpm	Revolution per minute
R_x	RC oscillator resistor
S	South pole
$S1$	First control signal
$S2$	Second control signal
$S3$	Third control signal
sw	Switch
t	Time
T	Time period
T_C	Torque of the Turbine
$T_{D-energize}$	De-energizing time period
$T_{Energize}$	Energizing time period
T_H	Torque of the high speed gear
T_L	Torque of the low speed gear
T_{net}	Net torque
T_{sleep}	Time period of the sleep mode
T_T	Torque of the Turbine
TSR	Tip speed ration
v_{wind}	Wind speed
V	Voltage
v	Volume of rotating object
V_{Bat}	Battery voltage

V_C	Capacitor voltage
V_{const}	Constant voltage
Vol	Volume of a cylinder
V_{res}	Reservoir capacitor voltage
V_{store}	Storage capacitor voltage
$V_{store (max)}$	Maximum voltage of the storage capacitor
W	Work done
w	Thickness
Z	Impedance
θ	Angle of rotation
ϕ	Phase angle
ΔC_{var}	Variable capacitance difference
ΔV	Potential difference
Δt	Time difference
dq	Charge difference
ζ	Zeta / Damping coefficient
ρ	Air density
ε_o	Absolute permittivity
ε_r	Relative permittivity
ω	Angular frequency
ω_C	Angular velocity of the capacitor
ω_{LC}	Resonant angular frequency
ω_n	Angular velocity
ω_T	Angular velocity of the turbine

ACKNOWLEDGEMENTS

This thesis was prepared through collaboration between Emirates Aviation University and Coventry University. It would not have been possible to complete this thesis without the support and help of many people.

First and foremost, the director of study Dr. Luay Yassin Taha deserves more thanks than I can possibly give. His constant help and support to me and my work goes far beyond what is expected. I am his student and I hope that I have made him proud. I do not have enough words to say, I can only hope he understands this thank you. I would also like to thank Prof. Paul Ivey, my supervisor from Coventry University for his guidance and valuable advices during the four years of my research.

Special thanks also go to the Senior Vice Chancellor of Emirates Aviation College Prof. Ahmad Al-Ali, who provided me with support throughout the entire period of my study.

I am very grateful to all the EAU staff, but especially Dr. Hesham Ibrahim, Alexendra Burow and Zaynab Alquraishy for their support and guidance in completing this long study. Thanks also to Mariam Alansay, who is amazing thinker and problem solver. She has helped in many ways and has always been a pleasure to work with.

My family have proved to be a great support and always treated my education with the highest importance. Special thanks go to my father, Tareq Aljadiri, for all his encouragement and support, and to my mother, Lucy Koreen, who has been a constant source of motivation. Thanks go to my sisters, Rasha and Sally, and my brother Ramy. They are amazing people who have helped me and stood by my side during the tough times of the study. Last but not least, I would like to thank my best friend, Muad Almansoori, for being there for me, helping, advising and supporting me.

CHAPTER 1

INTRODUCTION

1.1 MOTIVATION

In 1991, Mark Weiser described the concept of advanced computing whereby computing is made to appear everywhere in our daily life, stating that “the most profound technologies are those that disappear. They weave themselves into the fabric of everyday life until they are indistinguishable from it” (Weiser 1991). He predicted that devices in the future will be full of small embedded systems that people will use frequently to complete daily tasks efficiently. However, these devices will only become useful if they do not require continuous maintenance.

One example of these devices is portable and wearable electronics, which are low-power, usually small and light-weight hardware devices that are operational most of the time. Such devices are significantly important in improving the quality of life (Pentland 1998). However, maintaining them is quite difficult. Specifically, replacing batteries although most of these devices have a power supply with a long life, their batteries still need to be replaced after a certain period of time, which is a disincentive (Miao et al. 2003). It is not possible to increase the storage capacity by using larger batteries due to limitations on the maximum size, and the additional cost (Mitcheson 2005). One solution is providing power sources that can power the device for its entire operating period.

Wireless sensor networks (WSNs) are examples of important embedded devices in our daily life. Many small sensors are deployed in the environment to collect and transmit information (Boisseau et al. 2012). Many sectors make use of them, including automotive and aerospace industry. For example monitoring acceleration, fuel consumption, identification of incorrect tire pressure, verification of illumination, evaluation of the vital signals of the driver (Tavares et al. 2008), it can be used in aircraft safety critical systems and non-safety critical systems such as engine control system, flight control system, structural and engine health monitoring system, cabin environmental system and in-flight entertainment system (Yedavalli et al. 2011). In many other sectors, there is a frequent need to deploy WSNs,

which have been used extensively in various applications, including monitoring of buildings, machines, domestic environment, security, military tracking and human guidance systems (Gilbert and Balouchi 2012). Researchers are currently trying to develop WSNs that are able to work for years without any human intervention (Roundy et al. 2004). One possible way to power such WSNs is by harvesting energy from the environment. Energy harvesting is the process by which energy is derived from external sources (such as heat, light, acoustic noise or mechanical energy), captured and then converted into usable electrical energy (Mitcheson et al. 2008). In recent years, this method of generating electricity has become an important part of many advanced technology applications.

1.2 ENERGY HARVESTING

During the past 15 years, energy harvesting has become an important field within both the academic community and industry as demands for renewable energy sources have increased. Meanwhile, reductions in the power consumption of many electronic devices have made harvesting approaches more practical (Boisseau et al. 2012). The surrounding environment is a rich source of energy, whether solar, thermal or kinetic. The conversion of ambient energy into electrical energy is attractive for many applications, including WSNs, monitoring systems, biomedical implants, and wearable and portable power devices (Mitcheson et al. 2008). Generating electricity using the energy harvesting approach involves capturing and converting a particular kind of physical energy into utilisable electrical energy (in the form of voltage or current) (Vullers et al. 2009). Figure 1.1 illustrates this schematically, showing how a harvester system includes a capturing device and an energy converter. Unlike large-scale renewable energy generating systems, such as thermal generators, solar systems and wind turbines, energy harvesting systems mainly deal with low power levels (Torres et al. 2005).

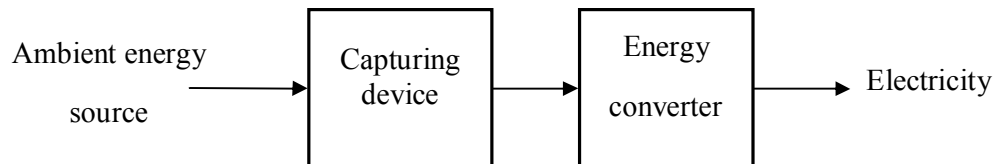


Figure 1.1: Schematic diagram illustrating a basic harvester system

1.3 AMBIENT ENERGY SOURCES

Environmental ambient energy sources are divided into four main types: mechanical, radiant, thermal and chemical (Boisseau et al. 2012). These sources are categorized according to power density, as shown in Figure 1.2.

This item has been removed due to 3rd Party Copyright. The unabridged version of the thesis can be viewed in the Lanchester Library Coventry University.

Figure 1.2: Power densities of different energy sources (Boisseau et al. 2012)

As Figure 1.2 shows, radiant sources provide the greatest power density. Although, solar energy is one of the most powerful sources of energy, harvesting solar power is unfortunately not possible in darkness. Similarly, it is not possible to harvest energy from thermal sources where there is no thermal gradient, or to harvest mechanical energy where there is no rotational motion, up/down movement, compression or vibration. Thus, environmental energy sources must be chosen carefully according to the type of application (Torres et al. 2005).

Several conversion approaches have been proposed for each kind of energy source to capture ambient energy and then convert it into electricity (Torres et al. 2005). The advantages and disadvantages of each type are discussed in detail in (Taha 2009), so this debate will not be repeated in this review. However, in general, each energy source needs to be evaluated separately in order to find the best energy harvesting method. Table 1.1 summarises the various types of energy sources and their conversion approaches for a micro scale devices.

Table 1.1: Various types of micro energy sources and conversion approaches (Taha 2009)

This item has been removed due to 3rd Party Copyright. The unabridged version of the thesis can be viewed in the Lanchester Library Coventry University.

This thesis focuses on wind energy harvesting, which can be an active power source for WSNs, and for portable and wearable devices in environments where no solar or thermal energy harvesting is possible. Wind is one of the most common types of mechanical energy sources, and is free, clean, inexhaustible, environmentally-friendly and sustainable. The wind's kinetic energy can be captured by wind capturing devices, converted first into mechanical power and then into electrical power to supply various applications (Grogg 2005).

The environmental impact of wind energy harvesters is relatively low. Unlike electricity extracted from fossil fuels, wind energy harvesters consume no fuel and emit no air pollution during operation. Although materials must be mined, manufactured, processed and transported in order to build a wind energy harvester, this process equally applies to all other types of power harvesters, and the energy consumed to manufacture the harvester is equivalent to the energy it produces within a few months of operation (UCSUSA.org 2013). According to a study by the Irish national grid “producing electricity from wind reduces the consumption of fossil fuels and therefore leads to emission savings” (Dbp.idebate.org 2010).

Wind energy can be harvested using three types of mechanical energy converters: electromagnetic (Williams et al. 2001), electrostatic (Sterken et al. 2003) and piezoelectric (Lu et al. 2004). These will be briefly reviewed in the following sections.

1.4 MECHANICAL ENERGY CONVERTERS

Mechanical energy harvesting involves converting mechanical energy into electrical power. In effect, there are three main steps in harvesting mechanical energy: (a) capturing the energy from the environment and converting it into mechanical power; (b) converting mechanical power into electrical power; (c) processing and storing electrical energy in a storage device or supplying it directly to a load (Boisseau et al. 2012).

Three main kinds of converters are used to turn mechanical energy into electrical energy: Piezoelectric devices that depend on piezoelectric materials to generate electrical charges when placed under stress or strain (Lu et al. 2004), Electromagnetic devices that are based on electromagnetic induction as an electromotive force is generated from relative motion between a coil and a magnet (Williams et al. 2001) as expressed by Faraday law and Lenz law and Electrostatic devices that use a variable capacitor structure to generate charges from a relative motion between two plates of the capacitor (Sterken et al. 2003).

The schematics of these three conversion devices are given in Table 1.2.

Table 1.2: Mechanical to electrical conversion devices (Boisseau et al. 2012)

This item has been removed due to 3rd Party Copyright. The unabridged version of the thesis can be viewed in the Lanchester Library Coventry University.

1.4.1 Piezoelectric Converters

A piezoelectric device converts mechanical energy into electrical energy by applying pressure on a piezoelectric material. The bending of this material causes charge separation across the material, producing an electric field and a voltage drop across it (Taha 2009). The voltage produced creates an unregulated current proportional to the pressure applied. Figure 1.3 illustrates a piezoelectric harvester in operation.

This item has been removed due to 3rd Party Copyright. The unabridged version of the thesis can be viewed in the Lanchester Library Coventry University.

Figure 1.3: Piezoelectric harvester in operation (Npl.co.uk 2012)

Typically, piezoelectric materials used for micro systems can produce voltage of 2 - 10 V (Rahman et al. 2012). Piezoelectric energy conversion produces higher voltage and power than electromagnetic or electrostatic systems. However, suitable piezoelectric materials are rare, expensive and sometimes cause high leakage voltages (Torres et al. 2005). Piezoelectric devices are used to harvest energy where stress and pressure are available. For example, a harvesting device can be placed inside a shoe, which provides enough bending of the

material to produce a voltage as the wearer walks, as shown in Figure 1.4. Another example is the use of a piezoelectric device in a total knee replacement (Figure 1.5) to measure force that provide useful information about tibiofemoral misalignment and soft-tissue imbalance. At the same time, the piezoelectric device can generate enough energy to transmit the measurements without requiring batteries (Almouahed et al. 2010).

This item has been removed due to 3rd Party Copyright. The unabridged version of the thesis can be viewed in the Lanchester Library Coventry University.

(a) (b)

Figure 1.4: Piezoelectric device placed in a shoe (a) Lab test setup (b) Harvester placed in a shoe (Rocha et al. 2010)

This item has been removed due to 3rd Party Copyright. The unabridged version of the thesis can be viewed in the Lanchester Library Coventry University.

(a) (b)

Figure 1.5: Piezoelectric harvesting device in a total knee replacement
(a) Component of implants (b) The test set-up (Platt 2003)

Concerning wind energy harvesting, some research has been done on converting kinetic wind energy into electrical energy utilising piezoelectric materials. A novel piezoelectric-based wind energy harvester was reported in (Tan & Panda 2007), which converts wind vibrations into electricity. Energy harvested from wind is first accumulated in a capacitor and, when enough energy has been harvested, it is used to power WSNs. It was suggested by the authors that this method provides a practical solution to powering remote sensors and various communication devices. Figure 1.6 (a) and (b) show the schematic diagram and photograph of the wind harvester.

This item has been removed due to 3rd Party Copyright. The unabridged version of the thesis can be viewed in the Lanchester Library Coventry University.

(a) (b)

Figure 1.6: Piezoelectric-based wind energy harvester system

(a) Schematic diagram (b) photograph of the system (Tan & Panda 2007)

A piezoelectric windmill was presented by (Priya et al. 2005) for generating electrical power from wind. The piezoelectric windmill consists of piezoelectric bimorph actuators arranged around the circumference of a windmill as shown in Figure 1.7. Using a gear mechanism, a rotational motion is generated and applied to the actuators. A prototype using 12 bimorphs under normal wind flow at a frequency of 6 Hz, successfully generated a power of 10.2 mW, as measured after rectification. Thus, this technology appears to offer a convenient solution to powering WSNs.

o 3rd Party Copyright. The
an be viewed in the Lanchester

(a) (b)

Figure 1.7: Piezoelectric windmill (a) schematic diagram (b) photograph of fabricated prototype (Priya et al. 2005)

Another approach was proposed in 2010 by IDTechEx. It used aero-elastic flutter and vibration of a membrane rather than a spinning turbine. The proposed harvester is about ten times more efficient compared to piezoelectric turbine-based systems. At 5.5 m/sec of wind the power output is 2 mW. The major advantage of the harvester is that it is significantly cheaper compared to most other wind based energy harvesters (Das 2010).

As well as being rare and expensive, piezoelectric materials have the drawback of being delicate so they can only support small masses and they suffer from fatigue and degradation of performance as a function of time (Bowen et al. 2000). Moreover, additional circuits are required for rectification and regulation of fluctuating harvested power. The circuitry for this consumes additional power which decreases the overall efficiency of the conversion system (Torres et al. 2005).

1.4.2 Electromagnetic converters

In an electromagnetic conversion device, a magnetic field is used to produce electrical energy. A mass can be allowed to oscillate in a magnetic field or a magnet can be used to oscillate inside a coil (Boisseau et al. 2012). According to Faraday and Lenz law, if a coil travels through a variable amount of magnetic flux, it induces a voltage and produces current. However, the amount of voltage produced is very low and unstable. Thus, power processing circuits are required (Torres et al. 2005). To harvest more energy, many factors can be changed: magnet strength, number of turns in the coil, changing the mass, or even changing the diameter of the coil's wire. However, all these options are limited by size constraints. On the other hand, the device has the advantage that it does not need any external voltage source to start generating power (Torres et al. 2005).

Figure 1.8 shows two types of vibration-based electromagnetic devices that harvest energy from direct wind flow: (a) a wind belt-based micro generator; (b) a Helmholtz resonator-based micro-generator (Kim et al. 2008). The output voltage of such devices depends mainly on wind speed. Another vibration-based device is an aero-elastic flutter-based electromagnetic energy harvester, as shown in Figure 1.9. It converts wind flow into mechanical vibration, which is then transformed into electrical power. However, aero-elastic flutter only starts when the wind reaches a certain speed and the direction of wind flow must be perpendicular to the device, which limits continuous power generation (Park et al. nd).

In 2013 a novel miniature airflow energy harvester (horizontal and vertical) for wireless sensing applications was proposed. The harvester consists of a wing that is attached to a cantilever spring. The wing oscillates in response to a steady airflow. It was found that the vertical airflow harvester has the highest power density among wind energy harvesters reported in the literatures so far. It produced output power of 90 μW at 2 m/sec. However, If the airflow speed becomes high (>10 m/sec), the displacement of the mass can be very large, which reduce the lifespan of the device (Zhu et al. 2013).

This item has been removed due to 3rd Party Copyright. The unabridged version of the thesis can be viewed in the Lanchester Library Coventry University.

(a) (b)

Figure 1.8: Electromagnetic harvesters using direct wind flow: (a) Windbelt-based micro-generator; (b) Helmholtz resonator-based micro-generator (Kim et al. 2008).

This item has been removed due to 3rd Party Copyright. The unabridged version of the thesis can be viewed in the Lanchester Library Coventry University.

(a) (b)

Figure 1.9: Aero-elastic flutter-based electromagnetic energy harvester: (a) Laboratory test (b) Field test (Park et al. nd).

Rotational motion-based electromagnetic devices are usually attached to turbines to extract energy from the wind. For example, the electromagnetic-based micro-windmill shown in Figure 1.10 is manufactured by HY mini.com to power digital devices, such as cell phones, iPods and digital cameras (Firebox.com 1998). A minimum wind speed of 4 m/sec is required to start charging these devices. The power is harvested, stored in lithium ion polymer rechargeable batteries and then connected to portable devices through a USB port. Recently, a group of researchers at the University of Texas have designed mini wind turbines, about 1.8 mm long, with micro-electromagnetic generators that can be used to charge cell phones (Mearian 2014). The researchers believe that hundreds of these micro devices could be embedded in a cell phone for recharging. A micro windmill, incorporating gears, inductors, switches and grippers, is shown in Figure 1.11, compared to a US Penny.

This item has been removed due to 3rd Party Copyright. The unabridged version of the thesis can be viewed in the Lanchester Library Coventry University.

Figure 1.10: Micro wind turbine by Hymini.com (Firebox.com 1998)

This item has been removed due to 3rd Party Copyright. The unabridged version of the thesis can be viewed in the Lanchester Library Coventry University.

Figure 1.11: Micro wind mill compared to a US Penny (Mearian 2014)

1.4.3 Electrostatic converters

Electrostatic converters are capacitive devices in which energy conversion takes place as the plates of a variable capacitor separate or the area of the plates is modified in response to externally applied mechanical energy (Boisseau et al. 2012). These devices can be divided into two categories:

- Electret-free electrostatic devices that use energy cycles to convert mechanical energy into electrical energy
- Electret-based electrostatic devices that use electrets to directly convert mechanical energy into electricity.

Electret-free devices operate in either charge- or voltage-constrained systems so there are two possible extremes of operation, as shown in Figure 1.12. In both cases, the mechanical work done is converted into electrical energy. Details of constant charge and constant voltage will be reviewed in Chapter 4. Electret-free based harvesters need an external power source for pre-charging the capacitor in order to generate electricity.

This item has been removed due to 3rd Party Copyright. The unabridged version of the thesis can be viewed in the Lanchester Library Coventry University.

(a) (b)

Figure 1.12: Two methods of obtaining energy using a variable capacitor: (a) Constant charge; (b) Constant voltage (Mitcheson et al. 2008)

Electret-based devices are very similar to electret free devices. The main difference is the additional electret layers that are applied to one or both plates of the capacitor for polarisation purposes. Currently available electrostatic harvesters tend to use electret-based devices more. However, the manufacturing process is complicated, being very similar to that for magnets. It entails injecting an excess of charge in a dielectric layer or heating the dielectric layer above its melting temperature. The layer is then left to cool down to maintain an electric field. This allows the dipoles of the dielectric layer to be oriented in the same direction as the electric field (Boisseau et al. 2012), as shown in Figure 1.13.

This item has been removed due to 3rd Party Copyright. The unabridged version of the thesis can be viewed in the Lanchester Library Coventry University.

(a) (b)

Figure 1.13: Electret based electrostatic converters (a) dipole orientation and (b) charge injection (Boisseau et al. 2012)

1.4.4 Assessment of mechanical energy converters

Each type of converter has both advantages and disadvantages, as described in Table 1.3.

Table 1.3: Advantage and disadvantages of mechanical energy converters

Type of converter	Advantages	Disadvantages
Piezoelectric	<ul style="list-style-type: none"> – High output voltage – High capacitance – No mechanical stops needed – High energy density – No separate external energy source needed – Compatible with micro fabrication – No need to control gaps 	<ul style="list-style-type: none"> – Not compatible with standard CMOS processes – Piezoelectric materials have poor coupling coefficients – Depolarization and ageing problems – Charge leakage and high output impedance – Brittle and expensive material
Electromagnetic	<ul style="list-style-type: none"> – No separate external voltage source is needed – No mechanical stops are needed – High output current – Long life – Robustness 	<ul style="list-style-type: none"> – Bulk and cannot be scaled well to smaller size – Difficult to integrate with micro systems – Difficult to fabricate – Low output voltage – Expensive material – Low efficiency at low frequencies
Electrostatic	<ul style="list-style-type: none"> – Easier to integrate with micro systems and electronics – High output voltage – Low cost systems can be built – High coupling coefficient – No smart materials needed – Can be scaled well to smaller size 	<ul style="list-style-type: none"> – Low capacitance – Separate voltage sources are sometimes needed – Mechanical stops needed – Capacitance causes damping, which reduces motion – High impact of parasitic capacitance – Need to control gaps or plates area

In most cases, piezoelectric and electrostatic devices are more appropriate for small-scale harvesters while electromagnetic devices are better for large-scale. When compared to conventional generators, the electrostatic harvesting system could lead to a system with similar power density to a conventional generator-transformer-rectifier combination, while the fewer components that would reduce system cost and increase overall efficiency. In spite of advances in energy harvesting using piezoelectric and electromagnetic approaches, the electrostatic approach retains a number of advantages: it is compact, sensitive to low mechanical energy, easier to integrate in small-scale systems, does not require smart materials, is simple to fabricate, its energy density can be modified geometrically, is low-cost and has a simple structure with less circuitry. However, it is also one of the least efficient with a low output power, so enhancing the output power density from electrostatic harvesters' remains challenging (Boisseau et al. 2012).

1.5 PROBLEM STATEMENT

Previous work in the literature focused on the design of electrostatic energy harvesters in terms of analysis, modelling, fabrication procedures and operation. The majority of the research on electrostatic energy harvesting technologies utilises only one type of mechanical energy – vibration. No researches were reported in harvesting rotational mechanical energy using electrostatic approach for low power applications. The previous studies are focused on electrostatic harvesters that use the resonance occurrence to produce energy from mechanical vibrations. These devices produce lower power levels compared to other mechanical energy harvesters. As explained earlier, the key element of an electrostatic device is its variable capacitor. Since parameters affect capacitance– area, distance and permittivity– several structures are possible. Most reported variable capacitors for electrostatic energy harvesting depend on vibration to modify the area of the capacitor plates or the gap between them. Because research studies on variable capacitor structures operating with rotational motion are very limited, this study aims to focus in depth on an electret-free multi-pole variable capacitor that works specifically for a wind-based electrostatic energy harvesting system.

The proposed harvester is a unique system that combines wind and electrostatic effects. The main trend in wind energy development is to produce large-scale wind turbines with conventional generation systems established on vast wind sites where average wind speed is

high. Thus, there is a need for research in small-scale wind energy harvesting systems that can be placed in remote areas to provide energy for low-power sensor networks. There are only an extremely limited number of studies in the literature on wind energy harvesting using an electrostatic approach. Electrostatic energy harvesters can be viewed as connecting blocks, one of which is the converter system. This means that many possible approaches can be adopted to improve the efficiency of the entire harvesting system.

1.6 RESEARCH SCOPE

In this thesis, we will first present a literature review on previous research work on electrostatic energy harvesters. Next, we will present a review study to address design considerations and design procedures for electrostatic harvesters. Then, we will give the theoretical background required for electrostatic energy harvesting. This helps in modelling the most appropriate variable capacitor and energy transfer circuitry for the wind harvester. We next describe the proposed harvester based on wind energy harvesting through a detailed study of the mechanical energy capturing device, the different structures of its variable capacitors, energy transfer circuits and controller. Finally, we simulate and test the operation of the harvesting system to prove its capability to harvest energy.

1.7 RESEARCH OBJECTIVES

The first objective of this research is to establish the design considerations and the design procedure for the electrostatic energy harvester and evaluate previous work related to various existing electrostatic energy harvesting designs and methods.

The second objective is to investigate the possibility of harvesting wind energy using an electrostatic approach based on capturing wind energy using a micro wind turbine before converting it into usable electrical energy. The produced energy can be stored in a battery to power small, permanently-operating devices in inaccessible locations and consuming just a few micro or milli-watts.

The third objective is to identify the optimal electrostatic-based wind energy harvester by developing a new harvester system with optimised architecture.

1.8 RESEARCH METHODOLOGY

In order to achieve these three objectives, the research is divided into five parts: design considerations, design procedure, principle of operation, including theoretical background, modelling approaches, and simulations and experiments.

The design considerations include the list of the factors affecting the design of the electrostatic harvester such as type of mechanical energy, variable capacitor structure, variable capacitor material type, energy transfer strategy and type of storage device.

The design procedure includes the flow chart that helps a circuit designer to design a suitable electrostatic harvester to power various applications using different mechanical energy sources.

The principle of operation includes the operating principles of both the mechanical and electrical parts of the system, including the wind turbine and the harvester's electrical system. Details of the theoretical background of energy conversion are also addressed in this part.

In modelling, the electrostatic-based wind energy harvester parts are integrated to investigate the feasibility of wind energy harvesting. This includes selecting a wind turbine, various models of multi-pole variable capacitor, the selected energy transfer circuit, the controller, the capacitance-sensing system and the RF transmitter.

Simulation is conducted by designing the harvester model in Matlab/ Simulink. This simulation model is capable of simulating actual harvesting cycles. Moreover, the simulations are capable of displaying the amount of harvested energy of multiple pole capacitors and the proposed capacitor array at various wind speeds. The simulations also display capacitance and energy optimisation.

Experimental testing includes testing of electrostatic harvester with the use of micro wind turbine, capacitance measurement of the variable capacitor for one cycle, charging and discharging of the capacitor, energy transfer circuit operation, and testing of data transmission using an RF transmitter.

1.9 RESEARCH QUESTIONS

Table 1.4 presents the research questions and the methodology to answer them.

Table 1.4: Research questions and methodology to answer them

Research questions	Methodology to answer research questions
Q1. What are the general design considerations for an electrostatic energy harvester?	<ul style="list-style-type: none">– A literature review of various types of electrostatic energy harvesters for several variable capacitor structures to extract the design factors.– Assessment and justification of the extracted design considerations for the harvester in terms of energy sources, construction, electrical properties and power processing needs.
Q2. What are the optimum parameters in a specific electrostatic harvester model?	<ul style="list-style-type: none">– Designing different models of the electrostatic harvester with different energy transfer strategies– Comparative assessment of different designs based on the theoretical and simulation results– Selection of the optimised design and integration into the harvester's architecture
	<ul style="list-style-type: none">– Prototype testing of the electrostatic harvester– Evaluating the experimental results and comparing the new proposed device with the existing devices

1.10 THESIS ORGANISATION

As mentioned previously this thesis is concerned with the design of an electrostatic-based wind energy harvester. The harvester is a combination of two main sub-systems (the wind-capturing device and the electrostatic converter). In order to design an optimised harvester system to harvest energy from wind efficiently, it is necessary to understand how each subsystem operates individually and the relationship between them. Thus this thesis presents a road map for designing a novel harvester. The road map is divided into number of chapters.

Chapter 1 provides an introduction to energy harvesting systems. It identifies all the types of ambient energy sources, highlights the three main types of mechanical energy converters and lists the advantages and disadvantages of each one. The problem statement, research scope, research objectives, research methodologies and thesis organisation are also explained in this chapter.

Chapter 2 presents the literature review of electrostatic energy harvesters regarding the various types of variable capacitor structures and energy conversion mechanisms to identify the best possible structure and conversion mechanism.

Chapter 3 discusses general design considerations, including all the factors affecting the design of the harvester and the design procedures that can be followed to design a suitable electrostatic energy harvester for a specific application.

Chapter 4 describes the operating principles of an electrostatic-based wind energy harvester. More details are given about the theoretical background underlying the capturing device, the variable capacitor, the energy transfer circuit and the capacitance sensing circuits.

Chapter 5 describes the new proposed electrostatic-based wind energy harvester with details of all its components.

Chapter 6 reports on the simulations and experiments conducted for this study, before discussing the results to verify validity of the proposed harvester.

Chapter 7 provides final conclusions and proposes future work.

CHAPTER 2

LITERATURE REVIEW

2.1 INTRODUCTION

As explained in Chapter 1, this thesis concentrates on electrostatic energy harvesters. The main unit of an electrostatic harvester is its variable capacitor, which makes use of a change in capacitance to either cause a voltage increase or a charge increase in the harvesting system. Many types of harvester have been reported in previous studies based on various capacitor structures and energy transfer strategies. A literature review of those types is presented in this chapter divided into four sections: work concentrating on variable capacitor structures; previous work on conversion mechanisms; a comparison of conversion mechanisms; and a comparison of various electrostatic devices.

2.2 ELECTROSTATIC ENERGY HARVESTERS

An electrostatic energy harvester consists of a variable capacitor and an energy transfer circuit (Boisseau et al. 2012). The electrostatic effect takes place between the parallel plates of the capacitor on which electrical charge is stored. The harvesting of electrical energy is achieved by fixing one of the plates and moving the other by an external mechanical motion to change one of the variable capacitor parameters: either plate area or plate separation (Miranda 2004). This allows mechanical movement to be converted into electrical energy according to the principle of electrostatics. The details of electrostatic energy conversion principle are addressed in Chapters 4 and Chapter 5.

2.3 VARIABLE CAPACITORS FOR ENERGY HARVESTING

The first variable capacitor for electrostatic power conversion was proposed in 1998 by Meninger and co-workers (Meninger 2001). The concept was later demonstrated by Roundy and co-workers utilising large machined variable capacitors (Roundy 2003). Since then,

several variable capacitor structures for electrostatic harvesting have been reported in the literature. The structures of these capacitors depend mainly on changing capacitance parameters. There are three types of variable capacitor: variable area, variable gap and variable dielectric constant. These three types are considered next.

2.3.1 Variable area capacitors

Philp (1977) reported a variable area vacuum-insulated varying-capacitance machine. This capacitor operated by rotational motion. Having evaluated its generation of high voltage direct current HVDC power, the author suggested that his capacitor machine offers two potential advantages over conventional rotating machines: first, it is capable of very high efficiency power generation; second, it is suitable for high voltage operation.

Nguyen et al. (2002) reported the design, fabrication and measurement of a novel micro electro-mechanical system MEMS tunable capacitor with angular vertical comb-drive actuators. The capacitor allows continuous rotation, making a large tuning ratio possible. The device fabrication process involves a single deep reactive ion etching step followed by release and assembly of the angular combs.

Sterken et al. (2003) proposed a variable area capacitor in which the vibrations cause the capacitor plates to move in opposite directions, changing the capacitance and hence producing electricity. The author reported that experimentally a 1 μW could be harvested from a 5 μm vibration at resonance frequency of 980 Hz.

Tsutsumino et al. (2007) developed an in-plane overlap variable area power generator. They proposed an electrode arrangement for reducing the in-plane unidirectional damping force. They confirmed that this generator model can imitate the response of the in-plane electret generator with sufficient accuracy.

Pasquale et al. (2008) presented the design approach for an electrostatic capacitive harvester based on a variable area construction. They derived the main analytical relations for capacitive structures and used these to provide a quantitative estimation of power scavenged in relation to operation frequency, and presented its ultimate applications.

Tvedt et al.(2008) modelled and simulated an electrostatic in-plane overlap varying energy harvester using a circuit simulator. They investigated both linear and nonlinear models. The nonlinear model included mechanical stoppers at the displacement extremes. They used both narrow- and wide-band large amplitude excitation signals to simulate environmental vibrations. The authors found that nonlinear behaviour is significant at large displacements due to the impact on mechanical stoppers. They also suggested that for sinusoidal excitation the mechanical stoppers could cause output power to decrease.

Kiziroglou et al. (2009) presented a novel electrostatic harvester design employing an external free-rolling proof mass. The vibration energy causes a change to the capacitor area. The authors described the fabrication process for a prototype device and the physical characterisations for dielectric sizes down to 100 nm. They demonstrated a voltage gain of 2.4, and suggested that the device is suitable for energy harvesting from low frequency motion sources, such as the human body.

Le et al. (2009) presented an in-plane overlap capacitor consisting of a metal strip set on two layer dielectrics opposing each other. They concluded that this capacitor had the disadvantage of fringing fields that have a significant effect on capacitance variation. However, they also suggested that the negative effect of the fringing field can be reduced by optimisation of the metal finger widths.

Halvorsen et al. (2009) designed, fabricated and characterized a MEMS electrostatic energy harvester using a variable area capacitor. The device operates in continuous mode and features high voltage output and large travelling distance of a big mass within a compact design using full bulk silicon thickness. The output power is about $1\mu\text{W}$ at an acceleration power spectral density of $0.03\text{ g}^2/\text{Hz}$.

Paracha et al. (2009) presented the design, fabrication and initial characterization results for a bidirectional, vibration silicon-based electric energy generator. The converter is based on an in-plane overlap plate configuration. The authors suggested that, with 6 V pre-charge voltage, the maximum theoretical power converted is $2.6\text{ }\mu\text{W}$ at 246 Hz vibration frequency from a $10 \times 10 \times 0.9\text{ mm}^3$ transducer.

O'Donnell et al. (2009) investigated the feasibility for directly generating HVDC power using a novel generator topology as an alternative solution to large offshore wind farms. They used variable-capacitance based on the work of Sanborn F. Philip (1977). The authors presented a generator that uses electrostatic fields to generate HVDC output with a minimum of power conditioning, and reported that its system power density is comparable to conventional generator–transformer–rectifier systems.

Reznikov et al. (2010) reported the generation of the electric power by a variable area permanently polarized capacitor used for energy harvesting from oscillations and rotation. Their experimental results demonstrated the generation of either high voltage pulses, or low voltage alternating current that need to be rectified, regulated and stored. They based their design for an electrostatic swing energy harvester on the linear displacement of a conductive shield between the electrets and passive electrode. The authors provided experimental data showing the harvester could provide a DC voltage greater than 3 V.

2.3.2 Variable gap capacitors

Mizuno et al. (2003) was the first team to propose a variable gap method in which mechanical vibration is used to vary the gap and hence the resonating capacitance, which can then be tuned to obtain optimum output power.

Maio et al. (2003) described the fabrication and initial testing of a micro-machined variable capacitor for power generation. The measured capacitance of the device varies from 100 pF to around 1 pF as the mass moves from initial to final position, corresponding to a hundred-fold increase in voltage if the device is operated in constant charge mode. The authors presented the initial tests of the capacitor on a vibration system generating a high voltage output of 2.3 kV when the capacitor was charged by a voltage source of 26 V. This corresponds to an energy conversion rate of 2.4 μJ per cycle, or 24 μW at a vibration frequency of 10 Hz.

Despesse et al. (2008) presented an in-plane gap closing structure with an interesting rectangular structure where the capacitance density can be increased by using triangles fingers. The gaps can be adjusted easily by adjusting the finger overlaps and then adapting

the structure to vibration conditions in order to maximize capacitance variation. The achieved output power was 16 μ W per gram over a frequency band between 20-100 Hz, with an efficiency of 60 %.

Pasquale et al. (2009) investigated the performance of micro systems based on electrostatic coupling, and tested the power scavenged by a capacitive micro-scavenger with an out-of-plane gap-closing layout. The authors investigated the performance of this energy harvesting strategy by comparing it both to a configuration with an in-plane motion of electrostatic benders and to the performance of bimorph piezoelectric transducers.

Guillemet et al. (2010) studied the vibration energy harvesting capabilities of an out-of-plane gap-closing converter. Their goal was to maximize the output energy harvested from a MEMS device while preventing the integrity of the conditioning circuit. The originality of their work lies in the optimisation, taking into accounts both electrical and mechanical aspects and studying at the same time the consequence of the voltage limitations on the transducer.

Cotia et al. (2012) presented the design, simulation and application of a micro-cantilever beam as a variable capacitor. The device consists of an array of cantilever beams with variable length, suspended over a bottom electrode. By applying a voltage between the electrodes, the electrostatic force pulls the beams in one by one to cause an increase in the capacitance as the gap between the cantilever beams and the target surface varies.

Guillemet et al. (2012) presented the design and testing of an electrostatic energy harvester based on a gap-closing comb drive structure. The capacitor is made from a thick silicon wafer, whose total capacitance varies from 40 to 290 pF. The authors' results show a parasitic capacitance of 30 pF. The device was tested with a charge pump circuit for 500 sec. The harvested power was 938 nW.

Janicek et al. (2013) reported a generator design based on an electrostatic converter that uses the principle of periodical modification of the gap between the electrodes of a capacitor. They designed and modelled the structure as a 3D silicon-based MEMS. The authors took an innovative approach to testing the structure under a very low resonant frequency of around 100 Hz. They also presented the design of a long cantilever spring with a minimum area of

the chip, its ability to work in 3D mode, and the capacity to be tuned to reach the desired parameters.

2.3.3 Variable dielectric constant capacitors

The methodology of producing electricity by changing the dielectric materials of a capacitor using mechanical energy topology was not previously common. However, it was adopted using flow energy topology by Boland et al. in 2005, who described a device that is a fixed-charged, Teflon-electret capacitor with air-filled gaps and liquid droplets that travel by vibration. As the liquid moves in and out of the gaps, a voltage is generated across the capacitor according to the position of the droplets. The authors also studied the possibility of using serial and parallel arrays of the device to increase power output. The power output produced from the parallel arrays was around 10 μ W.

Salem et al. (2007) presented a novel technique employing a switchable dielectric constant for enhancing the power delivered by electrostatic converters. Their approach provides power 103 times greater than that provided by conventional MEMS devices. They also considered potential technical challenges associated with viscous damping and time response of the device. They estimated the time response of the device as varying from 100 μ s to 300 μ s, depending on the device size.

Talal (2008) in her PhD thesis presented an electrostatic energy conversion method utilizes a change in the dielectric constant of the material between capacitor plates. The author suggested that by changing the actual material between the plates, it pumps energy into a storage device. The devices have fixed capacitance geometries such as gap and area but modify the dielectric permittivity by allowing a set of two fluids with two different dielectric constants to flow between fixed plates.

2.4 ELECTROSTATIC HARVESTER CONVERSION MECHANISMS

In the literature, there are three main techniques used for the electrostatic conversion mechanism: switched constant charge systems, switched constant voltage systems and continuous electret-based systems. These three approaches are reviewed next.

2.4.1 Switched constant voltage systems

Torres et al. (2009a) reported a voltage-constrained electrostatic CMOS harvester. The authors explained how much energy is available in such a system before and after harvesting, and offered energy conversion schemes for increasing net energy gain during all operational phases.

Torres et al. (2009b) reported a prototype circuit that pre-charges, detects and synchronizes to a variable voltage-constrained capacitor. The authors verified experimentally that it is possible to harvest energy using the electrostatic principle. Their experimental results showed that the system harvests 9.7 nJ/cycle by investing 1.7 nJ/cycle, for a net energy gain of approximately 8 nJ/cycle at an average of 1.6 μ W for every 200 pF variation.

Torres et al. (2010) reported a self-tuning battery-constrained electrostatic energy harvester integrated circuit IC that adapts to changing battery voltages to produce usable power from vibrations across the entire battery voltage operating range. Their prototype keeps the variable capacitor voltage constant so that kinetic energy in vibrations can generate and direct current into the battery when capacitance decreases. The reported pre-charger circuit is unlike other inductive based circuits, which charge the variable capacitor to battery voltage and adapt to a constantly shifting battery voltage. The proposed pre-charger circuit has a self-tuning reference system.

Kwon et al. (2010) presented a design for low-power switched-inductor converters capable of producing high net energy gains, using a switched-inductor, voltage-constrained electrostatic power stage.

2.4.2 Switched constant charge systems

Haas et al. (2004) presented a novel voltage step-up converter based on a charge-constrained variable parallel-plate capacitor in combination with an electrostatic actuator. Electrical equivalent circuit and system level Simulink models were developed. Based on these models, the authors analysed the design parameters and expected device performance to provide a starting point for prototype implementation.

Yen et al. (2005) presented a design for a variable capacitance vibration energy harvester that combines an asynchronous diode-based charge pump circuit with an inductive energy flyback circuit to deliver $1.8 \mu\text{W}$ to a resistive load. The complete harvester operates under constant charge with only one gated MOSFET for energy flyback control, which greatly simplifies switching control and avoids time management issues. The authors explained that the system requires a start-up voltage of less than 89 mV, indicating that it can be initially charged by a piezoelectric film.

Galayko et al. (2008) presented an analysis and system design for a capacitive harvester of vibration energy composed from a mechanical resonator, capacitive transducer and a conditioning circuit based on the buck DC-DC converter architecture with auto-adaptation to external vibration changes. The authors explained in detail the charge pump operation and presented a QV diagram of the operation.

Dudka et al. (2009) designed and modelled a calibration block for a harvester based on a charge pump concept which adapts the operating parameter of the conditioning circuit to the external vibrations. They improved on the basic architecture by adding a second output to the existing flyback circuit DC-DC convertor. This allows low DC voltage to be generated for the load without using an additional DC-DC convertor, which would require an additional inductor.

Arrafat et al. (2009) proposed a design for a piezoelectric voltage generator integrated with electrostatic structure to provide the necessary voltage. In this way, the system is self-initializing and autonomous. The harvester is CMOS-compatible based on a charge pump circuit.

Florentino et al. (2010) reported a variable capacitor and switch circuit architecture for the buck converter. The buck converter is used to step down the voltage harvested when the charge applied across the capacitor is constant. The authors investigated the performance of the switch circuit in relation to the amount of energy loss, suggesting that the main reason for losses is the size of the transistor. They developed their circuit in the Cadence software using high voltage components that can support voltages up to 50 V. The presented circuit loses less than 4% of transferred energy.

Kempitiya et al. (2011) presented an electrostatic generator with asynchronous control and charge flyback mechanism to optimise the useful energy generated by the harvester. The authors' theoretical and experimental investigations showed that there is an optimum value for the storage capacitor and the cycle number for maximum scavenging of ambient energy. The analysis also indicated that the most energy can be harvested when mechanical and electrical events are synchronised. Their theoretical results were confirmed by measurements on an electrostatic converter prototype with an asynchronous energy harvesting circuit.

2.4.3 Continuous electret based systems

Sterken et al. (2003) proposed a device with a vibration sensitive variable capacitor polarized by an electret as new approach to mechanical energy harvesting using an electrostatic converter. The vibration causes changes in the capacitance resulting in harvesting current to a load circuit. The authors proposed a prototype design based on an MPW-service. The prototype was able to generate power of 50 pW.

Naruse et al. (2008) developed an electrostatic micro power generator with vibration structure and new electret electrode for low frequency energy harvesting applications. The authors suggested that it has the advantage of being usable for high power structures because of both the controlled gap between electrodes and the low frequency vibrations. The generator was able to generate a 40 μ W of power output at very low frequency vibrations of around 2 Hz.

Edamoto et al. (2009) developed a vibration-based electret generator for energy harvesting applications. The spring material used was Parylene for low frequency vibrations. The adopted structure was a gap change for capacitance variation. At frequencies as low as 21 Hz, a large in-plane amplitude of 0.5 mm was achieved. The authors demonstrated LED operation from the generator using a low-power-consumption impedance conversion circuit.

Miki et al. (2009) developed an electret power generator driven by electromechanical vibration. The experimental data were directly compared with the model characteristics. The authors found that the circuit parameters should be optimized depending on the oscillation conditions. They also found that the electrostatic damping force acting on the seismic mass depends on the power management and rectification circuits.

Bu et al. (2010) reported an electrostatic energy harvester with an inter-digitised capacitive structure biased by electrets. The work proposed a novel collision-based energy conversion method. Based on their theoretical results, they proposed a method that generates high coupling efficiency at low vibration frequency. The authors found that the device is capable of harvesting output power of 0.58 μW and an available power density of 41.67 $\mu\text{W}/\text{mm}^3$ at 2 Hz collision input. The authors suggested that the collision method could be used to harvest vibration energy at random and low frequencies.

Suzuki et al. (2010) presented the concept, design, simulation, fabrication and evaluation of a novel micro generator based on electrostatic induction. The authors developed an asymmetric electret gammadion spring electrode for wide band vibration with three vibration modes. For mode 1, the maximum power output generated was 7.48 nW at 110 Hz; for mode 2, it was 2.19 nW at 165 Hz; and for mode 3 it was 1.72 nW at 243 Hz. They suggested that their method solves the problem associated with narrow operation frequency bandwidth, which strictly limits power output under normal wideband vibrations.

Altena et al. (2013) presented many improvements for an electret based electrostatic harvester. The device was initially able to generate a power output of 175 μW but after improvement with a higher resonance frequency and higher electret potential, it was capable of generating 497 μW AC power, which is the highest reported power for electret based harvesters. The authors suggested two improvements to the design: first, improvements to the electrical connections of the harvester; second, to the electrode geometrical setup.

2.5 COMPARATIVE STUDIES OF CONVERSION MECHANISMS

A number of comparative studies of the switched constant charge and constant voltage systems have been reported in the literature. A summary of these studies are presented next.

Menninger (Menninger 1999) and a group of researchers at MIT working on electrostatic generators were the first group to present an electrostatic micro generator work in the literature. They described and compared in detail the constant charge and constant voltage approaches. By using QV cycle plots, they reported that constant voltage operation is better than constant charge operation for maximising power generation. The authors were capable of achieving constant voltage operation by attaching a large fixed capacitor in parallel with the variable capacitor. They noted that the larger the parallel capacitor the more power is generated, although more initial energy loss occurs.

Further information on constant charge and constant voltage is given in Miranda's Ph.D. thesis (Miranda 2004). The author presented a simulation of a variable capacitor and power electronics in Matlab, using the parameters of an off-the shelf MOSFET. The author concluded that power electronics for constant charge are easier to implement than constant voltage. However, constant voltage systems generate low level voltages within the breakdown limits of standard IC process technologies.

Mitcheson et al. (2004) compared three main types of electrostatic micro generator conversion mechanisms: constant voltage, constant charge switched and electret based continuous. The authors considered that the switched types can be controlled easily to perform maximal power point tracking. However, this increases the complexity of the associated circuitry required to control the switching devices. The authors also suggested that, for large electrostatic forces, constant charge designs are preferable.

In 2004 Mitcheson and his team studied the power processing requirements of electrostatic harvesters, specifically for the constant charge approach. The authors highlighted issues with this approach, explaining that the harvester works with small amounts of charge at high voltage. The authors described how, when the generator experiences acceleration, the capacitance of the variable capacitor decreases and the voltage rises. In typical operation, the voltage generated on the capacitor plates can reach a few hundred volts so the harvested

voltage must be stepped down to lower voltages to be suitable for powering low power loads. The suggested solution for this problem was the use of a fly-back step-down converter.

Beeby et al. (2008) reviewed the use of kinetic energy harvesting as a potential power supply for wireless applications. The authors studied three types of electrostatic harvesters: in-plane overlap converters; in-plane gap closing converters; out-of-plane gap closing converters. The authors suggested that all the three types can be operated in both charge-constrained and voltage-constrained cycles. They argued that the voltage-constrained approach generates more energy than the charge-constrained approach. However, by using a parallel capacitor in charge-constrained systems, energy levels can reach those of voltage-constrained systems because parallel capacitors effectively constrain the voltage across the energy harvesting variable capacitor.

2.6 COMPARATIVE STUDIES OF CAPACITOR STRUCTURES

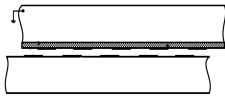

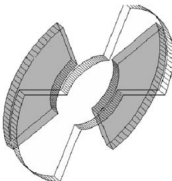
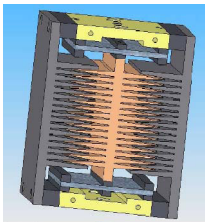
Roundy et al. (2002) presented a useful comparison between in-plane overlap and gap-closing converters. The authors suggested that the number of fingers for the in-plane gap closing converter is a function of the maximum deflection of the flexures; this is due to the fact that the fingers must be spaced far enough apart to accommodate the displacement. Therefore, lower maximum and minimum capacitances result from higher spring deflections. However, this is not the case with in-plane overlap converters, where more power is harvested when larger spring deflections are applied. The authors claim that in-plane overlap designs are more sensitive to parasitic capacitance than gap-closing converters.

Lim et al. (2008) compared detailed models of three different design concepts: in-plane overlap converter; in-plane gap-closing converter; out-of-plane gap-closing converter. The authors evaluated and compared the three design concepts based on simulations and practical considerations. The simulations results indicated that the highest power density is available from in-plane gap-closing converters, followed by out-of-plane gap-closing converters and finally in-plane overlap converters. The authors suggested that, to improve the power capabilities of the in-plane overlap, the surface area of the capacitor plates needs to be increased to produce more energy.

Boisseau and group of researchers (2012) reported on the assessments, limits and perspectives of various types of electrostatic energy harvester. One of the main limitations was capacitor gap control. This is an important factor that affects output power as it is greatly linked to capacitance variations that must be maximized. Therefore, the authors suggested that the air gap must be controlled precisely and minimized to achieve high capacitances. Moreover, it is also important to prevent from electrical breakdown problems.

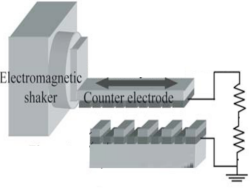
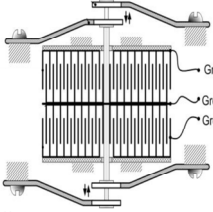
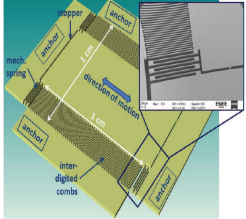
Eight main types of variable capacitors used for energy harvesting from previous studies were compared in this thesis. A summary of the results is given in Table 2.1.

Table 2.1: Comparison of variable capacitors used in electrostatic harvesters

Research team	Harvester type	Device structure	Capacitance range	Power capability	Features/ Fabrication difficulties
Le et. al (2009)	In plane overlap		203.7 - 134.7 pF	0.6 μ W	<ul style="list-style-type: none"> – Needs power processing – Resonance- based – Fringing field has negative effect on power output
Kiziroglou et. al (2009)	Rolling rod harvester		10 - 2 pF	=	<ul style="list-style-type: none"> – High output power of 250 μW when $V = 50V$, $R = 10 M\Omega$ – Needs power processing - step down converter – High cost fabrication processes.
O'Donnell et. al (2009)	Varying capacitance machine		40 – 9 pF	100 μ W	<ul style="list-style-type: none"> – Capacitance increases with the increase in the number of poles – Can be used for HVDC systems – 3 D finite-element analysis software is used to model the capacitor
Despesse et al. (2008)	In plane gap closing		-	16 μ W	<ul style="list-style-type: none"> – The gap between fingers must be higher than the relative displacement amplitude – The system needs an initial energy source to be polarized –

Continue . . .

... Continued

Tsutsumi no et. al (2006)	CYTOP electret generator		25.4 – 39.8 pF	280 μ W	<ul style="list-style-type: none"> – Needs power processing and rectification – Power output depends on thickness of electret, gap between electret, counter electrode and overlapping area – Power is generated when 20 Hz oscillation with 4 MW external load is used.
Ma et. al (2007)	Single wafer floating electrode		16.82 pF	60 nW	<ul style="list-style-type: none"> – Needs power processor, sensing transistor and diode bridge – Generator uses (CMOS) “floating gate” and post-CMOS photo-resist process
Nguyen. et. al (2002)	Tunable capacitor		1.34 – 0.32 pF	-	<ul style="list-style-type: none"> – Uses angular vertical comb-drive actuators – Uses glass substrate to reduce parasitic capacitances
Reznikov et. al (2010)	Electrostatic swing harvester		0.2 – 4.5 pF	0.75 μ W	<ul style="list-style-type: none"> – Used with oscillating, polarized charge pump – Homo-polar electret is used which contains real charges of only one sign and charge of opposite sign which is induced in available electrodes – Provides DC current output with voltage greater than 3 V
Guillemet et. al (2012)	In-plane gap-closing		40 -290 pF	938 nW	<ul style="list-style-type: none"> – Etched by DRIE (Bosch process) in a 380 μm-thick doped silicon wafer – Uses inductive flyback power circuit – Minimum value of capacitance is strongly affected by the parasitic capacitance.

2.7 SUMMARY

Electrostatic harvesters are compact converters with a simple structure. The energy density of these devices can be easily modified by changing the structure of the capacitor. This represents a potential solution to developing the market of energy harvesting powered applications by making it possible to develop low-cost energy harvesting devices. The design of an electrostatic energy converter depends mainly upon the structure of the variable capacitor and the conversion mechanism approach. Research studies have presented a wide range of possible structures and approaches that can be adopted. However, the proposed structures and approaches presented in the literature so far have both advantages and drawbacks.

The choice of capacitor structure depends on the type of mechanical energy applied: rotational motion or vibration. Both types can be extracted from kinetic wind energy. Variable area capacitor appears to be more suitable for harvesting rotational energy from wind. Area of the capacitor plates can be modified easily by the rotational mechanical energy. While a variable gap capacitor works mostly with vibrations. Moreover, variable area structures can be easily fabricated to electret free – air capacitors. It is relatively easy to increase capacitance by increasing the surface area of the capacitor plates.

The choice of conversion mechanism depends on the variable capacitor structure. As highlighted in the literature, the conversion mechanism can use either continuous or switched systems. The continuous approach is an electret-based approach that requires a polarisation source and special fabrication processes. While the switched constant voltage and constant charge approaches are easier to implement, they require switching control circuitry. Comparing the constant voltage and constant charge approaches, it is noticeable that the former offers more energy. Therefore, it is more appropriate for electrostatic energy harvesting provided that it generates low voltages within the breakdown limits of standard IC process technologies. On the other hand, the constant charge approach fits few types of electrostatic harvesters, especially for large electrostatic forces. The electrostatic force depends on the dimensions of the capacitor, the proof mass and the operating condition. It is more difficult to achieve high electrostatic forces using constant voltage structures than constant charge structures. For this reason, constant charge is more suitable when large electrostatic forces are required (Mitcheson 2008).

CHAPTER 3

DESIGN CONSIDERATIONS FOR ELECTROSTATIC HARVESTERS

3.1 INTRODUCTION

As discussed in Chapter 2, the design of an electrostatic converter depends mainly on the variable capacitor structure and the conversion mechanism. However, when looking at the overall energy harvesting system, there are many other design factors than need to be taken into consideration. While trying to understand how an electrostatic energy harvesting system works, we found various factors that affect the harvester design and the amount of power generated. The main aim of this chapter is to review all the possible factors that affect the design of the harvester in order to provide a design process. The focus is therefore on examining the design considerations that lead to the decisions for choosing the appropriate electrostatic harvester for various low power applications. This entails a review of the literature concerning design considerations and design procedures. This review produces a list of questions, which form the basis for this chapter.

3.2 DESIGN CONSIDERATIONS

Due to the variety of methodologies and approaches in designing electrostatic energy harvesters, a review and a comparative study was essential to identify the general design considerations for harvesters in terms of the source of mechanical energy, capacitor construction, electrical properties, energy transfer strategies and power processing needs. From all the topologies, methods and structures of electrostatic harvesters studied in this research, the following factors are the most significant for harvester design: type of mechanical energy, variable capacitor structure, variable capacitor material, energy transfer strategy and type of storage device.

The following sections summarise the key findings of the review regarding these factors. The aim of the findings is to provide a justification for the following work in this study.

3.2.1 Types of mechanical energy

Mechanical energy is generally the most adaptable and available energy source. Its high power density makes it the most suitable source for electrostatic energy harvesting (Miao et al. 2003). However, in mechanical energy harvesting, the amount of power harvested mainly depends on the specifics of the environment from which the kinetic energy is captured, the portion of the ambient energy surrounding the harvesting device, the type of mechanical energy, whether rotational motion or vibration, and the efficiency of the harvesting process (Halvorsen et al. 2007).

Most research on testing electrostatic energy harvesters utilises vibration as the energy source (Boisseau et al. 2013), while few studies have been conducted on testing electrostatic harvesters with rotational motion (O'Donnell et al. 2009). The type of mechanical energy is a critical factor that affects the design of the variable capacitor and the amount of harvested power, which highly depends on the frequency of the rotational motion or vibrations (number of revolutions per minute or number of cycles per second). Table 3.1 shows the output power obtainable from environmental kinetic energy sources using existing harvesting devices. It can be seen that the industrial environmental sources seem to have more energy to spare while human energy is very limited.

Table 3.1: Environmental kinetic energy sources (Vullers et al. 2009)

Source (Motion /vibration)	Harvested power
Human (eg. heart beat, respiration etc)	4 $\mu\text{W} / \text{cm}^2$
Industrial	100 $\mu\text{W} / \text{cm}^2$

T. Sterken et al. (2007) reported that the selection of the mechanical energy type for harvesting strongly depends on the application, which might be a very small, lightweight sensor, a wearable or a portable device. The authors gave a short overview of some examples of the mechanical energy produced by machines at different frequencies and amplitudes or accelerations, as shown in Table 3.2.

From Table 3.2, it can be observed that the machine motion (rotation or linear) produces more power than machine vibration. Thus, vibrations are used mostly with MEMS generators that harvest low power at low frequencies (Vullers 2009).

Table 3.2: Mechanical energy sources in industrial environments (Sterken et al. 2007)

This item has been removed due to 3rd Party Copyright. The unabridged version of the thesis can be viewed in the Lanchester Library Coventry University.

--	--

In order to obtain mechanical energy (rotational motion or vibration) from kinetic energy, a capturing device is required. This forms a significant part of an electrostatic harvester system as it is the first part of the system that must be capable of converting kinetic energy into mechanical energy with high efficiency. For electrostatic harvesters, a number of capturing devices are available based on variable capacitor models. These include wind turbines, wind vibros (Michler 2011), cantilever beams (Taha 2009), mechanical vibration machines (Mitcheson 2005), a mass on a spring (Torres 2005), and any device that convert rotational motion into linear motion or vice versa. At times, even the variable capacitor itself can be considered as a capturing device depending on its structure (Kiziroglou et al. 2009).

3.2.2 Variable capacitor structures

The capacitance variation of the variable capacitor is one of the most significant factors affecting the amount of energy that an electrostatic harvester can collect. In general, there are three important parameters in establishing the capacitance variation of a variable capacitor: plate area, plate separation and dielectric constant. Several capacitor structures have been reported in the literature as mentioned previously in Chapter 2, in terms of these parameters.

Roundy et al. (2004) classified three main types of electrostatic devices that can harvest energy from vibrations by modifying either the area of the capacitor plates or the gap between them. Schematics of these devices are shown in Figure 3.1.

This item has been removed due to 3rd Party Copyright. The unabridged version of the thesis can be viewed in the Lanchester Library Coventry University.

(a)

(b)

This item has been removed due to 3rd Party Copyright. The unabridged version of the thesis can be viewed in the Lanchester Library Coventry University.

(c)

Figure 3.1: Vibration-based electrostatic harvesting devices (a) In-plane overlap converter (b) In-plane gap-closing converter and (c) Out-of-plane gap-closing converter (Roundy et al. 2004)

The light areas represent the movable elements and dark areas the fixed elements. Lim et al. (2008) observed that the in-plane gap-closing mechanism can produce more energy per unit volume than the other two types. Additionally, the best energy output for the in-plane gap-closing converter is approximately 1.8 times greater than the energy produced by the out-of-plane gap-closing converter for load volumes between 5 mm^3 and 50 mm^3 . These converters mostly harvest energy from vibration not from rotational motion.

Other types of capacitor structures were compared previously in Chapter 2, Table 2.1, in terms of construction, fabrication method, practical maximum power and power processing needs. The conclusion was that a varying capacitance machine reported by (O'Donnell et al. 2009), which is a multi-pole capacitor, can produce more power than other structures. This device can be used to harvest energy from rotational motion and can be easily modified to obtain more energy by increasing the number of poles in the capacitor.

3.2.3 Variable capacitor materials

Most variable capacitors used for electrostatic energy harvesting consist of parallel conductive plates separated by air. Experiments have shown that capacitance increases when the space between the conductive plates is filled with dielectrics (Boylestad & Nashelsky 2011). Table 3.3 shows various dielectric materials, all of which have a dielectric constant greater than 1 and a characteristic dielectric strength that is the maximum value of the electric field that can be established before breakdown occurs. Although air has the lowest dielectric constant, it is still the most convenient dielectric material to be used, especially when harvesting mechanical energy.

Table 3.3: Dielectric materials (Floyd 2007)

This item has been removed due to 3rd Party Copyright. The unabridged version of the thesis can be viewed in the Lanchester Library Coventry University.

The capacitor's conductive plates are made of various types of material and composites, such as aluminium, silver, brass, tantalum or carbon nanotube (Floyd 2007). Comparing these materials in terms of conductivity, thermal conductivity, cost of material and equivalent series resistance (Zhang et al. 2009), it is observed that tantalum capacitors have a low equivalent series resistor but are expensive, harmful to the environment and unable to handle high charging voltages (radio-electronics.com 2012). Silver capacitors are more expensive but have many advantages, such as high precision, reliability and stability, and can operate at different frequency ranges (Floyd 2007). Brass capacitors have a low melt point, are easy to cast and can be recycled (Zhang et al. 2009). The nanotube capacitors reported by a group of researchers at MIT are constructed from an aluminium capacitor covered by millions of carbon nanotube. This capacitor has a long life and it can store energy for long time. However, it is very expensive and not yet developed for public use (Carbonnanotubebattery.com, 2009). Aluminium capacitors are inexpensive and highly conductive; moreover, aluminium can be easily formed into various capacitor plate shapes (Floyd 2007).

3.2.4 Energy transfer strategies

When considering energy transfer strategies, there are two modes of operation reported in the literature: voltage-constrained mode and charge-constrained mode (Mitcheson et al. 2008). In a voltage-constrained mode, switched-inductive circuits are used to transfer energy (Kwon 2010). The switched-inductor circuits dissipate little power because the energy transfer inductor and the switches used in the circuit conduct with close to zero volts across them. Moreover, this circuit delivers exactly the initial energy investment required by the capacitor, which saves a lot of energy (Torres et al. 2009a). In charge-constrained mode, one highly efficient energy transfer strategy reported in the literature (Kempitaya 2011) is the charge pump with flyback circuit. In its forward path, the charge pump converts mechanical energy into electrical energy that is then transferred to a temporary storage device. At regular intervals, the flyback circuit sends the harvested energy back to a reservoir to power both the load attached and the charge pump circuit itself (Dudka et al. 2009).

In some cases, a power processing circuit is required to improve the quality of the power delivered to a load or a storage device (Mitcheson 2006). For example, in a charge-constrained system, the fundamental difficulty in processing the output power is that it works with a small charge at high voltage. The voltage generated can be of the order of a few hundred volts, which must be converted to a lower voltage to be suitable for powering low power loads. Many power processing circuits for harvesters have been reported in the literature, such as buck converter, buck boost converter, linear voltage regulators, classical switching techniques and switched-capacitor regulators. These circuits are used to process and maintain the DC voltage at appropriate level. The selection of a suitable power processing circuit for the electrostatic harvester depends on the frequency, output voltage, current, resonance behaviour of the harvester, size of the harvester and the motion which drives the capacitor (D'hulst n.d.).

Table 3.4 summarises the advantages and disadvantages of three main types of conditioning circuits: linear voltage regulators, the classical switching regulators and switched-capacitor regulators. It shows that a switched capacitor regulator may provide a better solution to the sizing problem and a better up or down conversion of voltage than the other two regulating circuits.

Table 3.4: Advantages and disadvantages of power conditioning circuits
(D'hulst n.d.)

This item has been removed due to 3rd Party Copyright. The unabridged version of the thesis can be viewed in the Lanchester Library Coventry University.

3.2.5 Types of storage devices

Storage devices are of great importance in many harvesting systems because they enable harvested energy to be saved inside them before delivery to electrical systems, whenever and wherever energy is needed (Miranda 2004). Many battery technologies are available, such as nickel cadmium (NiCd), nickel-metal hydride (NiMH), lithium-ion (Li-ion), polymer Li-ion and thin film.

For electrostatic energy harvesters operating under constrained voltage systems, the most appropriate storage device is the lithium-ion (Li-ion) battery. Li-ion batteries require protection circuits to keep voltage and current within safe limits, and are subject to aging and expensive to manufacture (Torres et al .2006). However, these batteries also have many advantages, such as high energy density, lower weight than other types of rechargeable batteries, ability to handle many charge/discharge cycles, relatively low self-discharge rates and low maintenance needs (Kompis & Aliwell 2008). Another option is the thin film battery, which has a solid core so is less exposed to overheating. It can also be recharged thousand times before needing replacement (Kompis & Aliwell 2008).

In charge-constrained systems, the storage device used is a super capacitor that acts like reservoir to store energy (Kompis & Aliwell 2008). Super capacitors are electrostatic devices. Unlike batteries, they can be fully discharged for maintenance. The behaviour of these devices is more predictable and they are more tolerant of faults and damage. In the past, they have been little used because they are expensive, hold only a little electricity per unit volume and rapidly self-discharge. However, super capacitors have recently been improving much faster than lithium-ion batteries and their marketing is now more creative, so many applications not involving batteries now use super-capacitors, especially applications that depend on energy harvesting (Vullers et al. 2009).

The main characteristics of Li-ion batteries and super capacitors based on measurements carried out using the best available storage devices are presented in Table 3.5. It shows that Li-ion batteries and super-capacitors differ significantly in their main parameters. Both types can be used for the electrostatic harvester. Therefore, the choice between the two storage devices depends mainly on the requirements of the target application.

Table 3.5: Characteristics of Li- ion batteries and super capacitors (Vullers et al. 2009)

This item has been removed due to 3rd Party Copyright. The unabridged version of the thesis can be viewed in the Lanchester Library Coventry University.

3.3 DESIGN PROCEDURE

Designers propose a design procedure based on the relevant design factors. The proposed design process is a plan that helps the designers build an electrostatic harvester. The process involves many steps, some of which need to be repeated in order to optimise the final product.

For an electrostatic harvester, the design process includes many steps: identifying the type of mechanical energy, identifying the capacitor geometrical factor to be modified, which is either the area of the capacitor plates or the gap between them, selecting a suitable capacitor structure, and choosing the type of material for the capacitor plates. Later, a suitable energy transfer circuit, power processing circuits and a storage device need to be selected. Finally, a feasibility check is required to determine if the harvester design can proceed to a final fabrication and testing phase. This depends both on whether the harvester can produce sufficient power and whether its production stays within the cost limits. If the design passes the feasibility check, a final harvester design is produced for testing and fabrication. A flow chart of the design procedures is shown in Figure 3.2.

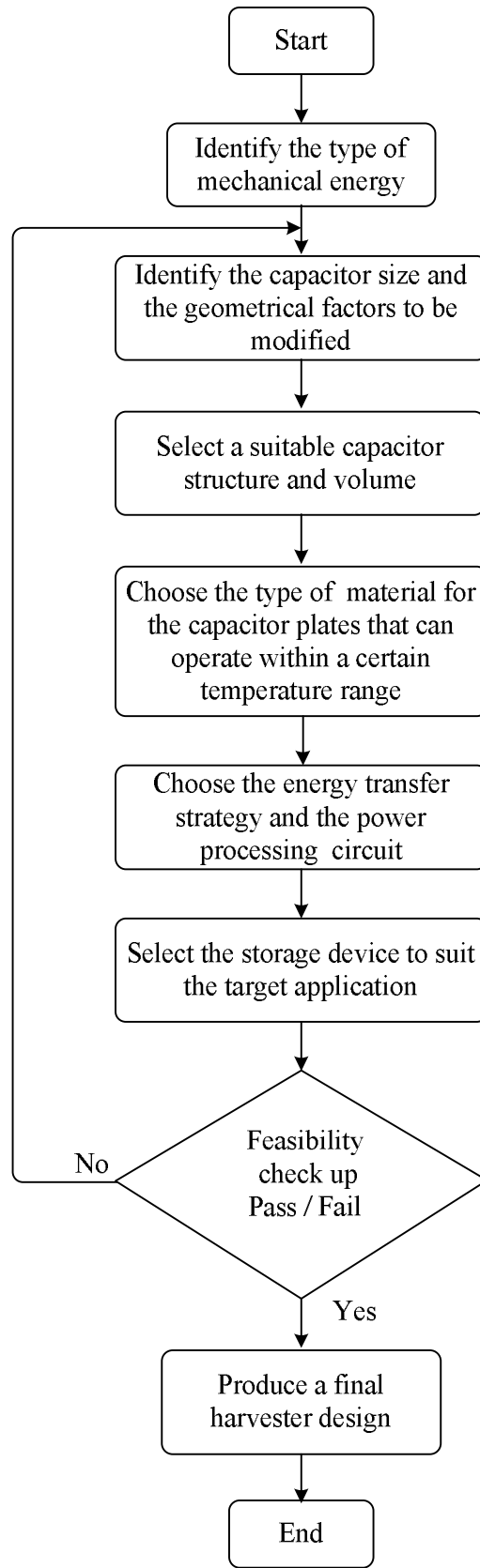


Figure 3.2: Flow chart of electrostatic energy harvester design procedure

3.4 SUMMARY

This chapter considered the design considerations and design procedures for various electrostatic energy harvesting devices. From the review of previous research, the following factors appeared to be the most important for the design of the harvester: type of mechanical energy, variable capacitor structure, variable capacitor material, energy transfer strategy and type of storage device.

Since the amount of harvested power depends on the type of mechanical energy, two types of mechanical energy were studied: rotational motion and vibration. It was observed that the mechanical motion provides more energy than vibrations. However, vibrations are preferable for low-power and low-frequency applications. Since this research is focused on wind energy harvesting, a micro wind turbine would be a suitable choice as a capturing device because it could extract rotational motion from the wind.

The chapter compared a number of capacitor structures to find the most appropriate structure for wind energy harvesting. This revealed that the varying capacitance machine reported for high voltage DC power generation could be used for energy harvesting. The capacitor structure used is a variable area, multi-pole capacitor that converts mechanical rotational motion into electrical energy. Although this capacitor was originally proposed for high power generation, a similar construction could be adopted for electrostatic-based wind energy harvesting.

With regard to the type of material to be used for wind energy harvesting in the air variable capacitor, the first option is to use silver for the capacitor plates as it is precise, stable and reliable, and can operate at different frequency ranges. The second option is to use aluminium as it is cheaper than silver, highly conductive and can be easily formed into various plate shapes.

The chapter also discussed energy transfer strategies for both constant voltage and constant charge systems. The inductive energy transfer circuit dissipates little power and delivers exactly the initial energy investment required by the capacitor, which saves a lot of energy, making it a suitable energy transfer circuit if a constant voltage approach is selected.

The chapter focused on the two most efficient devices for storing energy: lithium ion batteries and super capacitors. Choosing between them for electrostatic harvester in a constant voltage system depends on the requirements of the application.

Table 3.6 summarises the design specifications for the electrostatic-based wind energy harvester according to the design factors discussed so far and the proposed design procedure.

Table 3.6: Design specifications for electrostatic-based wind energy harvester

Design factors	Harvester specifications
Type of mechanical energy	Rotational motion
Energy capturing device	Micro wind turbine
Variable capacitor structure	Variable area/ Multi- pole capacitor (size and volume to match the micro wind turbine)
Variable capacitor material	Air variable capacitor with Aluminum conductive plates
Energy transfer strategy	Constant voltage system using inductive energy transfer circuit
Storage device	Lithium ion battery or super capacitor based on the power requirement of the target application

CHAPTER 4

ELECTROSTATIC WIND ENERGY HARVESTING PRINCIPLES

4.1 INTRODUCTION

As discussed in the previous chapter, many factors affect electrostatic energy harvester design and certain design procedures need to be followed. The design procedure described previously helped in setting the guidelines for the harvester's design. The design depends on type of capturing device, mechanical energy, variable capacitor structure, capacitor material, energy transfer strategy and storage device. The wind harvester captures and converts wind energy into mechanical rotational energy, which then moves the capacitor plates, thereby changing their effective area. This change makes the device's capacitance switch from maximum to minimum. Therefore, either the charge or the voltage changes while the other is kept constant.

In this chapter, the basic principles of electrostatic wind energy harvesting are introduced including: wind energy, historical background of wind turbines, types of wind turbine, power in wind, electrostatic converters, variable capacitors, constant charge systems, constant voltage systems, types of energy transfer circuits, capacitance sensing systems and controlling mechanisms.

4.2 ELECTROSTATIC BASED WIND ENERGY HARVESTERS

The electrostatic based wind energy harvester is a unique system that combines the concept of wind and electrostatic effects. It consists of two main blocks. First, a wind turbine converts wind energy into rotational mechanical motion. Second, an electrostatic converter converts the mechanical energy into electrical energy. Figure 4.1 illustrates the basic block diagram of the harvester. The details of each block will be reviewed in the following sections.

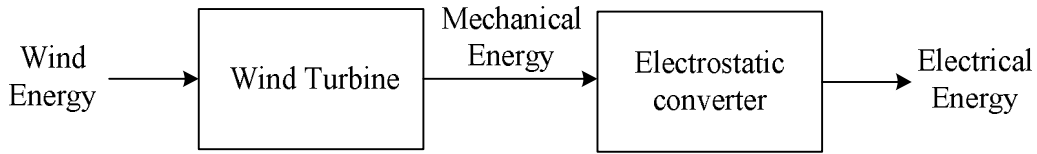


Figure 4.1: Basic block diagram of electrostatic based wind energy harvester

4.3 WIND ENERGY HARVESTING

Wind energy is one of the most cost effective renewable energy sources, creating no pollution or waste. In general, wind energy harvesting systems are one of the least expensive renewable energy sources and are becoming more affordable as the technology develops (Manuell 2009). However, to make wind a constructive electrical energy source, a suitable design of wind capturing device should be selected from the wide range of wind capturing devices are available that can efficiently capture energy from the wind.

4.3.1 The Wind

Wind is air movement across the earth's surface between high and low pressure areas, caused by the sun's rays heating the atmosphere randomly. This is affected by many factors, such as large bodies of water, open and covered areas with vegetation, the sun rays' angle of incidence. Heat energy absorbed from the sun is transferred directly to the air above the surface. As cool air has a higher density than hot air, hot air rises above it to form the high and low pressure areas. The rotational movement of the earth also helps in creating air turbulence. All these effects cause the varying winds across the earth surface (Grogg 2005).

Information about landscape and wind speed is very important when deciding where to install wind capturing devices such as wind turbines. For large scale wind harvesting, the minimum average wind speed should be about 5-6 m/sec. Wind speed is also a significant factor when selecting the type and size of wind turbine. Therefore, before installing wind harvesters, it is essential to determine wind speed as the number of hours per year that the wind at the site is at different speeds (Grogg 2005).

These data help to decide whether there is enough wind for a wind turbine to be cost-effective. A typical wind speed distribution curve, which is usually a smooth distribution, is shown in Figure 4.2. To produce electricity most efficiently, it is recommended to find the right combination of size, shape and materials, and the right location to install wind turbines (Grogg 2005).

This item has been removed due to 3rd Party Copyright. The unabridged version of the thesis can be viewed in the Lanchester Library Coventry University.

Figure 4.2: Typical wind speed distribution curve (Grogg 2005)

4.3.2 Historical development of wind turbines

The utilization of wind energy has a very long history, dating back to over 3,000 years ago (Manuell 2009). Modern developments in wind energy harvesting technologies have happened very fast in many dimensions. The world's first electricity generation wind turbine was built in 1819 to electrolyse water to produce hydrogen for gas lights. By the 1930s and 1940s, hundreds of thousands of small capacity wind turbine systems were in use in remote areas not served by electricity grids. The oil shocks of the 1970s, which increased awareness of energy problems, were joined by financial and regulatory encouragement for alternative energy sources. Within a decade or so, dozens of manufacturers installed thousands of new wind turbines (Manuell 2009). As shown in Figure 4.3, cumulative global wind power capacity grew rapidly from 1994 to 2012.

This item has been removed due to 3rd Party Copyright. The unabridged version of the thesis can be viewed in the Lanchester Library Coventry University.

Figure 4.3: Global wind power cumulative capacities (Hodge 2012)

4.3.3 Types of wind turbines

Wind turbines are classified in terms of the axis around which the blades rotate, with vertical axis and horizontal axis turbines being the two basic types of wind turbine configurations: the more common horizontal axis (HAWT) with the gearbox mounted on top of a tower, and the vertical axis (VAWT) with the gearbox at ground level. Figure 4.4 presents examples of the two types (Manuell 2009).

This item has been removed due to 3rd Party Copyright. The unabridged version of the thesis can be viewed in the Lanchester Library Coventry University.

Figure 4.4: Types of wind turbines (People.bu.edu n.d.)

The main advantage of HAWT is that they have high efficiency, access to high wind speed due to the tall towers and the blade pitch of these turbines can be controlled remotely while the main advantages of VAWT is that they do not require yaw control to keep them facing into the wind. Moreover, the heaviest mechanical components, such as the generator and gearing system, can be located down on the ground, where they can be maintained easily. As the blades spin around in pure tension, they can be relatively light-weight and inexpensive. On the other hand, there are several disadvantages of VAWT compared to HAWT. The main disadvantage is that the blades are close to the ground where wind speeds are low. In addition, wind close to ground has more turbulence, which increases stress on the wind turbine. Finally, at high wind speeds, they cannot be made to spill the wind as easily as the controlled blades of HAWT (Masters 2004).

Another important factor for wind turbines is the number of the blades. Wind turbines with many blades operate at much lower rotational speeds than those with fewer blades. This matters because, when rotation speed increases, turbulence caused by the blades increases too, which reduces the overall efficiency of the turbine. Most European turbines have three rotors while American turbines have just two, as shown in Figure 4.5. Three-blade wind turbines operate more smoothly and quietly. However, the third blade increases weight and cost (Masters 2004).

This item has been removed due to 3rd Party Copyright. The unabridged version of the thesis can be viewed in the Lanchester Library Coventry University.

Figure4.5: Two-blade versus three-blade turbines (Zipp 2010)

4.3.4 Micro wind turbine

On a small scale, micro wind turbines can be used for successful harvesting of electrical energy from wind energy, which can solve various challenges and develop new applications. In regions of low wind speed and in crowded areas, micro wind turbines are more suitable. These turbines have received attention in recent years and a great deal of research has been conducted to reduce their cost while increasing the generated output power (Leung 2010).

Researchers at Hong Kong University and Lucien Gambarota of Motorwave Ltd have developed a micro wind turbine technology small enough for private use in both rural and urban environments, as shown in Figure 4.6. Unlike large-scale wind turbines, micro wind turbines are light, compact and capable of generating power from wind speeds as low as 2 m/sec. In addition, they can be sited anywhere, and are cheap: a set of eight turbines costs only around \$150. Tests showed that turbines covering a surface area of one square meter in a wind speed of 5 m/sec could generate 131 kWh/yr (Hku.hk 2007).

This item has been removed due to 3rd Party Copyright. The unabridged version of the thesis can be viewed in the Lanchester Library Coventry University.

Figure 4.6: Micro wind turbines (Hku.hk 2007)

Leung et al. (2010) studied the performance of the micro wind turbine shown in Figure 4.7, which was specially designed for metropolitan areas where wind speeds are usually low. This turbine does not have to be connected to the grid; it can be linked directly to a small generator instead. The advantages of this micro wind turbine are that it is a cost effective device, can be propelled by a wind speed as low as 2 m/sec, has a fan-type blade configuration that has a functional advantage of increased power efficiency, has a twisted

blades to capture more efficient torque in different wind conditions, and designed in such a way that multiple turbines can be connected together to aggregate the power to meet any requirements in a flexible manner.

This item has been removed due to 3rd Party Copyright. The unabridged version of the thesis can be viewed in the Lanchester Library Coventry University.

Figure 4.7: Cost-effective wind turbine proposed by (Leung et al. 2010)

The micro turbine studied in (Leung et al. 2010) is the most suitable choice for electrostatic based wind energy harvesting systems because it is capable of generating mechanical power from low wind speeds, is small and light, can be stopped by a touch of the hand, does not represent any physical danger, has relatively low primary cost, and is appropriate for low power applications. Finally, an array of these small turbines can be connected together to increase the power output to meet any requirements.

4.3.5 Power from wind

Wind turbines work by first converting the kinetic energy in wind into rotational mechanical energy in the turbine. If a packet of air with a mass of m moves at a speed of v_{wind} , its kinetic energy is governed by (Manuell et al. 2009):

$$E = \frac{1}{2}mv_{\text{wind}}^2 \quad (4.1)$$

where E is kinetic energy from wind, m is the total mass of air and v is the instantaneous wind speed. Since

$$m = \rho A v_{\text{wind}} \Delta t \quad (4.2)$$

where ρ is the air density, A is the area visible to the wind, and Δt is the period of time over which the calculation is performed. From (4.1) and (4.2), the wind kinetic energy is given by:

$$E = \frac{1}{2} \rho A v_{\text{wind}}^3 \Delta t \quad (4.3)$$

Knowing energy is a product of power and time, mechanical power from wind can be written as (Masters 2004):

$$P_{\text{wind}} = \frac{1}{2} \rho A v_{\text{wind}}^3 \quad (4.4)$$

From equation 4.4, it can be seen that wind power is proportional to the cube of the wind speed. A power duration curve is typically used to analyse wind turbine efficiencies, which plots wind speed against power from the wind, as shown in Figure 4.8.

This item has been removed due to 3rd Party Copyright. The unabridged version of the thesis can be viewed in the Lanchester Library Coventry University.

Figure 4.8: Wind power distribution curve (Manuell et al. 2009)

More analyses are required to explore the maximum possible conversion efficiency of wind turbines in converting kinetic energy in the wind to mechanical power. These analyses are

based on simple physics principles, fluid dynamics and algebra to estimate the maximum power harvested by a wind turbine.

To calculate maximum power, let us consider a stream tube, which is an envelope drawn around the air mass passing through the wind turbine, as shown in Figure 4.9. The wind approaches the turbine with an initial velocity of v_1 before slowing down to v_2 by the time it reaches the rotor. Because the rotor captures part of the energy, the air behind the rotor has less energy so its velocity is further reduced to v_3 , keeping in mind that the mass of air leaving behind the rotors is the same as that moving toward the rotors (Masters 2004).

The wind turbine cannot extract all the energy from the wind because, if it did the air behind the rotor would have to be very slow or even still. This would mean that any further flow of wind towards the turbine would have nowhere to go so high pressure would build up. Therefore, v_2 cannot be zero. It can be seen from Figure 4.9 that the stream tube increases in volume behind the turbine rotor because that air moves at a low speed at low pressure, causing the air to expand to allow continued flow (Masters 2004).

This item has been removed due to 3rd Party Copyright. The unabridged version of the thesis can be viewed in the Lanchester Library Coventry University.

Figure 4.9: Stream tube (Masters 2004)

The practical power extracted from the wind is equal to the power calculated by equation (4.4) multiplied by the fraction of the wind power extracted by the blades, which is determined by the efficiency of the rotor and usually designated as C_p , for the performance power coefficient (Masters 2004). C_p is the ratio of the power in the rotor to the power in the wind, known as the Betz limit. Hence, the extractable power from the wind is given by:

$$P_{\text{mech}} = \frac{1}{2} \rho A v_{\text{wind}}^3 C_p \quad (4.5)$$

The original derivation of C_p is credited to the German physicist Albert Betz who concluded in 1919 that an ideal wind turbine would slow the wind to one third of its original speed. Hence, no wind turbine can convert more than 59.3% of the kinetic energy of the wind into mechanical energy. This is known as the theoretical maximum rotor efficiency and is defined as: $C_p = 0.593$ (Masters 2004).

However, not all wind turbines operate at this maximum limit so each turbine type has its unique value of C_p , which is a function of the wind speed that the turbine is operating in. Taking into consideration all the engineering requirement of a wind turbine, the limit in practice is lower than the Betz Limit, with values of 0.35-0.45 being common even in the best-designed wind turbines. After other factors in a complete wind turbine system, such as the gearbox and bearings, are considered, only 10-30 % of the power of the wind is actually converted into usable electricity (Masters 2004).

Rotor efficiency, C_p , is also a function of rotor speed. That is, if the rotor turns more slowly, efficiency drops because the blades are letting too much wind pass by unaffected. On the other hand, if the rotor speed is very high, efficiency decreases because of increased turbulence. Usually the efficiency of the rotor is represented as a function of its tip speed ratio, given by (Masters 2004):

$$TSR = \frac{rpm \times D}{60 v_{wind}} \quad (4.6)$$

where TSR is the tip speed ratio, rpm is the rotor speed and D is the rotor diameter. A typical efficiency plot for various rotor types versus the tip speed ratio is given in Figure 4.10. It can be noticed that the efficiency reaches a maximum point at different positions for different wind turbine designs. The highest efficiencies of the two bladed designs, the Darrieus concept (type of a VAWT) and the modern three blades are above 30% but below the Betz Limit. The American multi-blade designs have a maximum efficiency at around 30%(Masters 2004).

Having knowledge of how a turbine operates in different wind speeds is essential to understand the returns lost due to any down time for the turbine. It is also useful to understand what power a turbine should be producing so that if there is a problem with the

turbine this can be detected early. From the previous discussion, it can be seen that a turbine's mechanical power depends on various factors, such as the cross-sectional area of the turbine, wind speed, number of blades, gearbox, rotor efficiency, type of rotor and tip speed ratio. All these factors should to be taken into consideration when selecting the turbine for an electrostatic based wind harvester.

This item has been removed due to 3rd Party Copyright. The unabridged version of the thesis can be viewed in the Lanchester Library Coventry University.

Figure 4.10: Typical efficiencies for various rotor types (Masters 2004)

4.4 ELECTROSTATIC ENERGY CONVERTER

The conversion from mechanical energy to electrical energy is achieved using an electrostatic converter. The block diagram of the electrostatic converter is shown in Figure 4.11. Each block will be reviewed in the following sections.

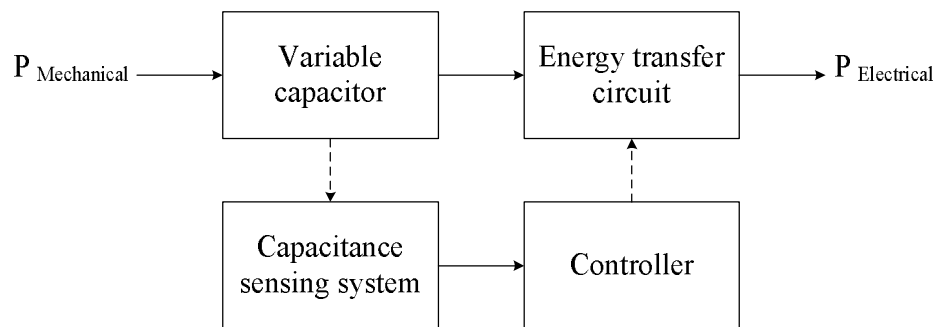


Figure 4.11: Block diagram of the electrostatic converter

4.4.1 Variable capacitor

Basically, a capacitor (fixed or variable) consists of two parallel plates isolated from each other, typically by air, vacuum or an insulating material. The capacitor stores energy in the form of an electrical field that is established by charging the capacitor with a battery of voltage V , which creates equal but opposite charges Q on the plates in accordance with Coulomb's law: "A force exists between two point source charges that is directly proportional to the product of the two charges and inversely proportional to the square of the distance between the charges" (Boylestad & Nashelsky 2011).

Figure 4.12 shows how parallel plate capacitors of a conductive material separated by an air have been connected through a switch and a resistor to a battery. If the parallel plates are initially uncharged and the switch is left open, no positive or negative charges will exist on either plate. The instant the switch closes; however, electrons are drawn from the upper plate through the resistor to the positive terminal of the battery. This will cause a rush of current, at first limited by the resistance, but after a certain time period, the current flow will decline. The movement of electrons continues until the potential difference across the parallel plates is exactly equal to the battery voltage. Thus:

$$C = \frac{Q}{V} \quad (4.7)$$

This item has been removed due to 3rd Party Copyright. The unabridged version of the thesis can be viewed in the Lanchester Library Coventry University.

Figure 4.12: The resistor – capacitor circuit (Boylestad & Nashelsky 2011)

The number of flux lines per unit area between the two plates is quite uniform. At the edges, the flux lines extend outside the common surface area of the plates, producing a fringing effect that reduces the capacitance; however, this can be ignored for most practical applications. The uniformity of the flux distribution also indicates that the electric field strength is the same at any point between the two plates, as shown in Figure 4.13.

This item has been removed due to 3rd Party Copyright. The unabridged version of the thesis can be viewed in the Lanchester Library Coventry University.

Figure 4.13: The electric field between the plates of a fixed or variable capacitor (Boylestad & Nashelsky 2011)

Many values of capacitance can be obtained for the same set of parallel plates by adding different insulating materials between the plates, by changing the gap between the plates or by modifying the capacitor plates' areas. Larger areas and smaller gaps increase capacitance while different amounts of charge can be deposited on the plate by using different dielectric materials. Therefore:

$$C = \epsilon_0 \epsilon_r \frac{A}{d} \quad (4.8)$$

where A is the area in square meters of the plates, d is the gap in meters between the plates, and $\epsilon_0 \epsilon_r$ are the absolute and the relative permittivity. Thus, the main factors affecting the capacitance are the areas of the plates, the gap between them and the type of dielectric material (Floyd 1984).

As mentioned earlier, capacitors are storage devices, with the energy stored being equal to the work done to charge it. When charging a capacitor, the voltage source does work to remove charges from one plate and deposit them on the other. For an uncharged capacitor, the numbers of positive and negative charges on each plate are balanced so that there is no

net charge and therefore no electrical field exists between the capacitor plates. If positive charges move from one plate to another to charge it up, it leaves one of the plates negatively charged. This process builds up charge on the capacitor, thereby creating an electrical field. The total amount of work done in this process is:

$$W = \int_0^Q dq \Delta V = \frac{1}{2} \frac{Q^2}{C} \quad (4.9)$$

This is equal to the electrical potential energy of the system:

$$E = \frac{1}{2} CV^2 \quad (4.10)$$

From equation 4.10, it can be noticed that the energy of the capacitor increases with the increase of the capacitance value or the DC voltage across the capacitor.

To assemble a variable capacitor suitable for an electrostatic-based wind energy harvester, all the previously discussed parameters need to be taken into consideration. Various capacitor structures were mentioned earlier in Chapters 2 and 3. The variation of those capacitors is achieved by varying either the area or the gap between the plates. In more physical terms, the mechanical energy causes the gap and/or overlap area of a parallel plate capacitor to vary under constant charge or voltage conditions to produce electrical energy (Torres et al. 2006). These two modes of operation are discussed next.

4.4.1.1 Constant voltage mode

In a constant voltage mode, a capacitor is pre-charged while connected to a constant voltage source. If the capacitance is reduced by relative motion of the plates, it results in charge being removed from the capacitor and pushed back into the voltage source, thereby increasing the energy stored in the source. The charge Q is given by:

$$Q = C_{\text{var}} V_{\text{const}} \quad (4.11)$$

If the plates operate in a sliding motion, as indicated in Figure 4.14, the force between the plates in the direction of relative motion remains constant.

Figure 4.14: Constant voltage approach (Mitcheson et al. 2008)

Figure 4.14 also demonstrates the charge – voltage QV diagram for this approach. From 1–2, the capacitor is pre-charged to the source voltage while at maximum capacitance. Then, from 2–3, in the harvesting part of the cycle, its capacitance is reduced while it is connected to the voltage source forcing the charge back into the voltage source. From 3-1, the capacitor operates under constant charge during which the capacitor is disconnected from the voltage source before its capacitance increases to be ready for the cycle to start again. The area enclosed by the QV diagram represents the harvested energy.

4.4.1.2 Constant charge mode

In constant charge mode, the variable capacitor is pre-charged at maximum capacitance and then disconnected from any external circuit before its capacitance is changed by mechanical motion, which results in a voltage increase with decreasing capacitance, as given by:

$$Q_{\text{const}} = C_{\text{var}}V \quad (4.12)$$

Thus, additional energy will be stored in the electric field between the plates as work is done against the electrostatic force. This additional energy can then be used to power a circuit. The most common way in which this approach is implemented is as shown in Figure 4.15.

This item has been removed due to 3rd Party Copyright. The unabridged version of the thesis can be viewed in the Lanchester Library Coventry University.

Figure 4.15: Constant charge approach (Mitcheson et al. 2008)

The two parallel plates of the capacitor are arranged in such a way that they can be separated to increase the gap between them under a constant charge. This creates a constant force between the plates. Figure 4.15 shows the QV diagram of the operation of the harvesting cycle. From 1-2, the capacitor is pre-charged to a low voltage in the first part of the cycle by connecting it to a voltage source. Then, from 2-3, the plates are disconnected from the source and separated under constant charge during the harvesting part of the cycle. Finally, from 3-1, the capacitor is discharged. The capacitance is then increased ready for the cycle to restart. The area traced out by the QV diagram again represents the harvested energy. Table 4.1 summarises the differences between the two modes.

Table 4.1: Comparison of electrostatic energy conversion mechanisms (Ambokar 2011)

This item has been removed due to 3rd Party Copyright. The unabridged version of the thesis can be viewed in the Lanchester Library Coventry University.

4.4.2 Energy transfer circuits

A number of basic architectures for energy transfer circuits have been reported in the literature, all of which fall into two main types: inductive circuits and charge pump circuits.

4.4.2.1 The inductive energy transfer circuit

Inductive energy transfer circuits are magnetic based circuits consisting of inductors that play an important role in transferring energy. There are two types of inductive energy transfer circuits: LC to LC approach (Torres et al. 2006) and L to LC approach (Torres et al. 2009b), as shown in Figure 4.16 (a) and (b).

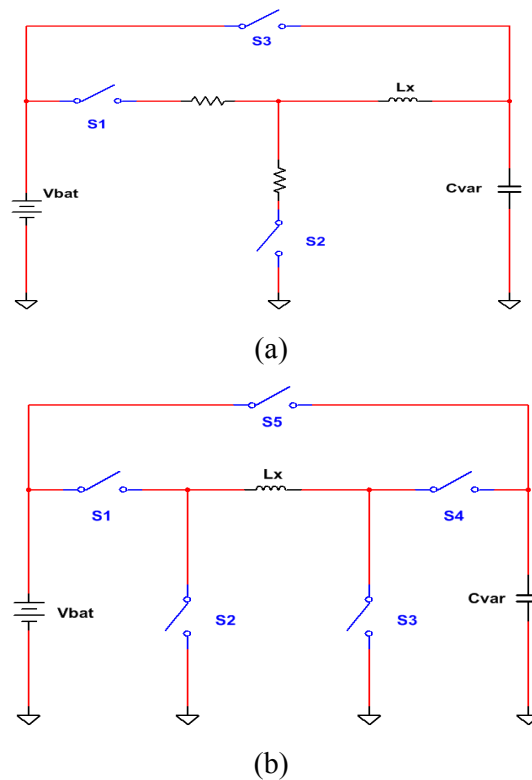


Figure 4.16: Inductive energy transfer circuits: (a) LC to LC approach (b) L to LC approach

Both approaches operate in constant voltage mode. As described in the previous section, the voltage across the capacitor is held constant throughout the pre-charge and the harvesting phase. As capacitance decreases in response to mechanical motion, charge is derived from the capacitor, which allows mechanical energy to be harvested and stored in the storage device (Torres et al. 2006).

The basic operation for both approaches is divided into three phases: pre-charge, harvest and reset phase, as shown in Figure 4.17. More energy can be harvested when the cycles goes faster. However, there is a physical limit based on the time required to complete the pre-charge phase.

This item has been removed due to 3rd Party Copyright. The unabridged version of the thesis can be viewed in the Lanchester Library Coventry University.

Figure 4.17: Energy harvesting cycle (Torres & Rincón-Mora 2010)

The pre-charge phase starts when the variable capacitor is at maximum capacitance. During this phase, the capacitor is charged to the battery voltage, which represents an energy investment from the battery.

$$E_{inv} = \frac{1}{2} C_{max} V_{Bat}^2 \quad (4.13)$$

As capacitance starts decreasing, the harvesting phase starts and charges flow into the battery producing a harvesting current, which enables energy to be harvested and stored.

$$I_{harv} = \frac{dq}{dt} = V_{Bat} \left(\frac{dC_{var}}{dt} \right) \quad (4.14)$$

$$E_{harv} = \int V_{Bat} I_{harv}(t) dt = \Delta C_{var} V_{Bat}^2 \quad (4.15)$$

During the reset phase, capacitance falls to its minimum and, since the voltage is constant, it retains remnant energy. The energy stored in the capacitor at minimum capacitance is simply:

$$E_{rem} = \frac{1}{2} C_{min} V_{Bat}^2 \quad (4.16)$$

As a result of the harvesting cycle, a net theoretical energy gain is generated:

$$E_{\text{net}} = -E_{\text{inv}} + E_{\text{harv}} + E_{\text{rem}} \quad (4.17)$$

$$E_{\text{net}} = \frac{1}{2} \Delta C_{\text{var}} V_{\text{Bat}}^2 \quad (4.18)$$

Equation (4.18) shows that theoretical net energy depends on variation in C from maximum to minimum capacitance, and the square of the battery voltage.

In the LC to LC approach, the circuit consists of a battery, three switches, an inductor and the variable capacitor. Since the inductor is a quasi-lossless device, it is used to transfer energy from the battery to the variable capacitor. The switches, on the other hand, naturally allow the current to pass in one direction, so these switches only dissipate ohmic losses. Considering the low power losses, and risk and complexity of other types of semiconductor switches, MOSFET switches appear to be more suitable for this approach. The circuit operation cycle consists of three steps. First, by closing S_1 for a short period of time, energy is transferred from the battery to the variable capacitor through the inductor. Second, by closing S_2 , the energy stored in the inductor continues charging the capacitor to the battery voltage. Third, the energy stored in the capacitor is transferred to the battery through S_3 as harvesting current (Torres et al. 2009a). For simplicity, the energy study of the LC to LC circuit during the pre-charge phase is divided into two stages. The circuit of each stage is given in Figure 4.18.

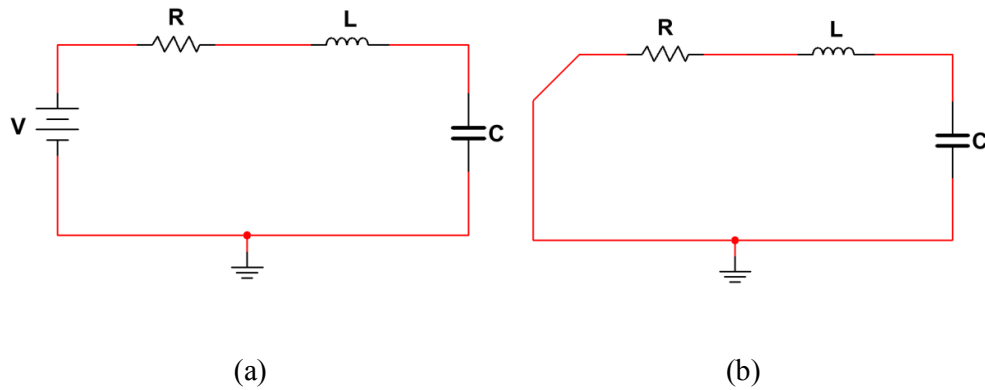


Figure 4.18: LC to LC circuit (a) Stage1 (b) Stage2

For Stage1, while energizing the coil L:

$$V = iR + L \frac{di}{dt} + \frac{1}{C} \int i dt \quad (4.19)$$

$$i = C \frac{dV_C}{dt} \quad (4.20)$$

Solving for V_C , and assuming $V = V_{Bat}$:

$$V_C(s) = \frac{\frac{1}{LC}}{s(s^2 + \frac{R}{L}s + \frac{1}{LC})} \cdot V_{Bat} \quad (4.21)$$

Then:

$$V_C(t) = V_{Bat} \left[1 - \frac{1}{\sqrt{1-\zeta^2}} e^{-\zeta \omega_n t} \sin(\omega_n \sqrt{1-\zeta^2} t + \emptyset) \right] \quad (4.22)$$

where $\omega_n = \frac{1}{\sqrt{LC}}$, $\zeta = \frac{1}{2} R \sqrt{\frac{C}{L}}$ and $\emptyset = \cos^{-1} \zeta$

From equation (4.20) and (4.22):

$$i(t) = C V_{Bat} \omega_n \sin(\omega_n t) \quad (4.23)$$

Using (4.23), the energies of C, L and R are given by:

$$E_C = \frac{1}{2} C V_{Bat}^2 [1 - \cos \omega_n t]^2 \quad (4.24)$$

$$E_L = \frac{1}{2} L (C V_{Bat} + \omega_n)^2 \sin^2 \omega_n t \quad (4.25)$$

$$E_R = \frac{1}{2} R (C V_{Bat} + \omega_n)^2 \left[t - \frac{1}{2\omega_n} \sin 2\omega_n t \right] \quad (4.26)$$

Considering the time period for energizing the coil is $t = \frac{2}{6\omega_n}$ then the energy at the end of Stage1 in both the coil and the capacitor is:

$$E_C + E_L = \frac{1}{2} CV_{Bat}^2 \quad (4.27)$$

For Stage2, while de-energizing L:

$$iR + L \frac{di}{dt} + V_C = 0 \quad (4.28)$$

$$i = C \frac{dV_C}{dt} \quad (4.29)$$

Solving for V_C :

$$V_C(s) = \frac{sV_C(0) + V_C'(0) + \frac{R}{L}V_C(0)}{s^2 + \frac{R}{L}s + \frac{1}{LC}} \quad (4.30)$$

Substituting $V_C(0)$ with $V_{C(Final)}$ of Stage1, which is equal to $\frac{1}{2}V_{Bat}$, gives:

$$V_C(t) = V_{Bat} \sin(\omega_n t + 30^\circ) \quad (4.31)$$

$$i(t) = \sqrt{\frac{C}{L}} V_{Bat} \cos(\omega_n t + 30^\circ) \quad (4.32)$$

Using (4.32), the energies of L, R and C are given by:

$$E_C = \frac{1}{2} CV_{Bat}^2 \sin^2(\omega_n t + 30^\circ) \quad (4.33)$$

$$E_L = \frac{1}{2} CV_{Bat}^2 \cos^2(\omega_n t + 30^\circ) \quad (4.34)$$

$$E_R = \frac{RC}{L} V_{Bat}^2 \left[\frac{1}{2} t + \frac{\sin(2\omega_n t + 30^\circ) - \sin(30^\circ)}{4\omega_n} \right] \approx 0 \quad (4.35)$$

Energy loss in the resistor is approximately 0 because $\frac{RC}{L} \approx 0$

Considering the time period for de-energizing the coil in stage 2 is also given by $t = \frac{2}{6\omega_n}$ then:

$$E_C = \frac{1}{2} CV_{Bat}^2 \quad (4.36)$$

From equation (4.36), it is clear that the total energy invested from the battery by the end of the pre-charge phase is equivalent to $\frac{1}{2} CV_{Bat}^2$ while the energy of L and R is approximately equal to zero. The complete mathematical analysis and derivations of the equations for both stage 1 and stage 2 are presented in Appendix A.

Details of the energy budget and strategies to reduce losses during the harvesting cycles under the LC to LC approach were studied previously by group of researchers from Georgia Tech Analog, Power & Energy IC research Lab. The figures shown next are from their published work in 2009 (Torres et al. 2009a).

Figure 4.19 illustrates the current and voltage waveforms of the pre-charge phase when C_{var} is at maximum capacitance. This phase includes energizing and de-energizing of the inductor. It can be seen that the voltage across the capacitor is charged to the battery voltage (Torres et al. 2009a).

Figure 4.20 shows the current and energy waveforms of the harvesting phase. As C_{var} changes from maximum to minimum capacitance, the harvested current increases to its maximum value before decreasing at the end of the harvesting phase while the harvested energy increases to E_{harv} (Torres et al. 2009a).

Figure 4.21 illustrates the voltage across C_{var} during the reset phase, when C_{var} returns from its minimum back to the maximum capacitance. In this phase, the voltage across the capacitor decreases to its minimum voltage, which can be used as the reference voltage to start the next cycle (Torres et al. 2009a).

This item has been removed due to 3rd Party Copyright. The unabridged version of the thesis can be viewed in the Lanchester Library Coventry University.

Figure 4.19: Inductor current and C_{var} voltage waveforms during the pre-charge phase (Torres et al. 2009a)

This item has been removed due to 3rd Party Copyright. The unabridged version of the thesis can be viewed in the Lanchester Library Coventry University.

Figure 4.20: Currents and energy waveforms during the harvesting phase (Torres et al. 2009a)

This item has been removed due to 3rd Party Copyright. The unabridged version of the thesis can be viewed in the Lanchester Library Coventry University.

Figure 4.21: Capacitor voltage waveform as C_{var} increases during the reset phase (Torres et al. 2009a)

In the L to LC approach, the circuit consists of a battery, five switches, an inductor and a variable capacitor. The circuit operation is a sequence of three steps. First, energy is transferred from the battery into the inductor by transferring energy through S1 and S3. Second, the energy stored in the inductor is transferred to the variable capacitor by connecting the variable capacitor to the inductor with S2 and S4. Third, the variable capacitor and the battery are connected together with S5 to transfer energy to the battery. The operation of the harvester is initiated by the timing control circuit while the variable capacitor is in contact with the capacitance sensing system (Torres et al. 2009b).

As in the previous approach, the energy study of the L to LC circuit is divided into two stages. The circuit of each stage is given in Figure 4.22.

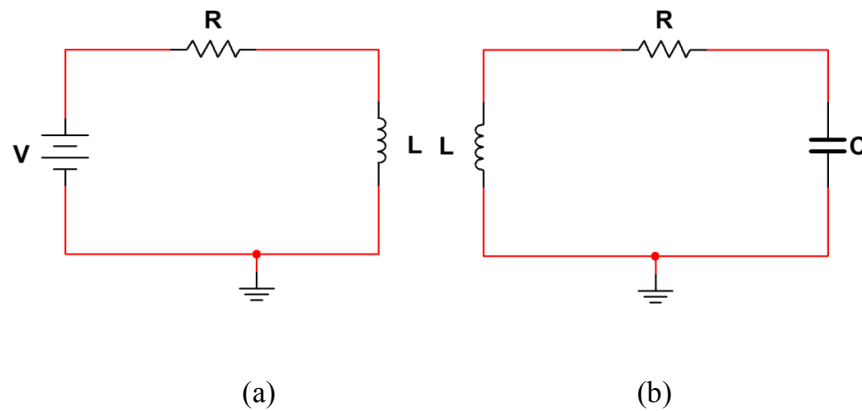


Figure 4.22: L to LC circuit (a) Stage1 (b) Stage 2

For Stage1, while energizing the coil L:

$$V_R = iR \quad (4.37)$$

$$V_L = V_{Bat} - V_R \quad (4.38)$$

$$i = \frac{V_{Bat}}{R} (1 - e^{-\frac{R}{L}t}) \quad (4.39)$$

Substituting 4.39 in 4.37 and 4.38:

$$V_R = V_{\text{Bat}}(1 - e^{-\frac{R}{L}t}) \quad (4.40)$$

$$V_L = V_{\text{Bat}}e^{-\frac{R}{L}t} \quad (4.41)$$

The energy of the coil during stage1 is:

$$E_L = \frac{1}{2}Li^2 \quad (4.42)$$

At the end of stage 1, energy E_L must be equivalent to the energy of C at C_{max} , which can be achieved when:

$$t = \frac{L}{R} \ln \frac{\sqrt{L}}{\sqrt{L} - R\sqrt{C_{\text{max}}}} \quad (4.43)$$

By approximation using the Taylor series, equation (4.43) becomes:

$$t = \sqrt{LC_{\text{max}}} \quad (4.44)$$

For Stage2:

$$i(0) = \frac{V_{\text{Bat}}}{R} \left[1 - \left(1 - \frac{R\sqrt{C}}{\sqrt{L}} \right) \right] = V_{\text{Bat}} \sqrt{\frac{C}{L}} \quad (4.45)$$

Since $V_C(0) = 0$ then:

$$V_C(s) = \frac{V_C'(0)}{s^2 + \frac{R}{L}s + \frac{1}{LC}} \quad (4.46)$$

$$V_C(t) = V_{\text{Bat}}e^{-\alpha t} \sin \omega_n t \quad (4.47)$$

where $\alpha = \frac{R}{2L}$ and $\omega = \frac{1}{\sqrt{LC}}$.

If $\alpha \ll 1$ then:

$$V_C(t) = V_{\text{Bat}} \sin \omega t \quad (4.48)$$

$$i(t) = C \frac{dV_C}{dt} = C\omega V_{\text{Bat}} \cos \omega t \quad (4.49)$$

Using equations (4.48) and (4.49):

$$E_C = \frac{1}{2} CV_{\text{Bat}}^2 \left[\frac{1}{2} - \frac{1}{2} \cos 2\omega t \right] \quad (4.50)$$

$$E_L = \frac{1}{2} CV_{\text{Bat}}^2 \cos^2 \omega t \quad (4.51)$$

If $t = \frac{2}{4\omega}$ then the total energy:

$$E_C + E_L = \frac{1}{2} CV_{\text{Bat}}^2 \quad (4.52)$$

From equation (4.52), it is clear that the energy invested from the battery by the end of the pre-charge phase is equivalent to the capacitor energy $\frac{1}{2} CV_{\text{Bat}}^2$ while the energy of L is equal to zero, which matches the energy harvested in the LC to LC approach. The complete mathematical analysis of the L to LC circuit is presented in Appendix (A). Figure 4.23 shows voltage, current and energy during the three phases of the energy harvesting cycle (Torres et al. 2009b).

This item has been removed due to 3rd Party Copyright. The unabridged version of the thesis can be viewed in the Lanchester Library Coventry University.

Figure 4.23: Voltage, current and energy during the three phases of energy harvesting (Torres et al. 2009b).

4.4.2.2 The charge pump circuit

A charge pump is a type of DC to DC converter that uses capacitors as storage component to create higher or lower voltages. The charge pump energy transfer circuit used for electrostatic energy harvesting uses a charge pump and a flyback circuit to transfer the harvested energy (Galayko et al. 2008). The block diagram of the harvester using the charge pump circuit and the implementation of the block diagram are shown in Figure 4.24 (a) and (b) (Yen & Lang 2005).

This item has been removed due to 3rd Party Copyright. The unabridged version of the thesis can be viewed in the Lanchester Library Coventry University.

(a)

This item has been removed due to 3rd Party Copyright. The unabridged version of the thesis can be viewed in the Lanchester Library Coventry University.

(b)

Figure 4.24: Charge pump with flyback circuit (a) block diagram and (b) circuit diagram

The role of the charge pump circuit is to transfer electrical charge from a large capacitor C_{res} to a smaller capacitor C_{store} by making use of variation in the variable capacitor C_{var} . The energy to pump the charge comes from mechanical vibration. During charge pumping, the

harvested energy is stored in C_{res} and C_{store} , which are connected together through the flyback circuit. Since C_{res} is much greater than C_{store} , V_{res} remains constant so that only V_{store} changes, which represents the increase in energy.

The flyback circuit operates as a Buck DC-DC converter to step down the voltage, transferring charges from C_{store} to C_{res} using the inductor as an energy buffer. The flyback operation is controlled by the switch represented by a MOSEFT transistor in Figure 4.24 (b).

Figure 4.25 (a) shows the evolution of V_{store} and the power generated during the charge pump operation. It can be seen from Figure 4.25 (a) that V_{store} becomes constant after a certain time period as the harvested power decreases to its minimum value. As the flyback circuit is used here to continue energy harvesting, it is necessary to decrease the voltage difference between C_{store} and C_{res} without losing the harvested energy. From Figure 4.25(b), it can be seen that power increases to a maximum value at some point. To continue energy harvesting, V_{store} should remain within the range of the threshold voltages of V_1 and V_2 . The theoretical values of V_1 and V_2 can be calculated by:

$$V_1 = V_{res} + 0.1(V_{store(max)} - V_{res}) \quad (4.53)$$

$$V_2 = V_{res} + 0.6(V_{store(max)} - V_{res}) \quad (4.54)$$

where $V_{store(max)}$ is the saturation voltage of the charge pump given by:

$$V_{store(max)} = V_{res} \frac{C_{max}}{C_{min}} \quad (4.55)$$

When V_{store} reaches V_2 , Sw should switch on, and the Buck DC-DC converter transfers the charge and energy from C_{store} to C_{res} . When V_{store} is reduced to V_1 , the switching device should turn off. The automatic generation of the switching events is made possible by using a control block that senses voltages V_{store} and V_{res} and detects if V_{store} is within the range between V_1 and V_2 (Dudka et al. 2009).

(a) (b)

Figure 4.25: Operation of the charge pump harvester: (a) V_{store} evolution; (b) Power evolution
(Dudka et al. 2009)

4.4.2.3 Comparison of energy transfer circuits

In general, inductive magnetic-based circuits have a number of advantages: the inductors used in the circuit are capable of producing high energy gains even when supplied by low power mechanical energy sources; the energy losses that occur during very short time periods can be ignored; and a single storage devices is enough for pre-charging and storing the harvested energy. The disadvantage of these circuits is the increased complexity of the control circuit to run the operation of the switching devices.

Comparing the two inductive energy transfer circuits reveals that energy losses are higher in the L to LC approach. Although the theoretical analysis proves that the invested energy for both circuits is the same, simulation and practical measurements show that the energy losses of the L to LC circuit are higher both because there are more switching devices in the circuit and because the initial energy investment is slightly higher due to resistive energy losses. The advantage of a charge pump circuit is the simplicity of its operation, with control of switching only requiring one switch. Its main disadvantages are that there is high energy loss if two capacitors with different initial energies are connected and the high voltages that can be generated are incompatible with the standard CMOS process.

4.4.3 Capacitance sensing systems

Since the operation cycle of the harvester mainly depends on the capacitance value, as demonstrated previously in Figure 4.17, the capacitance sensing system should be considered as an essential part of the harvesting system. Various methods are used to sense and monitor capacitance, such as mechanical, optical, magnetic and electric circuit (Webster 1999).

The mechanical method involves allowing brushes to sense the position of the conductive plates of the movable part of the capacitor. Some drawbacks with this method are that the brushes wear out after a certain time period and that they cannot operate in a rough environment. Moreover, the mechanical systems require high power to operate.

One optical method is to send light through the plate using a light-emitting diode and to detect the light coming out the other side with a photo diode. The drawbacks with this method are that dirt and dust can interfere with the light and that this method also consumes a lot of power as it has to be permanently operational.

The magnetic method can use a variable reluctance sensor or an inductive proximity switch. Both methods are based on magnetic or magnetic absorbing material. One drawback with this method is that other external magnetic sources can create interference with the sensor, which reduces the sensing accuracy. Additionally, the sensing devices used in this method are not cost effective.

Various circuits can be used in the electric method, such as capacitive bridge detector, capacitive pseudo bridge or an RC oscillator. These circuits depend on capacitance variation to measure the voltage, frequency or time period.

The following sections provide further details about the most suitable methods for monitoring capacitance for electrostatic energy harvesting.

4.4.3.1 Variable reluctance position sensor

Figure 4.26 shows a variable reluctance sensor. The sensor shown is a position sensor based on Faraday's law of electromagnetic induction. Basically, a variable-reluctance sensor consists of a toothed wheel made of a ferromagnetic material, attached to a rotating shaft, a coil and a permanent magnet. When the wheel moves closer to a permanent magnet, it induces EMF in the coil.

This item has been removed due to 3rd Party Copyright. The unabridged version of the thesis can be viewed in the Lanchester Library Coventry University.

Figure 4.26: Variable-reluctance sensor (Webster 1999)

The variable reluctance sensor is widely used in rotation sensing applications. It can be used to detect the capacitor plate's position and the presence of maximum and minimum capacitance. It is quite advantageous to use the sensor with the electrostatic harvester because it does not require any external power source to operate, and can be considered as an energy harvester itself. The variable reluctance technology available nowadays is quite mature and can be used directly without any modifications. However, it has low sensing accuracy; it forms quite a large assembly and has a complicated structure, which adds additional weight.

4.4.3.2 Inductive proximity switch

Inductive proximity switches can sense the distance to objects, specifically the proximity of metallic objects. The inductive sensor consists of an induction loop and sensing circuitry. The inductance of the loop changes in the presence of metal as it increases the current flowing in the loop. This change can be detected, opening and closing the proximity switch accordingly. Figure 4.27 shows the components of the switch. For an electrostatic energy harvester, it can be placed in a position close by and facing the capacitor plates. As the plates

are moved by the applied mechanical motion, the switch closes and opens. Normally, the inductive proximity switch is open until it detects the position of the plate, then it closes (Ab.com n.d.).

This item has been removed due to 3rd Party Copyright. The unabridged version of the thesis can be viewed in the Lanchester Library Coventry University.

Figure 4.27: Inductive proximity switch (Ab.com n.d.)

The inductive proximity switch has a high switching rate and can work in harsh environmental conditions. However, it also suffers from several disadvantages. First, it can only detect metallic objects and has a very limited operating range. Additionally, it requires an external power supply to operate. Finally, it has poor sensing accuracy and is not cost effective.

4.4.3.3 Bridge capacitive detector

The bridge capacitive detector, which is a basic AC symmetrical bridge, can be a very useful method to measure unknown capacitance values. The bridge circuit shown in Figure 4.28 is balanced by adjusting the capacitor values. The circuit shown is a somewhat simplified version of real-life practical AC bridge circuits (Pallas-Areny & Webster 2001). The practical circuit needs to have a variable resistor in series or parallel with the capacitor to balance out stray resistance in the unknown capacitance. In general, to balance the AC bridge, the impedance ratios of each branch must be equal:

$$\frac{Z_1}{Z_2} = \frac{Z_3}{Z_4} \quad (4.56)$$

In case of non-balanced impedance, the voltage at the output varies accordingly. In the electrostatic harvester, C_{var} capacitance varies as a result of the mechanical energy applied so

voltage values at the output are variable. The bridge capacitive detector has various advantages: high sensitivity, high accuracy and linear output. However, it consumes energy as it requires an oscillator to generate the AC signal and a rectifier to convert the output signal to DC.

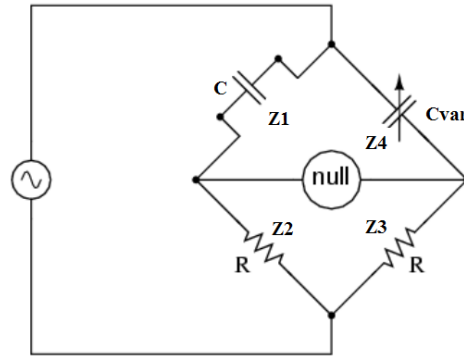


Figure 4.28: AC capacitive bridge detector

4.4.3.4 Oscillator circuit

The basic idea of using oscillators is to generate signals of variable frequencies that depend mainly on the capacitance variation of C_{var} . While many oscillator circuits are suitable for capacitance measurement, the most suitable one for an electrostatic harvester is the RC oscillator. The RC oscillator is a comparator circuit. The output signal of its oscillator has a frequency. Its frequency value depends on the values of the resistor and capacitor of the oscillator circuit R_x and C_x , as shown in Figure 4.29. The three resistors R_1 , R_2 and R_3 set the threshold voltages when the comparator output signal switches. The oscillation time period is set by the values of R_x and C_x . Since R_x is set to a fixed value, the only factor that changes the time period is C_x , which is the C_{var} of the harvester (Romanblack.com 2013).

$$f = \frac{1}{R_x C_{var}} \quad (4.57)$$

$$T = \frac{1}{f} = R_x C_{var} \quad (4.58)$$

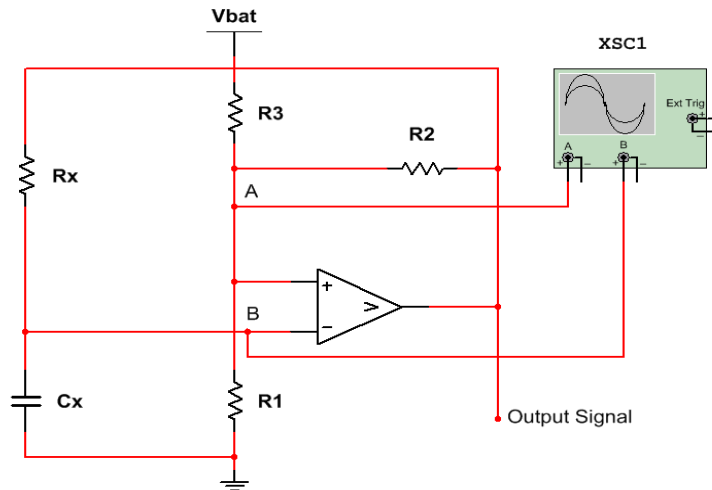


Figure 4.29: RC comparator oscillator for capacitance measurement

4.4.4 Controller mechanism

The controller is a critical part of the harvester system. In the electrostatic-based wind energy harvesting system, the controller is responsible for sending signals to control the operation of the switching devices. The controller has both input and output ports. It receives input from the capacitance sensing device and then, based on the capacitance value (maximum or minimum); it sends a control signal to operate one of the switching devices.

There are two possible ways to construct a controller for an electrostatic energy harvester: using off-the-shelf microcontrollers or a power electronic circuit. The power consumption of the microcontrollers is a very important factor when dealing with energy harvesting because it is essential for the microcontroller to consume as little power as possible while providing functions that reduce the overall system's power consumption. Currently, two extreme low power technologies are available: nanoWatt and nanoWatt XLP (Ivey 2009). There are two main factors affecting the power consumption of the two technologies: dynamic and static power. Dynamic power is the power consumed by the switching of digital devices while static power is the power consumed by disabling the main clock using leakage transistors. The primary requirement for a low power microcontroller is the power consumed while in sleep modes. There are three basic low power modes of operation: sleep, low voltage (LV) sleep and deep sleep. Figure 4.30 shows the current consumption of various modes of operation.

This item has been removed due to
 3rd Party copyright. The
 unabridged version of the thesis
 can be viewed in the Lanchester
 Library entry University.

Run Sleep V Deep
 Sccc Sccc Sccc

Figure 4.30: Microcontroller current consumption during various modes of operation
 (Microchip.com n.d.)

Sleep mode is used when the application requirement is to sleep most of the time, wake every second to process information and then go back to sleep. Low voltage sleep mode is most likely to be used when the requirement is to sleep most of the time, wakeup for few seconds to process data then go back to sleep. Deep sleep mode is to sleep most of the time but wakeup to process information once every hour, day, etc. Table 4.2 shows various types of extreme low power microcontrollers and typical current values during sleep mode and deep sleep mode. Note that all figures are typical values at minimum V_{dd} taken from the microcontrollers' datasheets. For an electrostatic-based wind energy harvester, the typical operation modes are run and sleep modes so the most suitable microcontroller device is PIC18LF45K50 as it has the lowest current consumption during the sleep mode.

Table 4.2: Extreme low power XLP microcontrollers (Microchip.com n.d.)

				Deep Sleep (nA)	μ A/MHz
PIC16F1823	2	8/14	20	-	34
PIC16F1509	12	20	25	-	30
PIC18LF45K50	32	28/44	10	-	110
PIC18LF47J13/J53	64-128	28/44	200	9	197
PIC24F16KL402	4-16	14/20/28	30	-	150
PIC24FJ64GB004	32-64	28/44	200	20	250
PIC24FJ128GA310	64-128	64/100	330	10	150

Another method for controlling the operation of the harvesters instead of using a microcontroller was proposed by Torres et al (2009). The first circuit they suggested was a prototype circuit that pre-charges, detects and synchronizes the operation of a variable voltage-constrained capacitor. Its circuit consists of a voltage detector that detects the difference between battery and capacitor voltage, and a slope detector. Both detectors send a voltage signal to the digital control circuit that sends signals to control the operation of the switching devices. Figure 4.31 shows the complete controller circuit of the harvester.

In 2010, Torres et al. (2010) presented a 1.5×1.5 mm $20.7\text{-}\mu\text{m}$ BiCMOS self-tuning electrostatic energy harvester integrated circuit (IC) shown in Figure 4.32 that adapts to changing battery voltages to produce usable power from vibrations across the battery voltage for the entire operating range. The controlling circuit consists of two comparators, a zero current sensor, a logic control circuit and gate drivers to control the switching devices. The pre-charger and its self-tuning reference and other control circuits consume sufficient power to operate yet dissipate low enough energy to produce a net energy gain. The system adjusts the energy invested to just what is required. This type of correcting loop is especially critical in reducing energy losses.

This item has been removed due to 3rd Party Copyright. The unabridged version of the thesis can be viewed in the Lanchester Library Coventry University.

Figure 4.31: Electrostatic energy harvester with state and slope detectors (Torres et al. 2009)

This item has been removed due to 3rd Party Copyright. The unabridged version of the thesis can be viewed in the Lanchester Library Coventry University.

Figure 4.32: Self tuning controller circuit (Torres et al. 2010)

4.5 SUMMARY

This chapter discussed the principles of converting wind kinetic energy to electrical energy using a wind turbine and an electrostatic converter along with a detailed description of each part of the harvesting system. The chapter was divided into two parts. The first part considered wind energy to mechanical energy conversion while the second part discussed mechanical power to electrical power conversion.

In the first part, wind energy, types of wind turbines, power in wind and energy capturing device efficiency were discussed. Since a wind energy harvester is a low power harvester, a micro wind turbine was preferred for the harvester in this study because it is a cost-effective device, can be propelled by a wind speeds as low as 2 m/sec, and is small and light. Moreover, an array of small turbines can be linked to increase power output to meet any requirement. Using the specification of the micro wind turbine, wind power can be calculated then multiplied by the efficiency of the device to find the total power passed on to the electrostatic converter.

The second part presented the electrostatic converter along with a detailed description of the variable capacitor, energy transfer strategies, capacitance sensing devices and the controlling

mechanism. Since change in capacitance depends on the capacitor structure by changing the area of the plates or the gap between them, two basic modes of operation were studied: constant voltage mode and constant charge mode. In the constant voltage system, keeping the voltage across the capacitor constant helps to restrict the voltage within reasonable levels which is a key advantage of this approach. Moreover, the capacitor uses a single voltage source both for pre-charging and storing the harvested energy. However, this mode has the disadvantage of requiring a complicated controlling circuit to control the switching devices. In contrast, the constant charge approach does not require such complicated power electronics circuits or an additional storage device. However, it has the disadvantage that the maximum voltage it produces exceeds the breakdown limits of most modern CMOS technologies by a considerable margin. Such voltages can only be handled by costly specialised technologies, such as silicon-on-insulator CMOS processes. However, their increased costs limit the extent that the market will adopt them. This indicates that the constant voltage approach is the preferable technology for a wind energy harvester.

Two inductive energy transfer circuits operating under a constant voltage system were studied. The LC to LC circuit was found to be preferred for an electrostatic converter because of its high energy transfer efficiency, its low energy losses during pre-charge, and the lower number of switching devices compared to the L to LC circuit. Many capacitance sensing circuits were presented; with the RC oscillator being found the most suitable as it is a simple circuit, very accurate in measuring capacitance values and consumes very little power. Finally, the discussion of the controlling mechanism found that the best controller is the XLP microcontroller as it can be easily programmed and reconfigured to fit any requirement. It also consumes little power in both run and sleep mode. Finally, it has comparators that can be used to build the RC oscillator, meaning that off-the-shelf microcontrollers can be used as controller and capacitance monitoring system at the same time.

CHAPTER 5

ELECTROSTATIC-BASED WIND ENERGY HARVESTER

5.1 INTRODUCTION

As explained in Chapter 4, the wind harvester consists of two sub-systems: wind turbine and electrostatic converter. The principles of operation and the theoretical background of each part were described. This chapter presents a novel electrostatic-based wind energy harvester. The assumption behind the proposed design is that the micro wind turbine is used as a capturing device, while the variable capacitor used is a multi-pole capacitor with variable area subjected to change according to the applied rotational motion. This system is used to harvest energy to wirelessly transmit information about wind speed. The new harvester consists of five blocks: wind energy - capturing device, variable capacitor, energy transfer circuit, controller and RF transmitter.

5.2 PROPOSED HARVESTER SYSTEM

Figure 5.1 shows the block diagram of the proposed electrostatic-based wind energy harvester.

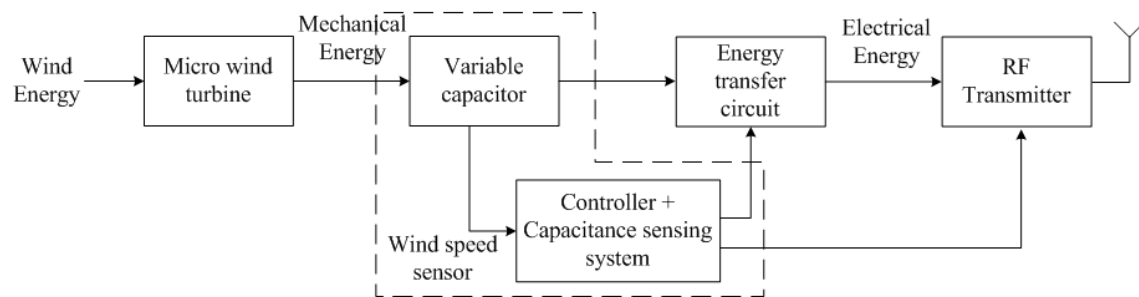


Figure 5.1: Block diagram of the proposed electrostatic-based wind energy harvester

The first stage of power conversion is from wind energy to mechanical power, using a micro wind turbine. The second stage is the conversion of rotational mechanical power to electrical power using the electrostatic converter, which consists of a variable capacitor, energy transfer circuit and controller. The energy transfer circuit operates under a voltage-constrained mode as described earlier in Chapter 4. It has three phases to complete a harvesting cycle: pre-charge, harvest and reset (Torres et al. 2009a). The controller monitors the capacitance in order to generate the appropriate timing signals necessary to control the energy harvesting cycle. It also sends information about wind speed to the RF transmitter, which then wirelessly transmits data about detected wind speed. Details of each block are explained in the following sections. Currently, most available wind energy harvesting systems are built from micro wind turbines with electromagnetic generators. The cost of such systems could be reduced by the direct generation of DC power using electrostatic converters. Although the power densities of electrostatic harvesting systems are less than those of electromagnetic generators, an electrostatic harvester could lead to a system with similar power density to an electromagnetic generator-transformer-rectifier combination, while the fewer components would reduce system cost and increase overall efficiency. Figure 5.2 shows schematically a two wind turbine systems: with electromagnetic generator and with electrostatic converter.

This item has been removed due to 3rd Party Copyright. The unabridged version of the thesis can be viewed in the Lanchester Library Coventry University.

Figure 5.2: Wind energy generation system concepts: (a) Wind turbine with electromagnetic generator (b) Wind turbine with electrostatic converter (Abdulmunam et al. 2012)

5.3 MICRO WIND TURBINE

The first block in the wind harvesting system is the micro wind turbine that captures and converts wind energy into mechanical energy in the form of rotational motion. Recently, the development of micro wind turbines has gained attention with a great deal of research being conducted to improve their performance in harvesting energy at low wind speeds. In this research, the micro wind turbine chosen is a twisted fan-type blade configuration. The twisted blades help in capturing more efficient torque in different wind conditions while the fan-type configuration has the functional advantage of increased power efficiency (Leung et al. 2010). The main advantage of this turbine is its cost effectiveness as it can be mass produced by injection moulding. Moreover, multiple turbines can be connected together to increase the amount of captured energy from the wind to meet any requirement (Leung et al. 2010).

Figure 5.3 illustrates the AutoCAD model of the micro wind turbine linked via a gear box to the shaft of the variable capacitor. The gear box is a speed increaser to increase number of harvesting cycles for various wind speeds. Investigations on the performance of a specially designed micro wind turbine for urban environments by Leung et. al (2010) showed that the maximal angular velocity of the wind turbine is between 100 - 750 rpm for wind speeds between 2 m/sec – 10 m/sec. Without any loading, the micro wind turbine can rotate freely so that angular velocity increases linearly with increasing wind speed, as shown in Figure 5.4.

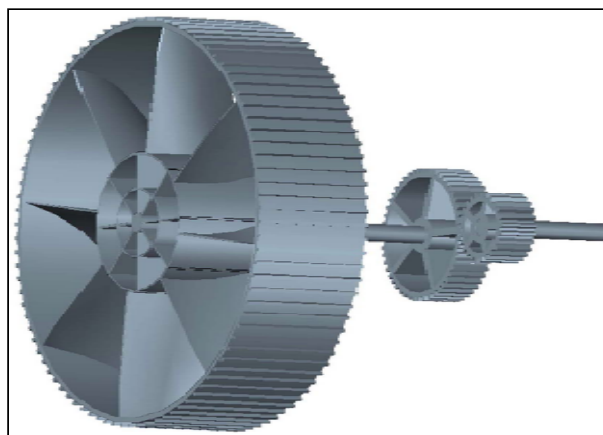


Figure 5.3: AutoCAD model of the micro wind turbine linked to a gear box

Figure 5.4: Maximal angular velocity versus wind speed (Leung et al. 2010)

The mechanical output power can be calculated by multiplying the angular velocity of the turbine by the torque captured by the turbine. Figure 5.5 shows the relationship between mechanical output power and angular velocity of the wind turbine at a wind speed of 7 m/sec. The plot indicates that the maximum mechanical power obtained is around 1.1 Watts at the optimal angular velocity. The curve also shows that mechanical power first increases as angular velocity increases then reaches its maximum at the optimal angular velocity before decreasing again.

Figure 5.6 shows the relationship between the power coefficient C_p and the tip speed ratio of the micro wind turbine. As indicated by the plot, the tip speed ratio of the turbine is between 0 and 1, which matches with the traditional small-size multi-bladed wind turbines that normally operate at a tip speed ratio between 0 to 2. The maximum power coefficient of the turbine indicates that the 12.5 % of kinetic wind energy is transformed into mechanical energy for various turbines with 3–12 blades. There is no significant improvement in maximum output power with eight or more blades with the best possible tip speed ratio being 0.5 to 0.6 for an 8 to 12-bladed turbine.

This item has been removed due to 3rd Party Copyright. The unabridged version of the thesis can be viewed in the Lanchester Library Coventry University.

Figure 5.5: Mechanical power versus angular velocity at wind speed of 7 m/sec
(Leung et al. 2010)

This item has been removed due to 3rd Party Copyright. The unabridged version of the thesis can be viewed in the Lanchester Library Coventry University.

Figure 5.6: Power coefficient of micro wind turbine with different number of blades
(Leung et al. 2010)

In order to analyze the mechanical system, the variable capacitor moment of inertia was calculated using mathematical analysis and simulation. To calculate the inertia analytically, the following steps were required. First, measurement of the dimensions of all the rotating objects, such as the head of the inner rod, the rest of the inner rod, the rings between the plates and the capacitor plates. Second, the moments of inertia of all the objects related to the axis of rotation passing through the centre of mass and perpendicular to all plates were determined using equation (5.1):

$$I_i = \int_v \rho d^2(x,y,z) d(x,y,z) \quad (5.1)$$

where v is the volume of the rotating object, ρ is the density of the material at any given point (x,y,z) and $d(x,y,z)$ is the distance from any given point (x,y,z) to the axis of rotation. Third, the total inertia of the variable capacitor using the principle of superposition was calculated (Abdulmunam et al. 2013). In the simulation approach, AutoCAD function MASSPROP (Docs.autodesk.com 2010) was used to determine the moment of inertia of the object relative to the axis of rotation parallel to the axis at x , y and z passing through the centre of mass (Abdulmunam et al. 2013). Applying Newton's second law for the micro wind turbine and the capacitor shafts, the following equation can be written (Krishnan & Srivatsa 2007):

$$T_T - T_L = I_T \frac{d\omega_T}{dt} \quad (5.2)$$

$$T_H - T_C = I_C \frac{d\omega_C}{dt} \quad (5.3)$$

where T_T is the turbine torque applied by the wind, T_L is the transmitted torque on the low speed gear applied by the high speed gear, T_H is the transmitted torque on the high speed gear applied by the low speed gear, and T_C is the resistance torque on the rotor of the capacitor applied by the stator. I_T and ω_T are the moment of inertia and the angular velocity of the micro wind turbine, respectively, while I_C and ω_C are the moment of inertia and the angular velocity of the variable capacitor, respectively. Figure 5.7 presents the torques applied in the system. Assuming the gear box is ideal, with no backlashes or losses, and assuming that shafts are rigid, where n_1/n_2 is the gear box ratio, the following can be written (Krishnan & Srivatsa 2007):

$$\frac{T_L}{T_H} = \frac{\omega_C}{\omega_T} = \frac{n_1}{n_2} \quad (5.4)$$

Figure 5.7: Torques applied to the electrostatic-based wind energy harvester system
(Krishnan & Srivatsa 2007)

From (5.2), (5.3) and (5.4), the net torque T_{net} can be derived as follows:

$$T_{\text{net}} = T_T \left(\frac{n_2}{n_1} \right) - T_C = I_{\text{net}} \frac{d\omega_C}{dt} \quad (5.5)$$

where:

$$I_{\text{net}} = I_T \left(\frac{n_2}{n_1} \right)^2 + I_C \quad (5.6)$$

Equation (5.5) indicates that net torque depends on the moment of inertia of both the turbine and the variable capacitor, the angular acceleration of the turbine and the gearbox ratio. Since I_{net} is positive and the angular acceleration $d\omega_C/dt$ must be positive for the capacitor to rotate, then the following can be written:

$$T_T \left(\frac{n_2}{n_1} \right) - T_C > 0 \text{ or } T_T > \left(\frac{n_1}{n_2} \right) T_C \quad (5.7)$$

Thus, in order to rotate the rotor of the capacitor, it is necessary for torque T_T to be greater than $\left(\frac{n_1}{n_2} \right) T_C$ (Abdulmunam et al. 2007). It is possible to directly drive the capacitor without the gear box. However, the gear box is beneficial as it is required to increase number of harvesting cycles to harvest more energy within certain time period.

5.4 ELECTROSTATIC CONVERTER FOR WIND ENERGY HARVESTING

The electrostatic converter consists of three parts, a multi-pole variable capacitor, an inductive energy transfer circuit and a controller.

5.4.1 Multi-pole variable capacitor

The multi-pole capacitor is a variable capacitor made of two parallel plates: rotor and stator. The stator is the stationary part of the capacitor while the rotor is the rotating part that rotates according to the applied mechanical motion. Each rotor and stator is divided into a number of poles. The number determines the amount of capacitance variation within a single rotation. The multi-pole capacitor can be constructed from a single or multiple sets of rotors and stators. This capacitor was chosen for the proposed wind harvesting system for several reasons. It is compact, can be easily coupled with the micro turbine system, has a simple structure that is simple to fabricate, and has a capacitance that can be modified geometrically, which can allow the harvester to collect more energy per cycle.

The main requirement in a multi-pole variable capacitor is to have at least two plates in each comb of the capacitor, where the number of neighbouring sheets of positive and negative charge is three, as shown in Figure 5.8. In general, when there are N sets of stator – rotor plates, the number of parallel capacitors is $(2N_{SR} - 1)$ (Serway, Beichner & Jewett 1996). It can be observed from Figure 5.7 that $N_{SR} = 2$, which means that there are three parallel capacitors, as represented by $C_1//C_2//C_3$ so that the total capacitance is determined by (Serway, Beichner & Jewett 1996) :

$$C_{var}(N_{SR}, A, d) = (2N_{SR} - 1)\epsilon_o\epsilon_r \frac{A_{eff}(\theta)}{d} \quad (5.8)$$

where N_{SR} is the number of stator rotor sets, A_{eff} is the effective area of the plates, θ is the angle of rotation, d is the distance between the parallel plates and $\epsilon_o\epsilon_r$ are the absolute and relative permittivity of the dielectric material, respectively.

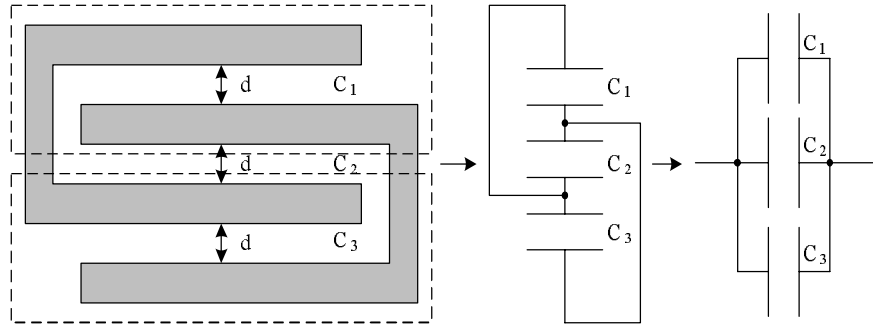


Figure 5.8: Multi-pole capacitor plates equivalent to three capacitors in parallel C_1 , C_2 & C_3

There are several structures to realize a multi-pole capacitor, as illustrated in Figure 5.9. Although all the capacitors shown have the same maximum and minimum capacitances, the capacitance variations per cycle are different, as shown in Figures 5.9 and 5.10. It can be noticed from Figures 5.10 and 5.11 that the number of times capacitance changes from maximum to minimum capacitance within 360° increases as the number of poles increases. Thus, increasing the number of poles is a very important factor in increasing the amount of harvested energy per cycle. The results of the energy study per cycle will be discussed in Chapter 6.

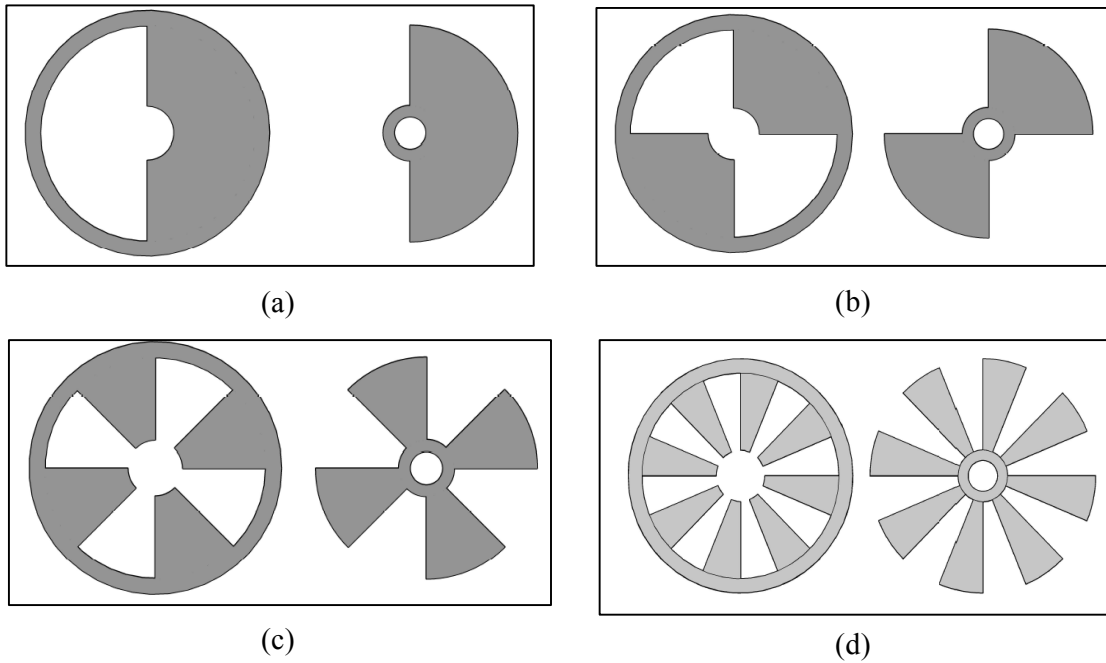
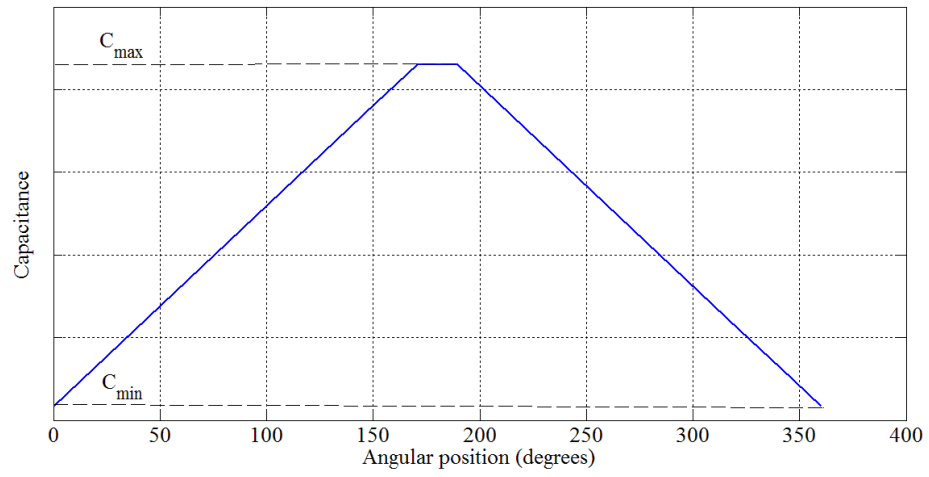
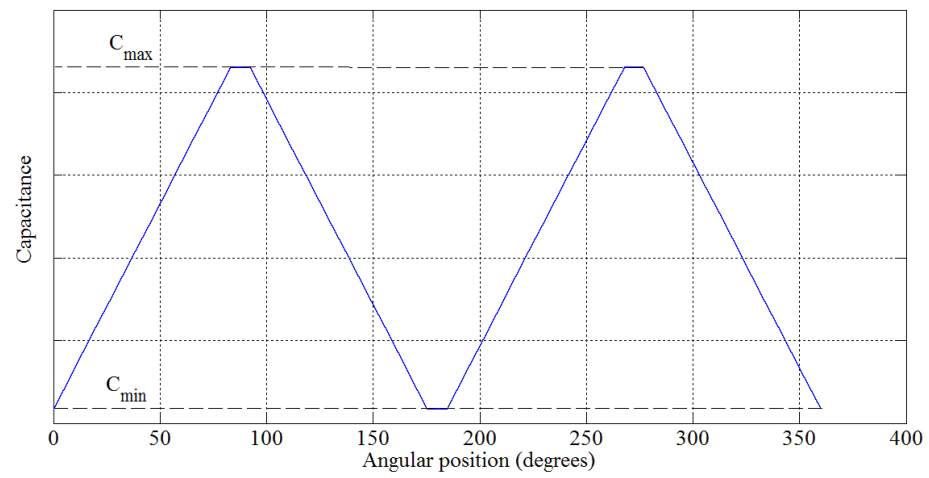


Figure 5.9: Multi-pole capacitors: (a) one-pole, (b) two-poles, (c) four-poles and (d) eight-poles

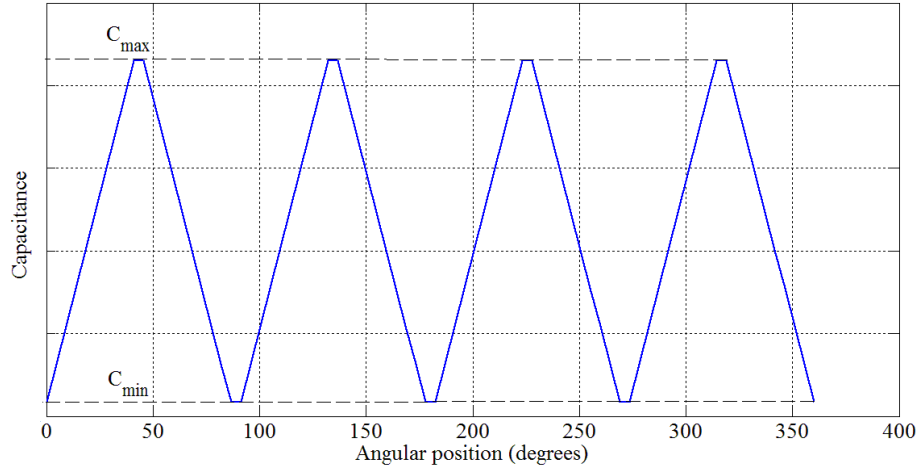


(a)

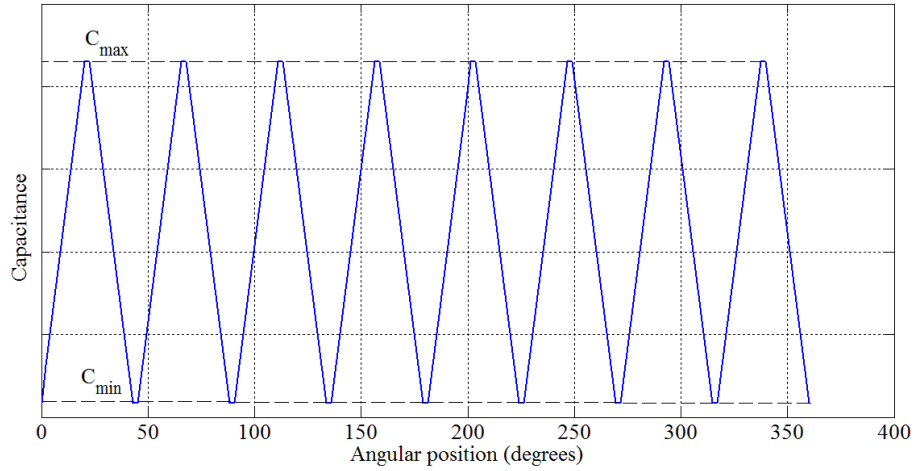


(b)

Figure 5.10: Capacitance variation: (a) one-pole, (b) two-poles



(a)



(b)

Figure 5.11: Capacitance variation: (a) four-poles and (b) eight-poles

5.4.2 Capacitance optimisation

As discussed in Chapter 4, the harvested energy can be maximised by increasing the capacitance variation ΔC_{var} . To increase the difference between C_{\max} and C_{\min} , an optimised capacitor design is required. It follows from equation (5.8) that capacitance can be optimised

by adjusting the number of stator – rotor sets N_{SR} , the effective area of the capacitor plates A_{eff} , the number of poles in each plate N_{Pole} and the distance between the plates d . The results of the energy optimisation study will be addressed in Chapter 6. The optimised capacitor design is given in Figure 5.12. Both the stator and the rotor are divided into eight sets of sector-shaped plates, with each set consisting of an array of parallel plates separated by air as the dielectric material. Using an array of capacitor plates increases the effective area and thus capacitance value increases. Since there are eight sector-shaped plates, this capacitor is called an eight-pole capacitor.

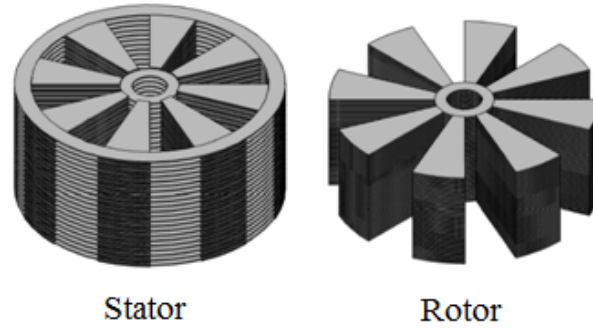


Figure 5.12: AutoCAD model of the eight-pole variable capacitor

The capacitance variation of this capacitor depends on modifying the effective area of the plates as a function of the angle of rotation. The effective area is a critical parameter for computing the minimum and maximum capacitance. The maximum and minimum effective areas of the capacitor shown in Figure 5.12 are determined by:

$$A_{eff\ max} = N_{Pole} \times \frac{1}{2} \theta (r_3^2 - r_1^2) \quad (5.9)$$

$$A_{eff\ min} = N_{Pole} \times \frac{1}{2} \theta (r_3^2 - r_2^2) \quad (5.10)$$

where r_1 , r_2 and r_3 are the radii of the circles, as shown in Figure 5.13.

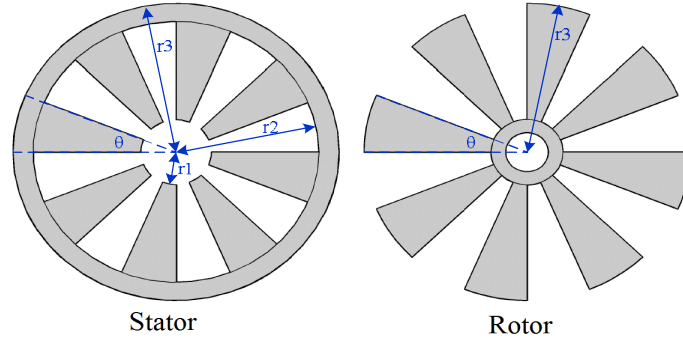


Figure 5.13: Stator and rotor of the eight-pole variable capacitor

Using equations 5.8, 5.9 and 5.10, the theoretical value of the capacitance variation with angular position was calculated for the eight-pole capacitor when $r_1 = 10$ mm, $r_2 = 40$ mm, $r_3 = 45$ mm, $N_{\text{Pole}} = 8$, $N_{\text{SR}} = 50$ and $d = 1$ mm. Figure 5.14 presents the result of this calculation, indicates that the theoretical capacitance varies from a maximum of 2.56 nF to a minimum of 0.61 nF. These theoretical capacitance values can then be processed using a MATLAB curve fitting tool to obtain a mathematical expression of capacitance in terms of angular position. This indicated that of the best fit is a Fourier polynomial of degree 3. The resulting capacitance is expressed by:

$$C_{\text{var}} = a_0 + \sum_{i=1}^3 a_i \cos(i\omega t) + b_i \sin(i\omega t) \quad (5.11)$$

Where $\omega = 0.1396$ rad/sec and a_i , b_i values are listed in Table 5.1.

Table 5.1: Parameters of capacitance variation with angular position

i	0	1		3
a_i	-	-	-	1.015×10^{-10}
b_i		-	-	-2.605×10^{-25}

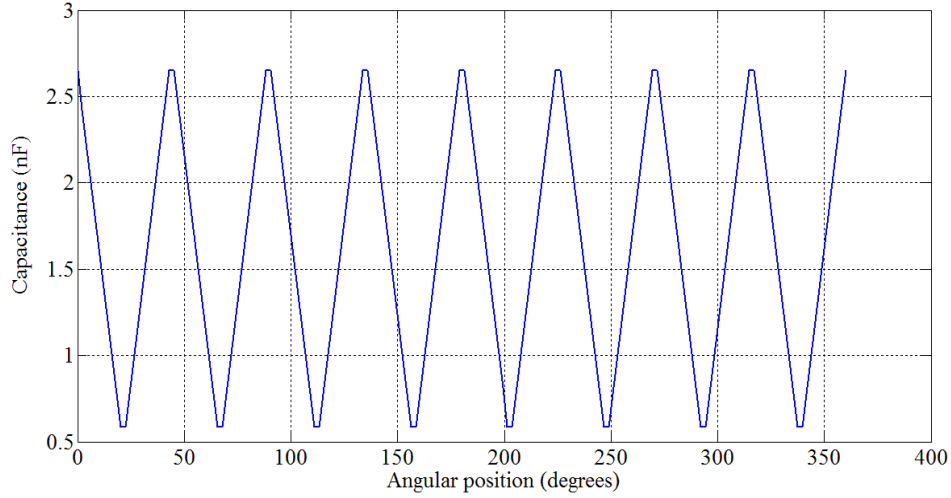


Figure 5.14: Theoretical capacitance variations with angular position

5.4.3 Multi-pole capacitor array (MPCA)

Simulation testing of the optimised eight pole capacitor proved that, although wind energy in the environment is boundless, only small portions of energy can be drawn at a time, which means the actual harvested power is low. This happens due to the limitation on the maximum number of poles per capacitor, which restricts capacitance variation in each single rotation. To improve the efficiency of wind energy harvesting and the capability of the capacitor to draw more energy packets, a discrete multi-pole variable capacitor can be divided into an array of small capacitors. Figure 5.15 (a) and (b) illustrates two types of multi-pole capacitor: discrete and array. An MPCA has various advantages over a discrete multi-pole capacitor: it can operate at lower wind speeds, harvest more energy per revolution (because the small circumference of individual capacitors means less time elapses to complete one harvesting cycle); it can harvest energy even if one or more capacitors are not working, is suitable for integrated circuit fabrication and uses space more efficiently.

Figure 5.16 demonstrates the theoretical variation of an MPCA with $N_C = 4$, where N_C is the number of multi-pole capacitors in the array. The idea is to utilise space in smaller capacitors rather than one large capacitor. The overall capacitance of the four small capacitors in Figure 5.15 (b) is the same as the capacitance of the single capacitor shown in Figure 5.15 (a).

Simulations were conducted using Matlab/ Simulink to determine the amount of electrical energy that can be harvested using the multi-pole capacitor and capacitor array at various wind speeds. The results of this simulation are given in Chapter 6.

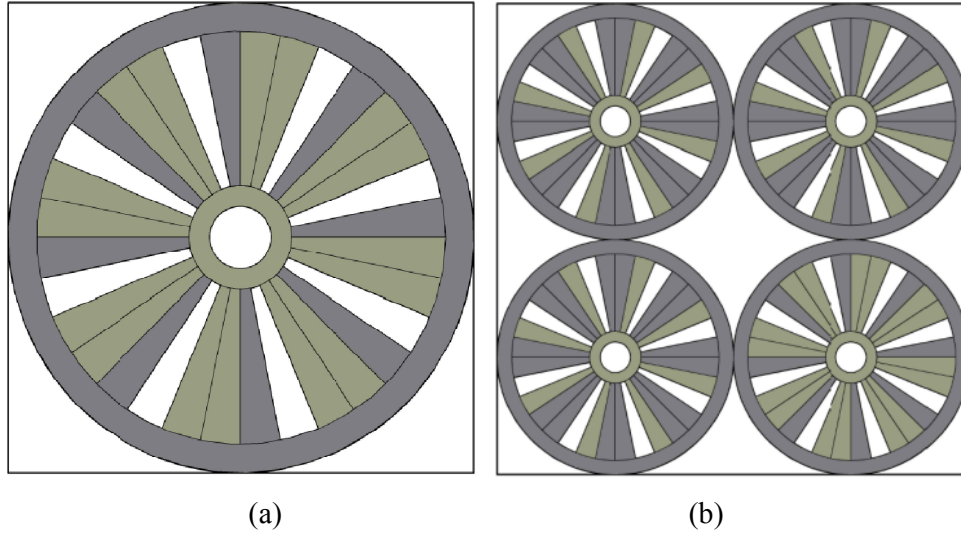


Figure 5.15: Types of multi-pole capacitor: (a) single variable capacitor; (b) MPCA

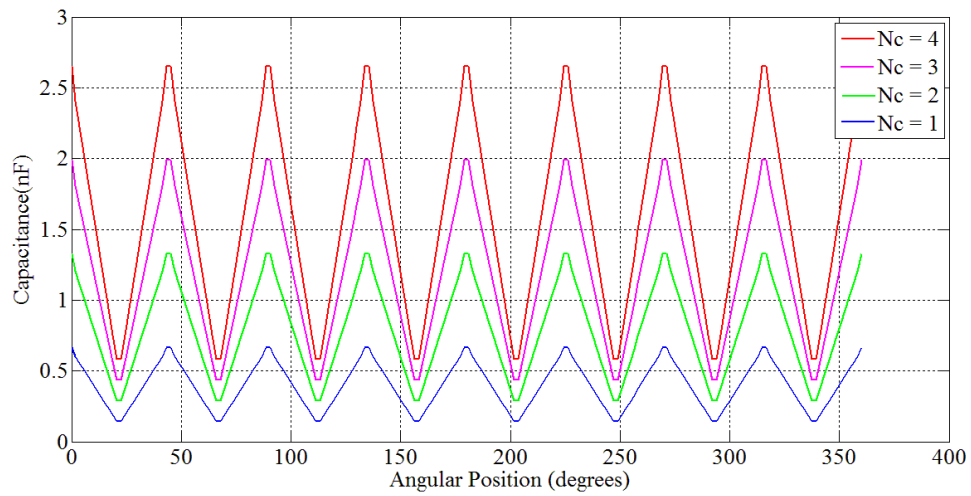


Figure 5.16: Capacitance variations with angular position of the MPCA

5.4.4 LC to LC inductive energy transfer circuit

As described in Chapter 4, the LC to LC energy transfer circuit is a simple circuit with low energy losses and high energy harvesting efficiency (Torres et al. 2009a). Furthermore, it uses the same storage device for pre-charging and storing of the harvested energy. The LC to LC circuit shown in Figure 5.17 operates in a voltage-constrained mode with three phases to complete the energy harvesting cycle, as shown in Figure 4.9 in Chapter 4.

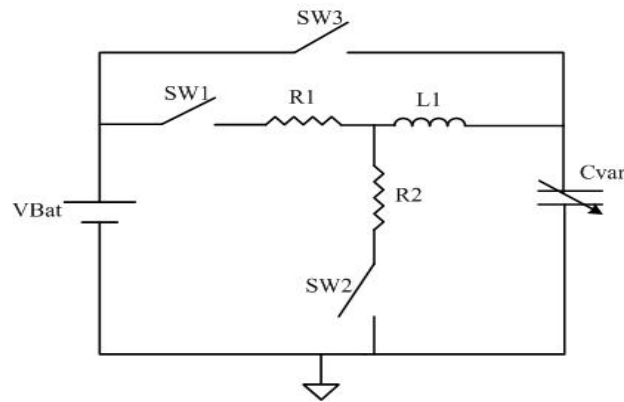


Figure 5.17: LC to LC inductive energy transfer circuit

In theory, this method of energy transfer is a lossless transaction (Torres et al. 2009a). The energy is transferred from the battery to the inductor and C_{var} through sw1 and sw2. Once the voltage reaches its maximum and C_{var} changes from C_{max} to C_{min} , the harvesting phase starts with current passing from C_{var} back to the battery through sw3. The transaction is lossless because the inductor is energized from the battery through sw1 so, while energizing the inductor, the current rises and voltage remains very low throughout the entire energizing phase. In the same way, de-energizing the inductor to the variable capacitor keeps the voltage across sw2 very low. During the harvesting phase, both sw1 and sw2 shut off, which means there are no losses during harvesting phase. The main target of the pre-charge phase is to deliver no more or less than the initial invested energy, as described in Chapter 4. Thus, reducing losses during this phase is very important. Although the pre-charge circuit is not completely free of energy losses in real life applications due to losses from the switching devices and the parasitic effect, these losses are all limited to a small fraction of the entire harvesting process so the total energy loss is rather low (Torres et al. 2009a).

During charging of L and C_{var} , the energy invested at the beginning is given by:

$$E_{LC} = C_{\text{var(max)}} V_{\text{Bat}}^2 [1 - \cos(\omega_{LC} t)] \quad (5.12)$$

where ω_{LC} is the resonant frequency. Thus, E_{LC} reaches E_{inv} when $[1 - \cos(\omega_{LC} t)]$ is equal to 0.5, which is achieved when:

$$t = \frac{2\pi}{6\omega_{LC}} \quad (5.13)$$

This means that sw1 should allow the battery to energize L and C until C_{var} charges to 0.5 V_{Bat} . After that, sw2 should allow L to finish charging C_{var} to V_{Bat} . The total pre-charge time (energizing and de-energizing) is thus double the time given in (5.13).

In the harvesting phase, C_{var} decreases from maximum to minimum capacitance due to the rotational motion. This drives the harvesting current and energy to the battery. The simplest way to transfer the charge back to the battery is to use a MOSFET switch because, despite the voltage drop across the transistor, it more closely resembles an ideal switch, except that it requires a control circuit to control it (Torres et al. 2009b). The harvested charge, current, energy and charge are given, respectively, by:

$$I_{\text{harv}} = \frac{Q_{\text{harv}}}{t_{\text{harv}}} = \frac{\Delta C_{\text{var}} V_{\text{Bat}}}{t_{\text{harv}}} \quad (5.14)$$

$$E_{\text{harv}} = \int V_{\text{Bat}} I_{\text{harv}}(t) dt = \Delta C_{\text{var}} V_{\text{Bat}}^2 \quad (5.15)$$

$$Q_{\text{harv}} = \Delta C_{\text{var}} V_{\text{Bat}} \quad (5.16)$$

The reset phase is started by dis-engaging all three switches, while the capacitor is left open-circuited. When it increases from minimum to maximum in charge-constrained mode, it forces V_C to decrease, as given by (Torres et al. 2009b):

$$V_{C(\min)} = \left(\frac{C_{\text{var}(\min)}}{C_{\text{var}(\max)}} \right) V_{\text{Bat}} \quad (5.17)$$

In this case, the capacitor retains recovered energy that does not return to the battery so this energy is lost. However, this can actually increase the overall energy gain of the harvesting system because changes in V_C are a good indicator of the state of C_{var} so it can detect when C reaches its maximum capacitance. This simplifies the operation and reduces the complexity of the control circuit and capacitance sensing system.

5.4.5 Harvester controller

The controller is the main part of the harvester system. In the electrostatic-based wind energy harvesting system, the controller is responsible for several functions. First, it monitors maximum and minimum capacitance. Second, it sends control signals to operate the switching devices. Third, it sends information about harvesting time and wind speed to the RF transmitter. Generally, extreme low power XLP microcontrollers are recommended for energy harvesting applications as they are efficient with low energy losses (Ivey 2009).

Since capacitance value is an important factor in starting the pre-charge, harvest and reset phases, the harvester controller is needed to measure the capacitance. The main method for measuring capacitance is to use the internal comparator of the microcontrollers. The comparator can be used to build the RC oscillator, as described in Chapter 4. The main reasons for using the microcontroller's comparator for the oscillator circuit are that it has a better comparator than many dedicated comparator ICs and that its output has good push-pull low resistance FETs. As explained in Chapter 4, the frequency of the output signal value depends on the values of the resistor and capacitor of the oscillator circuit. As C_{var} varies, the controller measures the time period very precisely. Then a simple calculation is performed to scale the time period to a specific capacitance value. If the controller detects the maximum capacitances range, it sends a signal to start the pre-charge and harvest phase. When the range of minimum capacitances is detected, the harvest phase ends and the rest phase starts. During the harvesting cycle, the microcontroller produces three control signals, S1, S2 and S3, as given in Figure 5.18 which control the operation of the three switching devices.

During the pre-charge phase, a control signal S1 goes high in order to close sw1 for a short time period, calculated using equation (5.12). After a small delay, control signal S2 goes high to close sw2 in order to continue charging C_{var} . The delay is included between every switching transition to prevent short-circuit conditions and high peaking voltages. Control signal S3 then goes high to start the harvesting of energy by closing sw3. Figure 5.19 demonstrates the operation cycle of the harvester with three control signals.

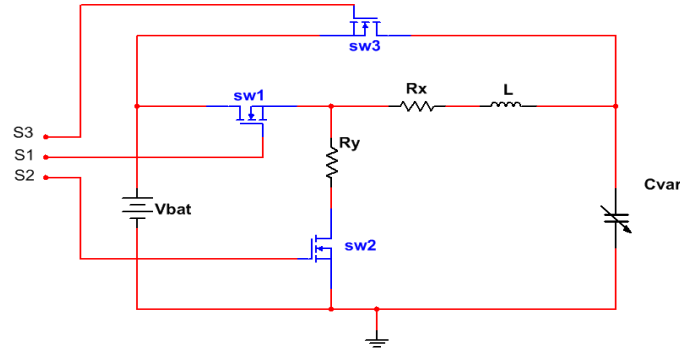


Figure 5.18: LC to LC energy transfer circuit with S1, S2 and S3 control signals

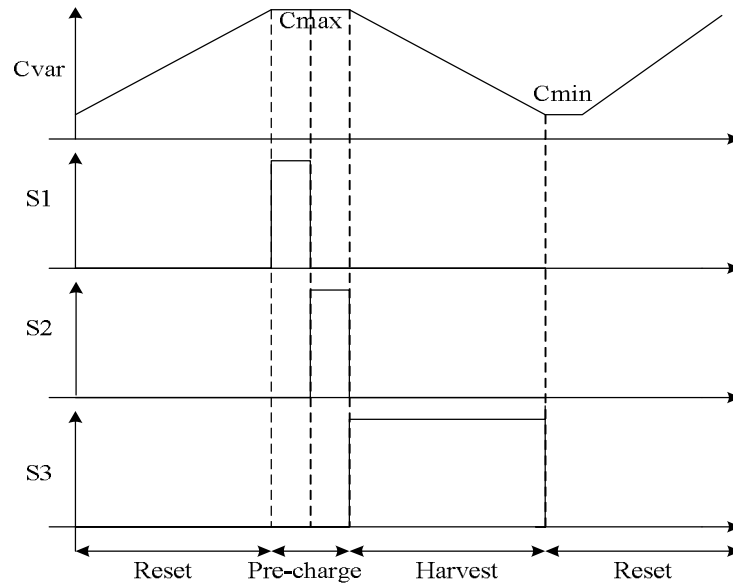


Figure 5.19: Operation cycle of the harvester with S1, S2 and S3 control signals

The final role of the controller is to operate and send information to the RF transmitter. When the controller detects maximum capacitance, it sends a signal to the transmitter before

starting the pre-charge phase. Once minimum capacitance is detected, it sends another signal to the transmitter before starting the reset phase. As long as wind is available, the transmitter keeps sending trigger signals to the receiver side, which will then calculate the time taken between the two trigger signals and calculate the detected wind speed.

The flow chart in Figure 5.20 summarises the operation of the controller used in the electrostatic-based wind energy harvesting system. T_{sleep} is the time period of the controller sleep mode; T_{energize} is the time required to charge the inductor L ; $T_{\text{D-energize}}$ is the time required to discharge the inductor L to C_{var} .

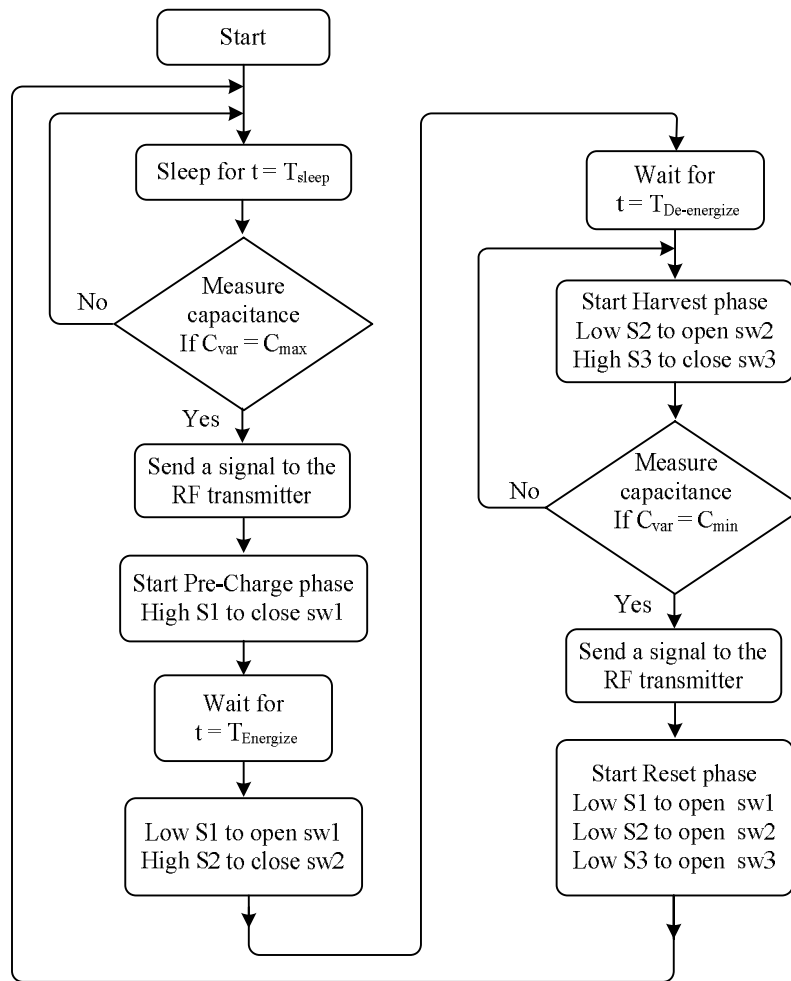


Figure 5.20: Flow chart of the controller operation

5.5 RF TRANSMITTER

Self-powered autonomous sensors are needed in order to site wind speed sensors in remote areas or hazardous environments that may not be easily accessible for replacing or recharging the devices' batteries. Otherwise, such sensors will fail to operate once the batteries' energy is exhausted. Electrostatic-based wind energy harvesters provide a suitable way to power miniaturized autonomous wind speed sensor, weather, moisture, humidity, temperature, pollution, etc...

Significant developments by microcontrollers and RF circuit manufactures have helped in reducing the power consumption of both working and the standby modes for these devices. A wireless sensor node generally consists of four blocks: sensor, microcontroller, radio transmitter and power source. The power consumption of the sensor node is typically 1 μ W - 50 mW, as shown in Figure 5.21. The total amount of power needed to perform a typical measurement and data transmission is 5 μ W – 1 mW (50 – 500 μ J) depending on the type of sensor and RF device. Unfortunately, electrostatic energy harvesters cannot supply the sensor with power continuously. However, the harvested energy can be stored in a battery before being used to perform measurement and transmission functions as soon as enough energy is available. The system then returns to sleep mode to wait for a new cycle (Boisseau et al. 2012).

This item has been removed due to 3rd Party Copyright. The unabridged version of the thesis can be viewed in the Lanchester Library Coventry University.

(a)

(b)

Figure 5.21: Wireless sensor node (a) Blocks and (b) Power consumption
(Boisseau et al. 2012)

This research demonstrates a useful application using an RF transmitter that transmits information about wind speed to a base station by modulating radio waves to carry data. The transmitter device is connected to the microcontroller, which provides the data to be transmitted.

The performance of the RF transmitter depends on many factors including transmission power. Increasing power permits more data in total to be transmitted over a longer distance. However, the greater electrical power required reduces the operating life of the battery while transmission faces more interference, although performance can be improved by using matched antennas. Effective operational distance is generally reduced by obstacles such as walls, floors or metal constructions that absorb radio wave signals (Kennedy & Davis 1992).

The RF transmitter used with the wind harvester is a low-power AM transmitter (AM-RT4-433FR) (Tan et al. 2007) that is very simple to operate, uses little current (typically 4 mA,) consumes low power, its operating voltage is between 2 - 14 V, can transmit data at 4KHz and its range of wireless link is 100+ meters. Data can be supplied directly from a microcontroller or encoding device, thus using fewer components, which keeps hardware costs low. Figure 5.22 shows a photograph and schematic diagram of the RF transmitter (Farnell.com 2006). As the flow chart of the controller shows, triggering signals are sent to the RF transmitter to transmit information wirelessly about wind speed.

This item has been removed due to 3rd Party Copyright. The unabridged version of the thesis can be viewed in the Lanchester Library Coventry University.

This item has been removed due to 3rd

(a)

(b)

Figure 5.22: RF transmitter: (a) Photograph and (b) Schematic diagram
(Farnell.com 2006)

The electrical energy consumed by the RF transmitter depends on the amount of digital data bits being transmitted. Each 12 bits require 20 msec for transmission. During the active time, the transmitter must be supplied with at least 3.3 V and a current of 4 mA, while it consumes almost no energy during the idle time. The average power and energy consumed by the RF transmitter are approximately 13.2 mW and 132 μ J respectively as shown in Table 5.2. The total power practicality required for one digital 12-bit data word is 167 μ J under the assumption that there are some other power losses during the entire transmission time (around 35 μ J) (Tan et al. 2007). For example, if 4 packets of 12-bit data are transmitted, total energy required is 668 μ J. The testing of the RF transmitter is reported in Chapter 6.

Table 5.2: RF transmitter electrical characteristics

Transmission time	Duration	Voltage	Current	Average Power	Energy
Active time	10 msec	3.3V	4 mA	13.2 mW	132 μ J
Idle time	10 msec	3.3V	0 mA		

5.6 SCHEMATIC DIAGRAM OF THE ELECTROSTATIC BASED WIND HARVESTER

The schematic diagram of the complete harvester, highlighting the main parts required is shown in Figure 5.23. The system consists of the variable capacitors C_{var} , the capacitance detector circuit, the controller, the LC to LC energy transfer circuit and the RF transmitter. Simulation and experimental testing of the harvester circuit are reported in Chapter 6.

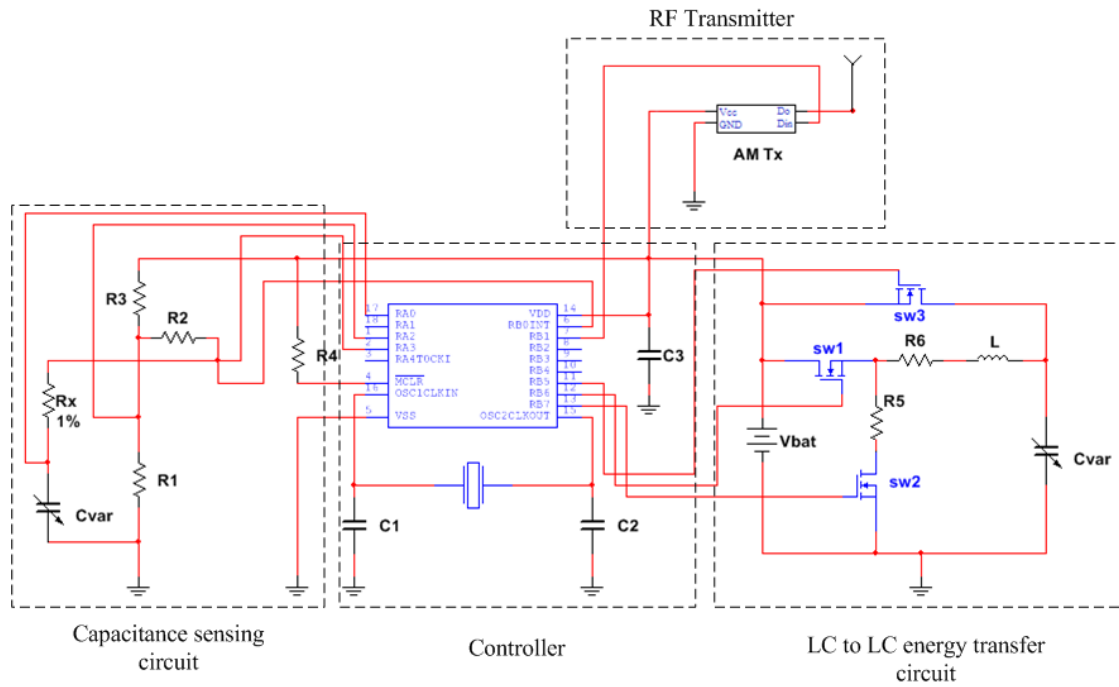


Figure 5.23: Schematic diagram of the electrostatic-based wind harvester

5.7 SUMMARY

This chapter presented the design of a novel energy harvesting system along with details of the sub-systems used. A micro wind turbine was selected for the wind harvester based on previous research by (Leung et al. 2010), and following a theoretical torque analysis. Results from the analysis indicate that, in order to rotate the rotor of the capacitor, it is necessary for the turbine torque T_T to be greater than $\frac{n_1}{n_2} T_C$. The chapter then considered two types of multi-pole capacitor: discrete and array. Both capacitors were described in details with a special focus on the advantages of the array type. The chapter described the energy transfer using an LC to LC energy transfer circuit and the controller operation along with the flow chart. In the proposed system, the harvester's controller is used for monitoring maximum and minimum capacitance, sending control signals to operate the switching devices and sending information about harvesting time and wind speed to the RF transmitter. The chapter then discussed which type of RF transmitter to be selected in order to ensure efficient data transmission. Finally, a circuit diagram of the overall system to be used for the experimental testing was presented.

CHAPTER 6

SIMULATION MODELLING, PROTOTYPE TESTING AND RESULTS

6.1 INTRODUCTION

In the previous chapter, a novel wind-based electrostatic harvester was proposed along with details of the sub-systems used. This chapter reports the simulation and experiments necessary to test the wind harvester. The simulation involves the testing of the three phases of the harvesting cycle (pre-charge, harvest and rest), testing of the multi pole capacitor, capacitance and volume optimisation, testing of the multi-pole capacitor array and finally energy optimisation. All simulations were performed using Matlab/ Simulink programs. The chapter concludes by evaluating the results from the simulation.

The experiments involve recording, discussion and comparison of the capacitance measurement of the prototypes, the charging and discharging of the capacitor during the pre-charge phase, and testing of the complete harvester with RF transmitter.

6.2 SIMULATION OF THE ELECTROSTATIC HARVESTER

In principle, the harvester electrical system can be simulated using several software tools such as Multisim or Spice. However, Matlab/Simulink was chosen as the simulation platform because it is capable of accurately simulating the time-varying variable capacitor and the switching devices. The simulation in this chapter was carried out using the Simscape blockset, which includes electrical elements, sensors and sources (Mathworks.com n.d.). These elements were used to realise the electrostatic converter circuit.

The complete Simulink model of the LC to LC energy transfer circuit and the variable capacitor is given in Figure 6.1. In order to operate the Simulink model, three control signals, S1, S2 and S3, were used to activate the switches. In addition, a mathematical function block

was connected to the variable capacitor to simulate capacitance varying over time. The values of the circuit parameters are shown in Table 6.1.

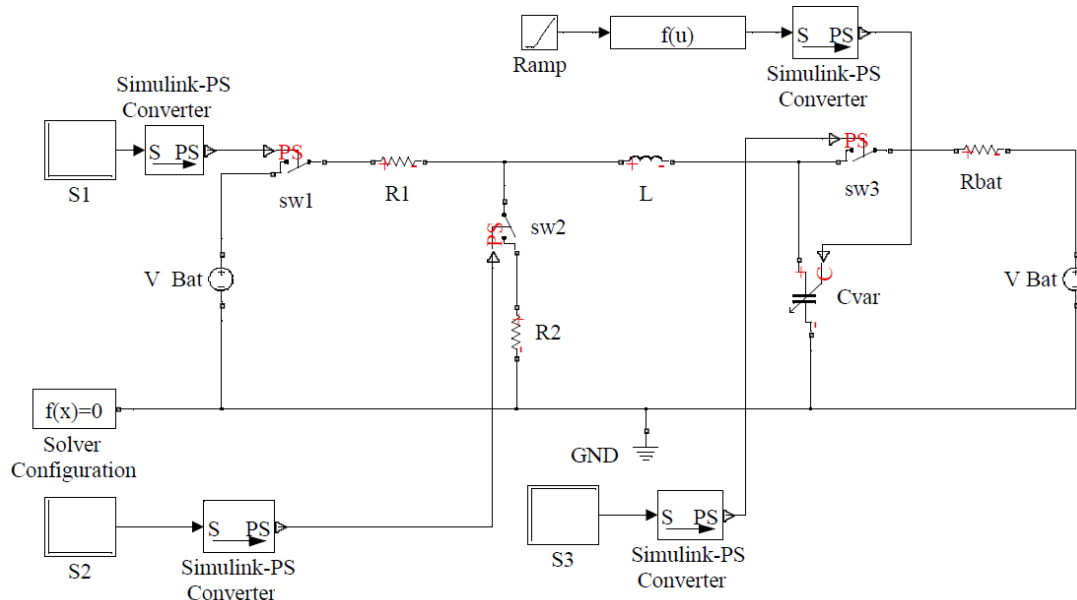


Figure 6.1: Simulink model of the electrostatic converter

Table 6.1: Parameters used to verify the Simulink model of the electrostatic converter

V_{Bat} (V)	L (mH)	C_{max} (nF)	C_{min} (nF)	R_1 (Ω)	R_2 (Ω)	R_{Bat} (Ω)
7.4	100	2.5	0.6	100	100	0.18

To simplify the process and reduce simulation errors, the Simulink testing of the electrostatic converter was divided into three stages to show pre-charge, harvest and reset phases separately. The ranges of wind speed for the simulation were chosen according to the yearly wind speed recorded in a sample area (Dubai international airport, Dubai, UAE), as shown in Figure 6.2. For the simulation testing reported in the following sections, the range of wind speed used was between 2 m/s and 10 m/sec.

This item has been removed due to 3rd Party Copyright. The unabridged version of the thesis can be viewed in the Lanchester Library Coventry University.

Figure 6.2: Average daily minimum (red), maximum (green), and average (black) wind speed (Weatherspark.com 2012)

6.2.1 Simulation of the pre-charge phase

Figure 6.3 shows the Simulink model of the LC to LC pre-charger circuit. The pre-charge phase starts when C_{var} is at maximum capacitance. Thus, the capacitor used in the simulation is a fixed capacitor with a value equivalent to C_{max} . When S1 is high, sw1 closes to allow charging of the inductor and capacitor. When S1 is low and S2 is high, sw1 opens and sw2 closes to allow charge to transfer from the inductor to the capacitor.

As the results of the pre-charge phase simulation in Figure 6.4 show, current I decreases to 0 A, capacitor voltage V_C rises to V_{Bat} and the energy of the capacitor reaches 68 nJ at the end of the pre-charge phase. The figure for energy produced by the simulation agrees with the theoretical value of the maximum invested energy calculated in Chapter 5, which was given earlier as:

$$E_{inv} = \frac{1}{2} C_{max} V_{Bat}^2 \quad (6.1)$$

The simulation test case of $C_{max} = 2.5$ nF and $V_{bat} = 7.4$, which gives an energy investment of 68.45 nJ, matches with the calculated value of energy from equation (6.1).

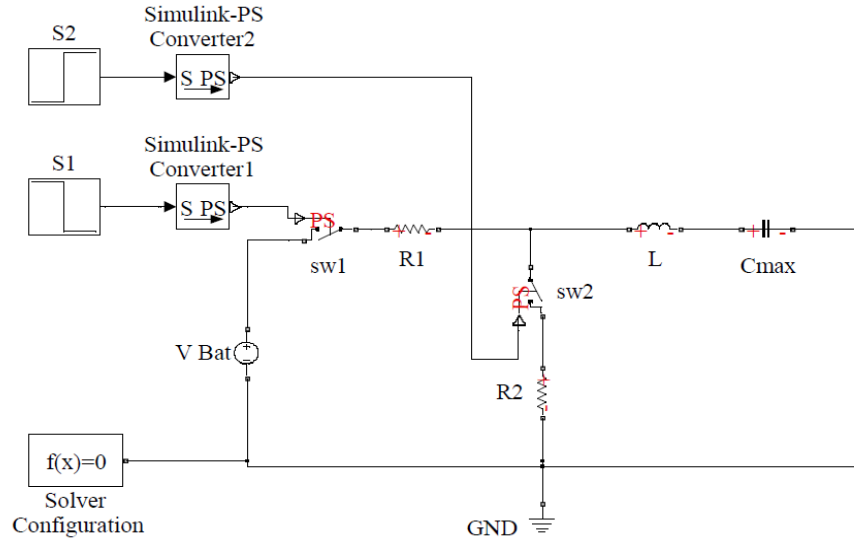


Figure 6.3: LC to LC pre-charger Simulink model

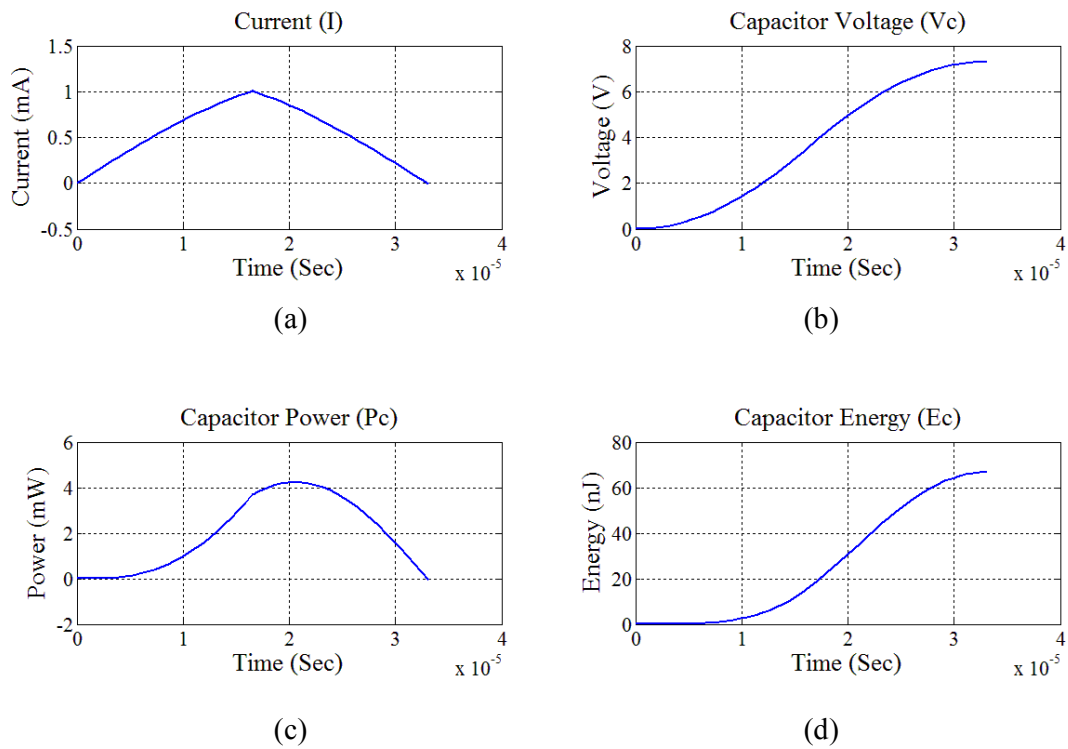


Figure 6.4: Pre-charge phase: (a) Current; (b) Voltage across C_{\max} ; (c) Power of the capacitor; (d) Invested energy by C_{\max}

Figure 6.5 shows the energy invested in R_1 , R_2 , L and C_{\max} . The main purpose of using the pre-charger circuit is to charge the capacitor with the minimum energy investment from the battery and minimum energy losses in both the resistors and the inductor. It can be seen from the simulation results that, when the inductor is energizing and de-energizing, its energy L is completely transferred to the capacitor while losses in the resistors are particularly low because the time period for energizing and de-energizing is very short.

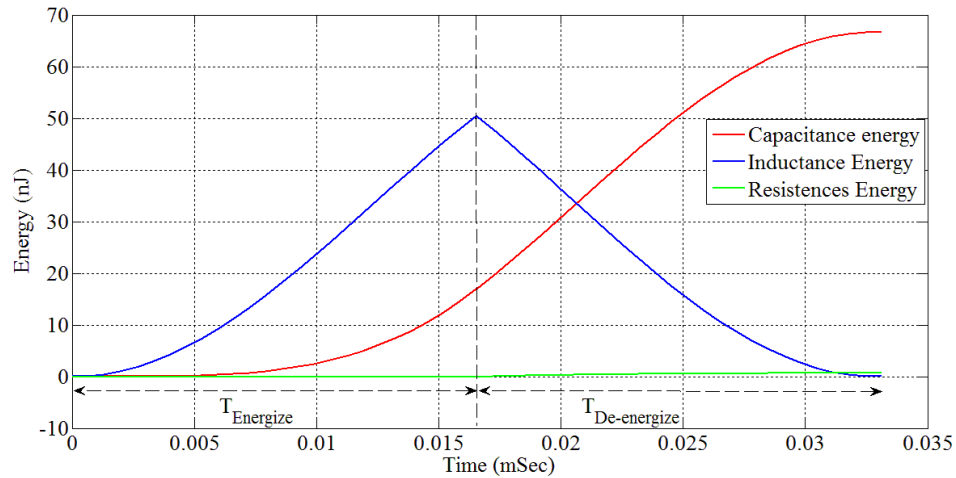


Figure 6.5: Energy invested in the resistors, inductor and capacitor

6.2.2 Simulation of the harvesting phase

Figure 6.6 presents the Simulink model of the LC to LC electrostatic converter during the harvesting phase. The variable capacitor C_{var} was connected directly to the battery through switch sw3 controlled by signal S3. As C_{var} changed from maximum 2.5 nF to the minimum capacitance of 0.6 nF under a constant voltage of 7.4V, the harvesting current increased to charge the battery, thereby increasing harvested energy.

Figure 6.7 and 6.8 plot the harvesting current and the harvested energy. The harvesting time used was 14.1 msec, which corresponds to a wind speed of 10 m/sec. For wind speeds from 2 to 10 m/sec, a Matlab program was written, and the curve-fitting tool was used to find the capacitance functions and harvesting time. The results from this program are given in Table 6.2.

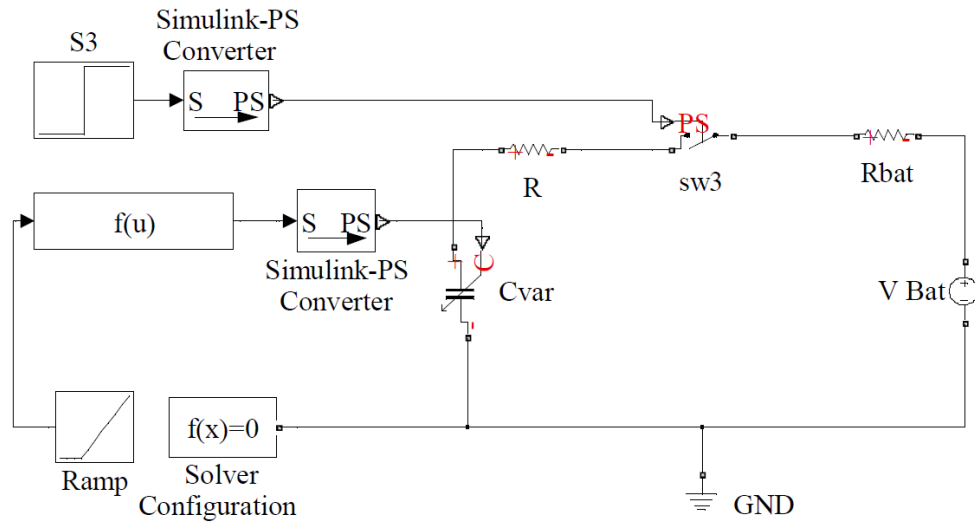


Figure 6.6: Harvesting phase of the LC to LC electrostatic converter

Table 6.2: Capacitance function and harvesting time period

Wind speed (m/sec)	Capacitance function	Harvesting time (msec)
2	$f(t) = -2.92 \times 10^{-8} t + 2.5 \times 10^{-9}$	70.7
4	$f(t) = -5.84 \times 10^{-8} t + 2.5 \times 10^{-9}$	35.3
6	$f(t) = -8.76 \times 10^{-8} t + 2.5 \times 10^{-9}$	23.6
8	$f(t) = -1.16 \times 10^{-7} t + 2.5 \times 10^{-9}$	17.7
10	$f(t) = -1.46 \times 10^{-7} t + 2.5 \times 10^{-9}$	14.1

The plots indicate that both the harvesting current and the harvested energy level are acceptable (in nA and nJ scales). Both current and energy increased at the beginning of the harvesting cycle. However, the harvested current decreased to 0 A at the end of the harvesting time while energy stayed at the maximum. The average value of the harvested current and the maximum harvested energy from the simulation agreed with the calculated values using the following equations given in Chapter 5:

$$I_{\text{harv}} = \frac{\Delta C_{\text{var}} V_{\text{Bat}}}{t_{\text{harv}}} \quad (6.2)$$

$$E_{\text{harv}} = \Delta C_{\text{var}} V_{\text{Bat}}^2 \quad (6.3)$$

Figures 6.9 shows the results of comparing the simulation and the calculated values of current and energy gain for various wind speeds from a minimum of 2 m/sec to a maximum of 10 m/sec.

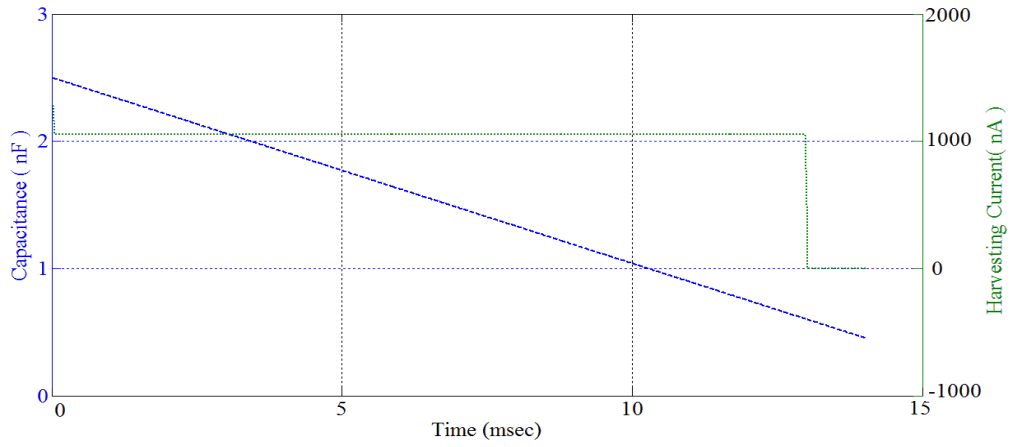


Figure 6.7: Current during the harvesting phase

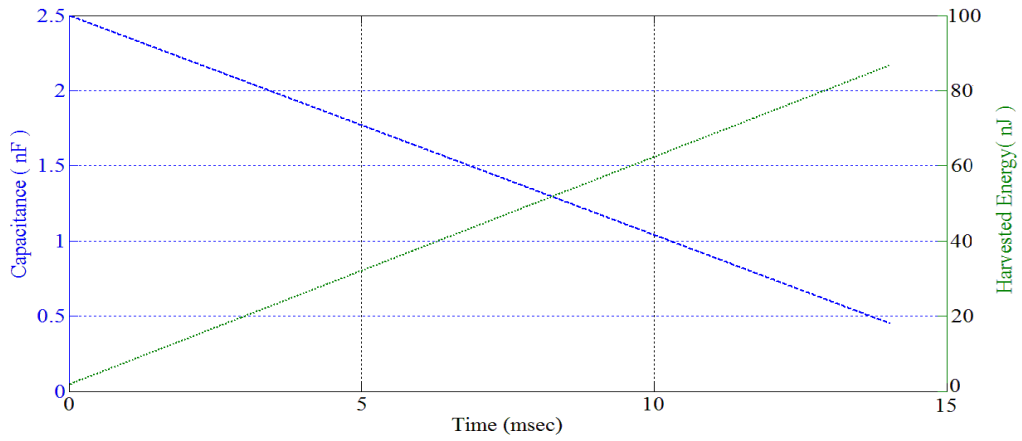


Figure 6.8: Harvested energy during the harvesting phase

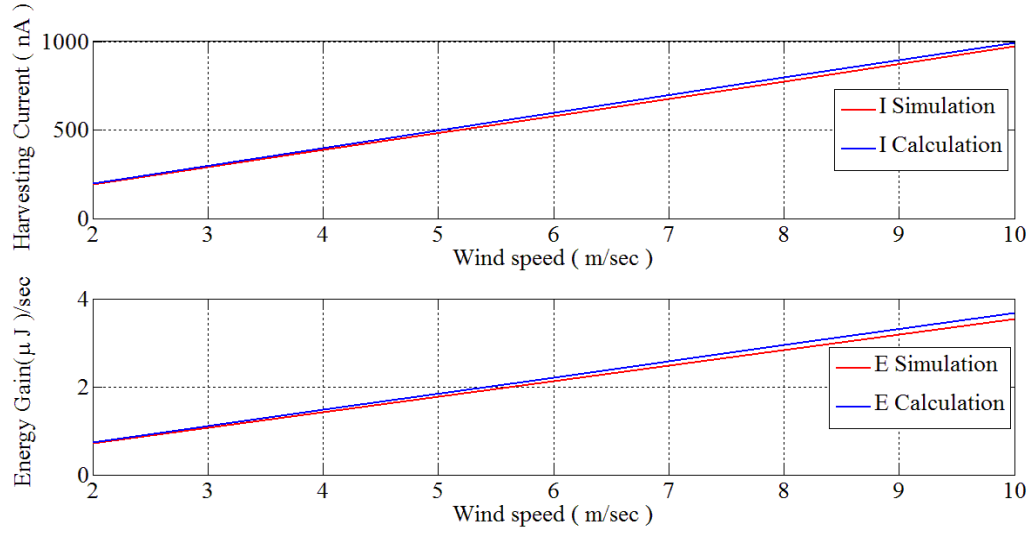


Figure 6.9: Comparison between simulated and calculated values of current and energy gain

6.2.3 Simulation of the reset phase

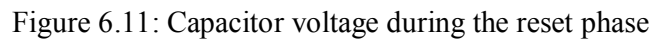
Figure 6.10 presents the Simulink model of the reset phase. During this phase, the capacitor is left open-circuited. All three switches open when S1, S2 and S3 are low. Capacitance C_{var} increases from $C_{min} = 0.6$ nF to $C_{max} = 2.5$ nF while V_C decreases from V_{bat} to $V_{c(min)}$.

The minimum capacitor voltage was given earlier as:

$$V_{C(min)} = \left(\frac{C_{min}}{C_{max}} \right) V_{Bat} \quad (6.4)$$

The theoretical value of the minimum voltage was calculated to be 1.77 V, which agreed with the value of 1.68 V produced by the simulation.

The plots shown in Figure 6.11 show a minimum voltage of $V_C = 1.68$ V, which was achieved when C_{var} was at maximum capacitance. Note the harvesting time used was 14.1 msec, which corresponds to a wind speed of 10 m/sec.



As described earlier in Chapter 5, a multi-pole capacitor is a variable capacitor comprising rotor and stator, with each divided into a number of poles. The number of poles determines the amount of capacitance variation within a single rotation. A multi pole capacitor can use a single piece or multiple sets of rotors and stators.

Figure 6.12, 6.13, 6.14 and 6.15 show the harvested energy using multi-pole variable capacitors. The variation of capacitance within one cycle of rotation and harvested energy per cycle is recorded. The results indicate that the harvested energy increased with an increase in the number of poles.

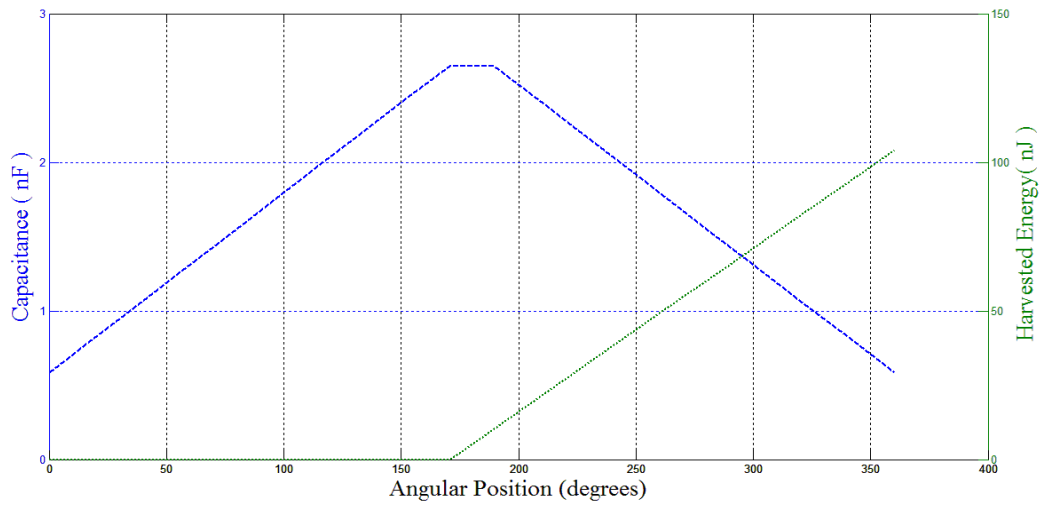


Figure 6.12: Harvested energy of a single pole capacitor $N_{\text{Pole}} = 1$

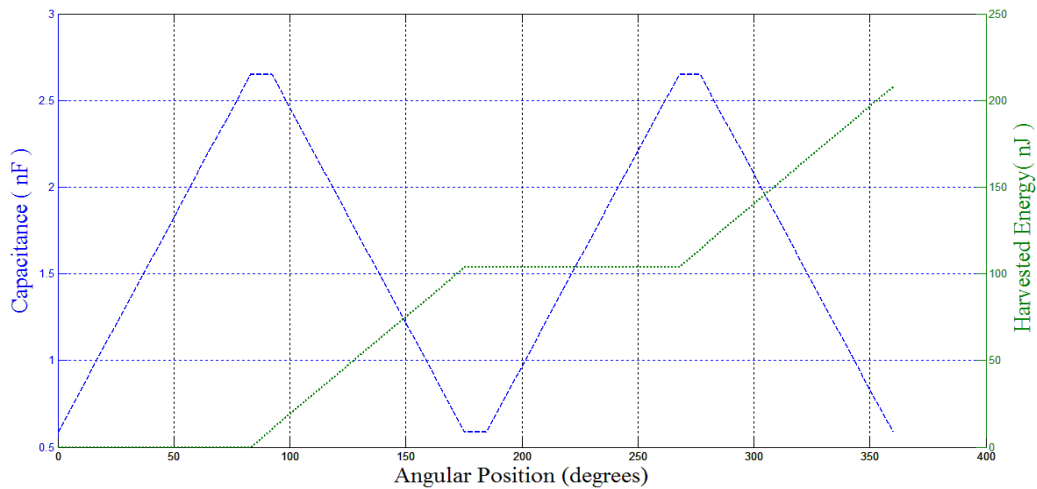


Figure 6.13: Harvested energy of two-pole capacitor $N_{\text{Pole}} = 2$

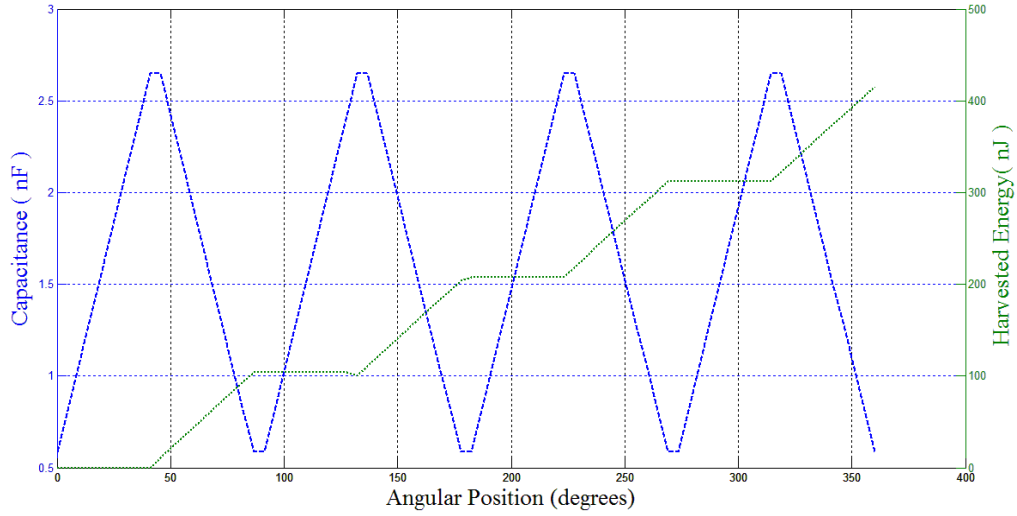


Figure 6.14: Harvested energy of four-pole capacitor $N_{\text{pole}} = 4$

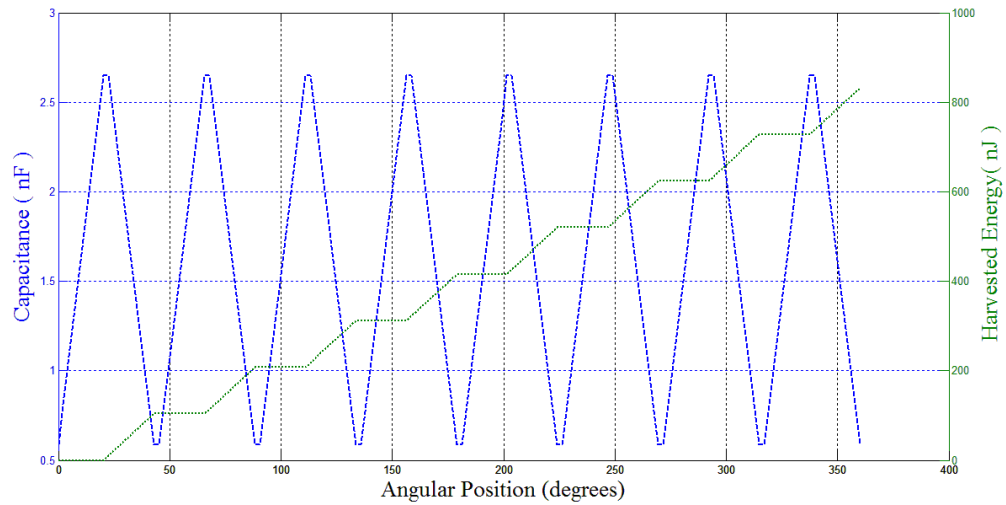


Figure 6.15: Harvested energy of eight-pole capacitor $N_{\text{pole}} = 8$

Table 6.3 presents the harvested energy per cycle and the harvested energy per second at various wind speeds. The results from Table 6.2 are plotted in Figure 6.16. The results indicate that the harvested energy increased as the number of poles increased, while the harvested energy gain in $\mu\text{J}/\text{sec}$ also increased at higher wind speeds. The simulation results matches with the calculated values of the harvested energy using equation (6.3).

Table 6.3: Harvested energy of multi-pole capacitors

N_{Pole}	$E_{\text{Harv/cycle}}$ (μJ)	Harvested Energy ($\mu\text{J/sec}$)				
		2 m/sec	4 m/sec	6 m/sec	8 m/sec	10 m/sec
1	0.104	0.73	1.47	2.20	2.94	3.67
2	0.208	1.47	2.94	4.41	5.88	7.35
4	0.416	2.94	5.88	8.83	11.77	14.71
8	0.832	5.88	11.77	17.66	23.55	29.43

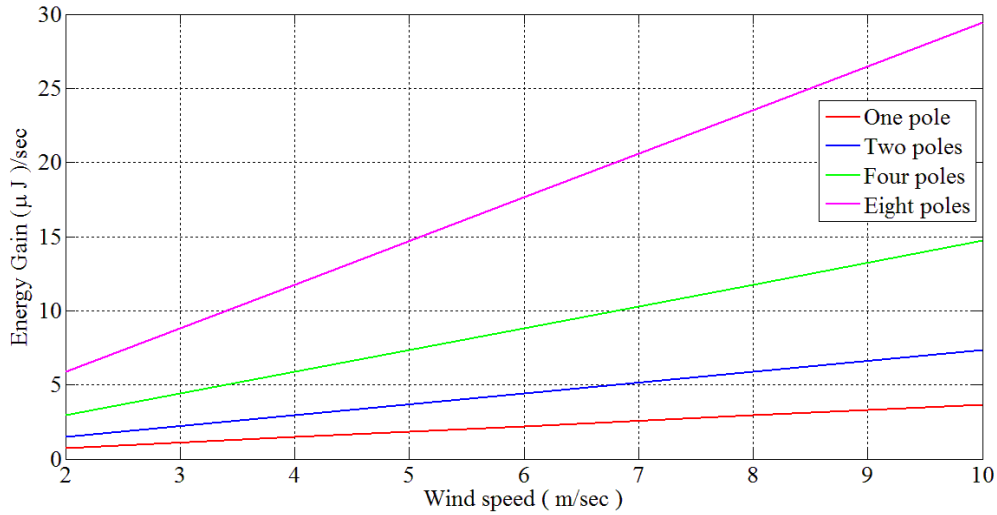


Figure 6.16: Harvested Energy of multi-pole capacitors

As observed previously, the amount of harvested energy increases as the number of poles in a capacitor increases. A Matlab program was written to calculate and plot the optimum pole number for a given variable capacitor attached to a gear box. The plots are shown in Figure 6.17. The maximum number of poles was calculated by finding the time required to complete a rotation for the given variable capacitor at various wind speeds in the presence of increaser gear box. The time was then divided by double the pre-charge time period given in Equation (5.13) to find the maximum possible divisions per rotation which was then divided by 2 to get the maximum number of poles.

Observation of the plots indicates that the maximum number of poles varies with wind speed conditions and gear ratios. Increasing the number of poles beyond specified limits causes leakage of the electrical field and increases the speed of capacitance variation, which means the energizing and de-energizing time would be insufficient to pre-charge the capacitor.

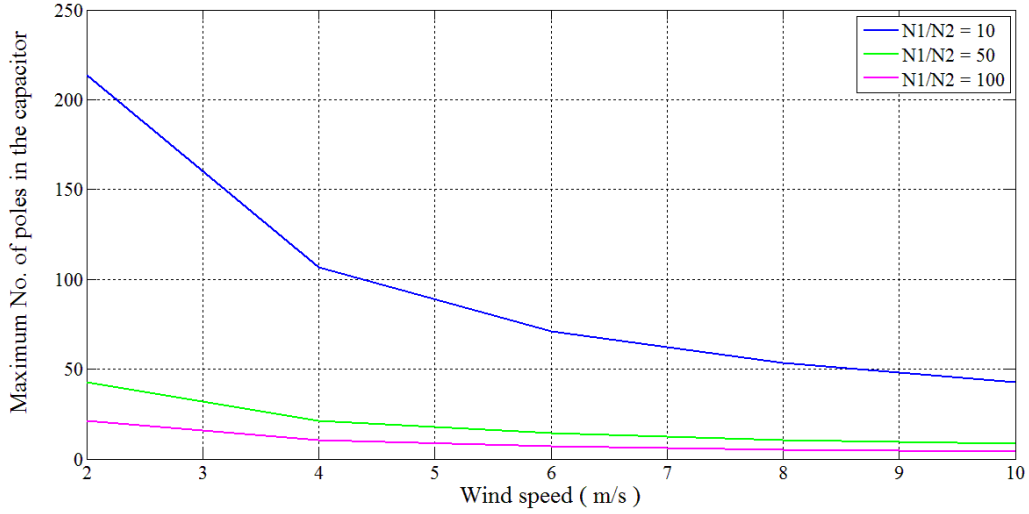


Figure 6.17: Maximum number of poles in a multi-pole capacitor

6.2.5 Capacitance and volume optimisation of the multi-pole capacitor

Capacitance difference ΔC_{Var} values are significant factor affecting the harvested energy beside battery voltage, as given in equation (6.3). Thus, capacitance optimisation is required. Capacitance is a function of angular position, area of the plates, gap between plates, number of poles and number of stator-rotor sets, as explained in Chapter 5 and given by the following:

$$C_{Var}(N_{SR}, A, d) = (2N_{SR} - 1) \epsilon_o \epsilon_r \frac{A_{eff}(\theta)}{d} \quad (6.5)$$

Capacitance optimization was performed to observe the effect of these parameters on capacitance difference. The results given in Figure 6.18 indicate that the highest ΔC_{Var} can be obtained when the effective area difference, and the number of stator-rotor sets is maximised while the distance between the plates is minimised.

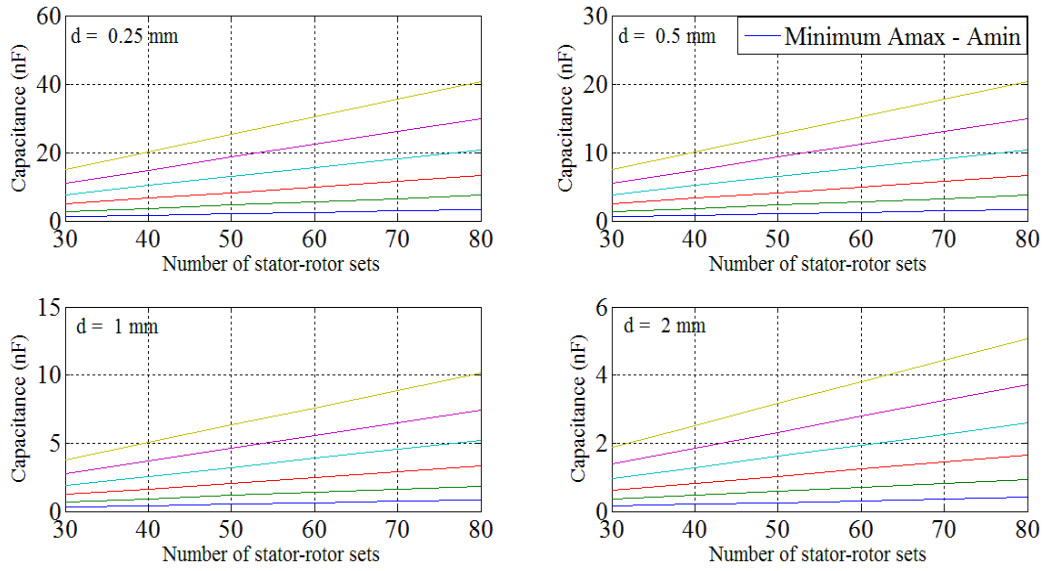


Figure 6.18: Capacitance optimisation of the multi-pole capacitor

Capacitor volume is another important factor that needs to be taken into consideration before fabrication. Since the capacitor's shape is similar to a cylinder, as shown in Figure 6.19, its volume can be calculated by:

$$\text{Vol} = \pi r^2 h \quad (6.6)$$

$$h = 2N_{\text{SR}}w + (N_{\text{SR}} - 1)d \quad (6.7)$$

where h is the height of the capacitor cylinder and w is the thickness of the individual plate.

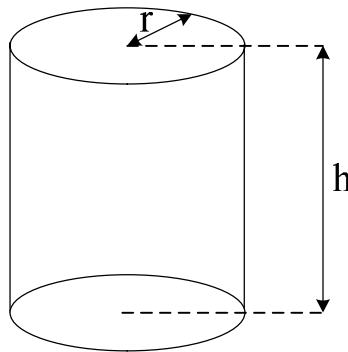


Figure 6.19: Cylindrical shape variable capacitor

From equations 6.5 and 6.6, it can be seen that the capacitor's volume is related directly to the capacitance parameters. Thus, it is related to the amount of energy harvested per unit volume.

Figure 6.20 illustrates the simulation results for the volume optimisation for different radius values (20 mm – 80 mm) and gap distances between the plates (0.25 mm - 2 mm). The plots are linear and show considerable volume changes for all bands of the selected N_{SR} . The maximum volume was obtained when $N_{SR} = 80$, $w = 1$ mm, $d = 2$ mm and the radius was 75 mm.

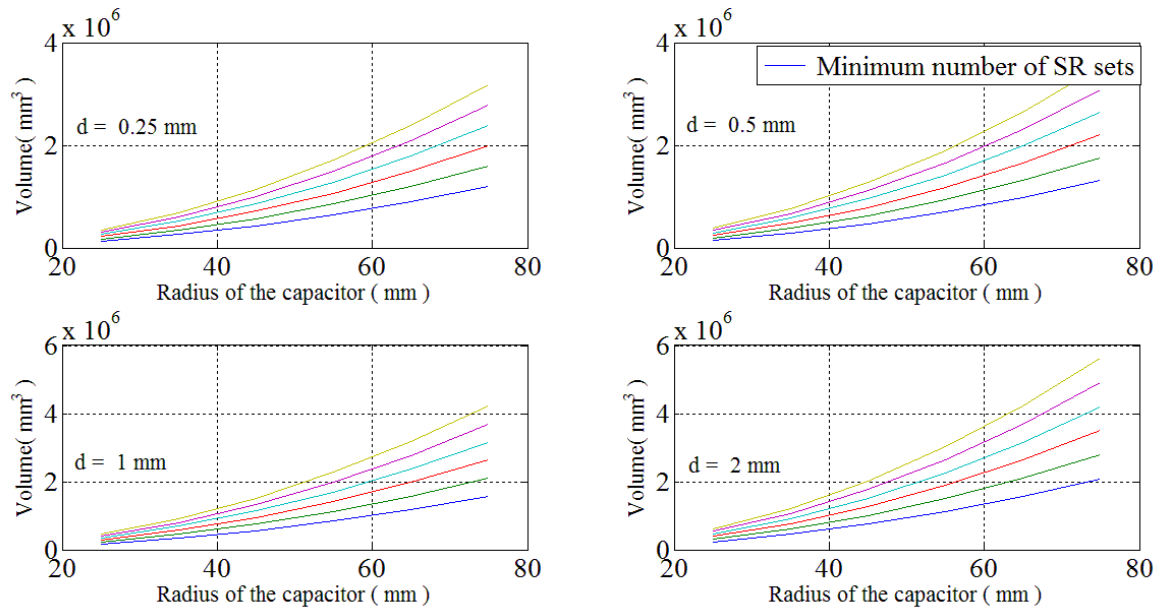


Figure 6.20: Volume optimisation of the multi-pole capacitor

6.2.6 Simulation testing of the multi-pole capacitor array (MPCA)

This section reports on the testing and plotting of the harvested energy of the MPCA. The simulation assumed that there were four capacitors in the array, where $N_C = 4$. The testing was completed in three stages: pre-charge, harvest and reset. Figures 6.21 and 6.22 present the three stages. Note that each capacitor is represented by a subsystem.

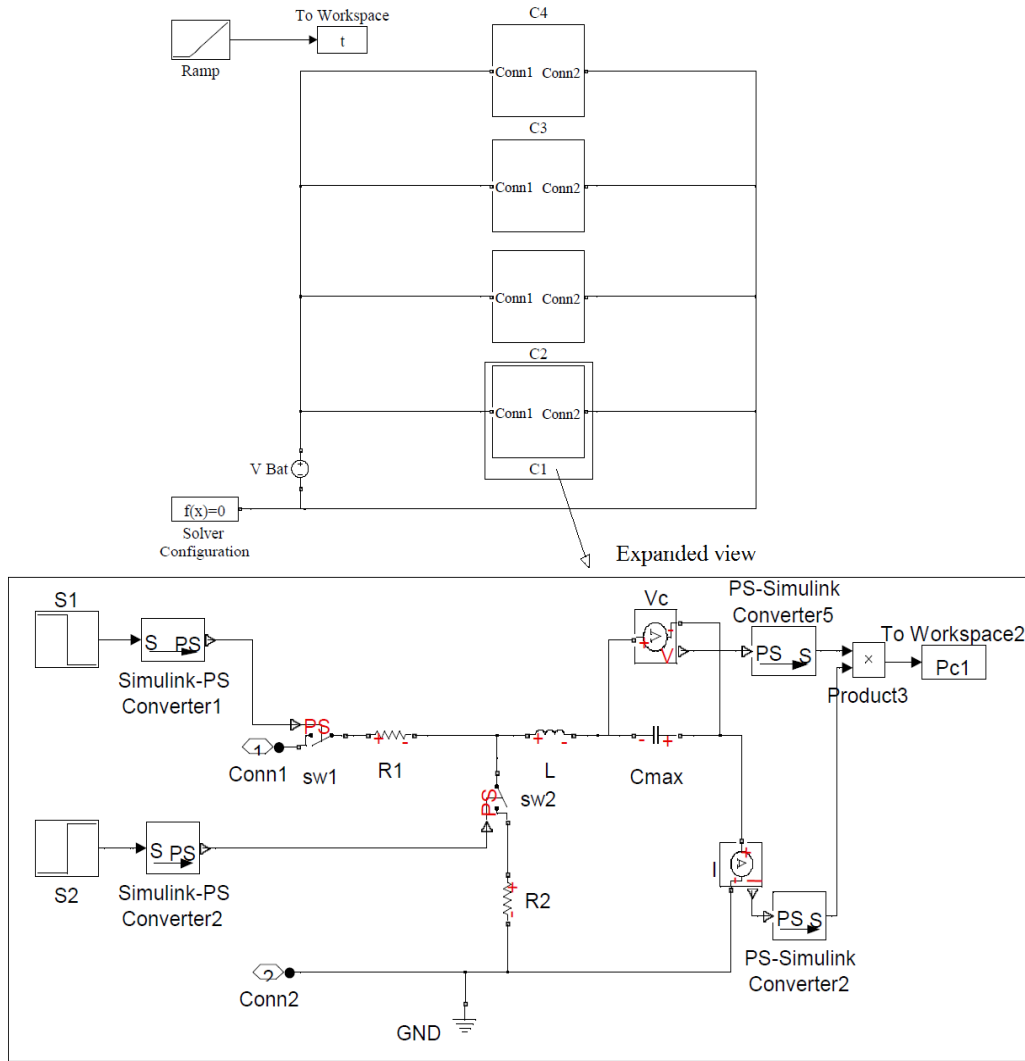


Figure 6.21: Pre-charge phase of the MPCA

Figure 6.23 shows the energy gain harvested at various wind speeds using the MPCA. Several observations can be made from the results. First, the amount of energy harvested using the MPCA is a considerable improvement compared to the discrete multi-pole capacitor. Although the capacitance is the same, the energy harvested under the same wind speed conditions is higher. For example, the energy harvested using an array of 10 capacitors was 10 times greater than the energy harvested from a single capacitor.

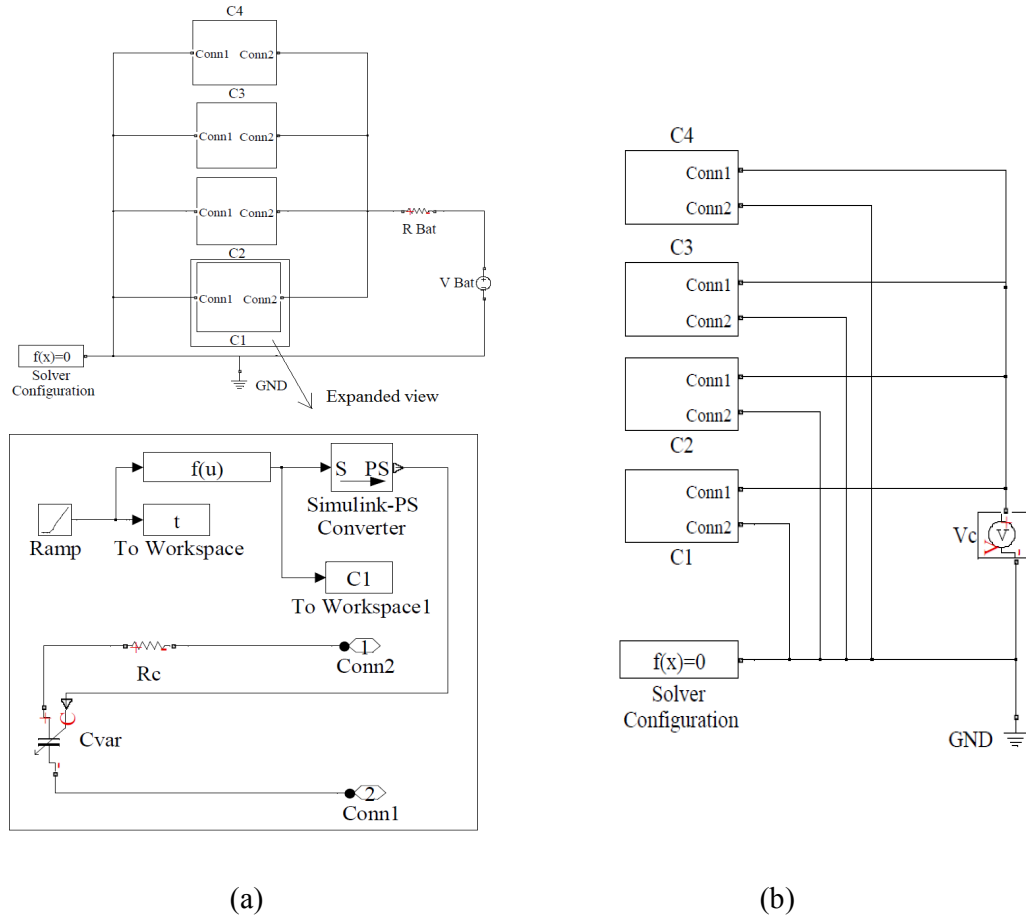


Figure 6.22: MPCA: (a) Harvesting phase and (b) Reset phase

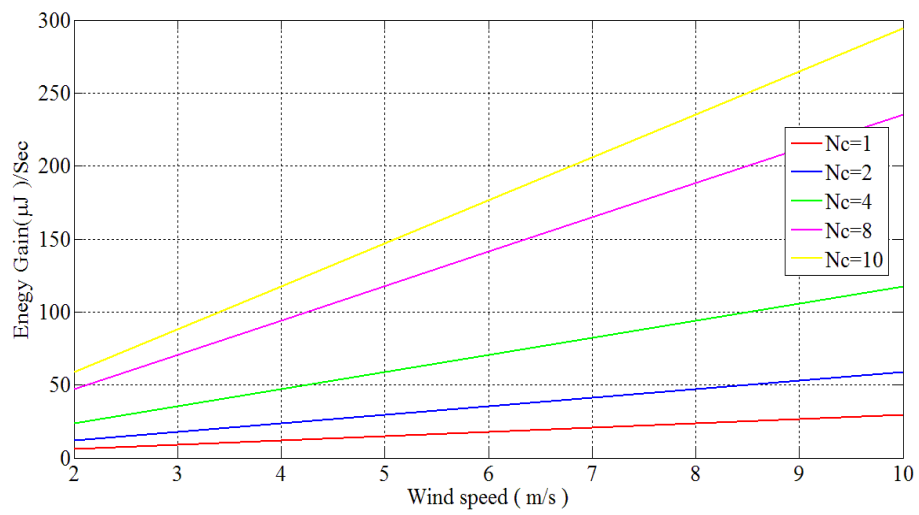


Figure 6.23: Harvested energy using the MPCA

6.2.7 Energy optimisation

Figure 6.24, which reports the results of harvested energy optimization, indicates that more energy is harvested with a higher-voltage battery but limited to maximum working voltage of the capacitor, the type of the storage device and the maximum voltage of the target application. Moreover, more energy can be harvested when more capacitors are used in the array. The plots in Figure 6.25 indicate that the harvested energy could be increased by modifying capacitance by increasing the number of capacitors in the array and reducing the harvesting time, which means a higher speed of rotation that relates directly to wind speed. Furthermore, the amount of harvested energy could be improved by increasing the number of poles in the capacitor and the number of those capacitors in the array (Figure 6.26).

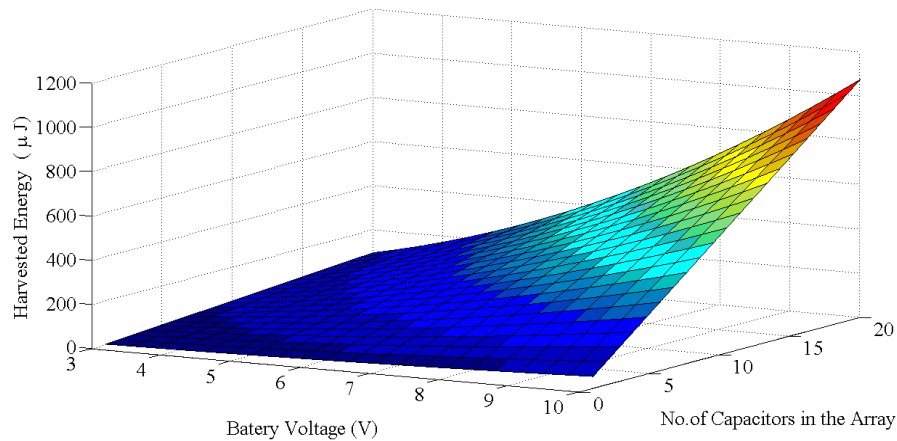


Figure 6.24: Energy optimisation for various battery voltages and capacitor arrays at 10 m/sec

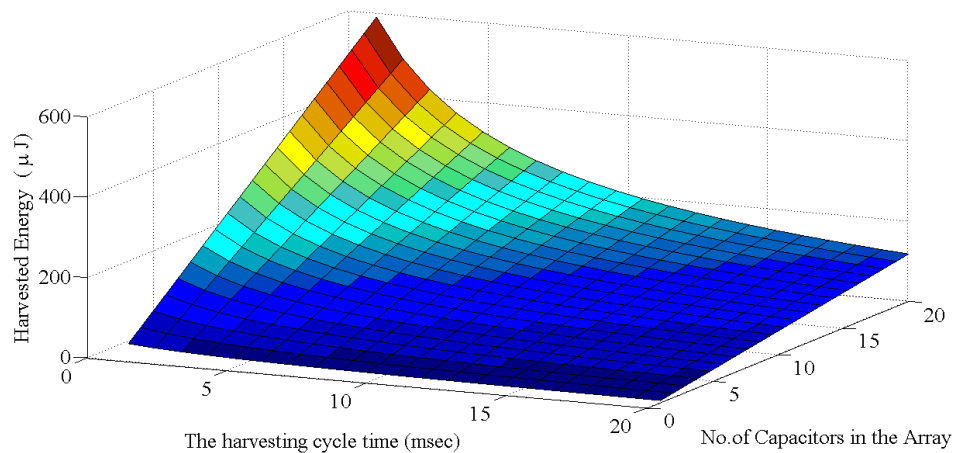


Figure 6.25: Energy optimisation for various harvesting time periods and capacitor arrays (2 -10) m/sec

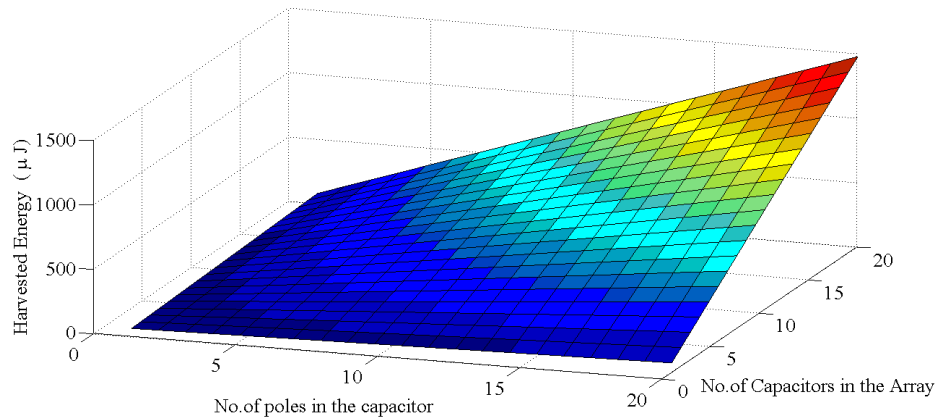


Figure 6.26: Energy optimisation for various numbers of poles in the capacitor and numbers of capacitors in the array at 10 m/sec

6.2.8 Charging time of selected battery power systems

The development of silicon-based electronics with low power consumption has helped in producing a broad variety of battery-powered portable, wearable and implantable devices. The power consumptions of a range of these devices are shown in Table 6.4 (Vullers et al. 2009). Note that the power consumptions of these devices are reducing all the time with the technological developments and could be reduced further in future. All these devices need compact, low-cost and lightweight batteries which enable the required portability and energy autonomy. Energy harvesters can be used a suitable choice to charge the batteries of these devices.

Table 6.4: Selected battery power systems (Vullers et al. 2009)

This item has been removed due to 3rd Party Copyright.
The unabridged version of the thesis can be viewed in
the Lanchester Library Coventry University.

In order to evaluate the feasibility of the proposed wind harvesting system, the specifications of selected battery powered devices were studied (Cellphoneshop.com 2014), (Atbatt.com 2014). The charging time in hours were calculated for various wind speed conditions. A battery charge time calculator available online (Csgnetwork.com 2011) was used to perform the calculation based on the simulation values of the harvested current per second. All calculations for efficiency loss were performed, no matter which battery was selected, using the generally accepted efficiency loss of 20 %. This allowed the time required to charge the batteries of various devices in different wind conditions to be estimated as given in Table 6.5. Note that all values are based on the simulation with the theoretical results not taking into consideration losses during the energy harvesting cycle.

Table 6.5: Charging times of selected battery power systems

VBat (V)	I (mAh)		Wind speed (m/sec)				
			2	4	6	8	10
			Charging time - Hours (h) Minutes (m)				
3.7	1000	Nokia cell phone	18h	4h 30m	2h	1h 7m	43m
3.7	700	Ericson cell phone	12h 36m	3h 9m	1h 24m	47m	30m
3.7	800	Samsung cell phone	14h 24m	3h 36m	1h 36m	54m	34m
3.7	900	LG cell phone	16h 12m	4h	1h 48m	1h	38m
3.7	600	Panasonic phone	10h 48m	2h 42m	1h 12m	40m	26m
3.7	250	iPod	4h 30m	1h 7m	30m	17m	11m
3.7	2000	iPhone	36h	9h	4h	2h 15m	1h 26m
7.4	750	Canon NB-2LH camera	13h 30m	3h 22m	1h 30m	50m	32m
3.7	660	Olympus Li-42B camera	11h 53m	2h 58m	1h 19m	44m	28m

6.3 EXPERIMENTAL TESTING OF THE ELECTROSTATIC HARVESTER

6.3.1 Variable capacitor prototype

Various variable capacitor prototypes were fabricated for testing purposes. The first prototype was originally fabricated and then designed using AutoCAD for effective area measurements. The first prototype was used to investigate the possibility of operating a

rotary multiple capacitors with micro wind turbine. Although the capacitor was found not useful for harvesting maximum energy from wind but the experimental testing results helped in putting the guidelines that lead to the design of the optimised structure proposed in Chapter 5.

Figure 6.27 shows the AutoCAD model of the multi-pole rotary variable capacitor. The capacitor is constructed from a rotor and a stator. The stator consists of eight sets of arrow shaped plates. Each set consists of an array of nine plates separated by air. The rotor consists of a set of nine rectangular rotating plates. The variable capacitor plates were made of aluminium and the inner rod was made of stainless steel. Stainless steel was used due to the great resistance to weather and corrosion and for the purpose of electrical conduction. Aluminium was used because it is inexpensive material, highly conductive and can be easily formed into the arrow and rectangular shaped plates.

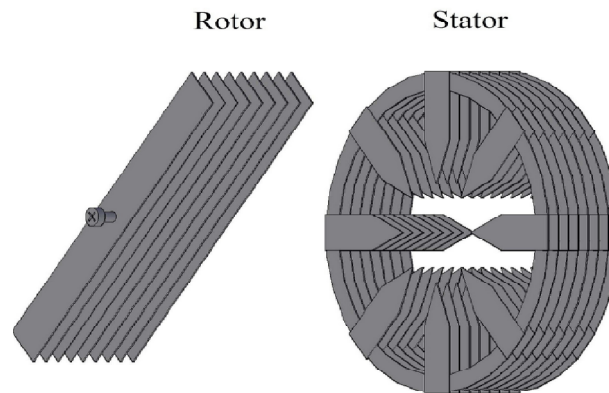


Figure 6.27: First Prototype of a multi pole capacitor

The effective area of the capacitor plates were calculated using an AutoCAD area calculation function. The stator consists of eight arrow shaped plates pointing to the centre. The arrow shape of the stator plates was chosen to match the rectangular rotor plates in order to get maximum effective area as shown in Figure 6.28. The variable capacitor was modelled with the initial angle of rotation set at 0° . The maximum effective area was then measured by applying a rotation of 1° recording the effective area and iteratively repeating the process for 360° . A sample of the process is shown in Figure 6.29 at an angle of 5° . The recorded data was then processed using Matlab where the capacitance of the variable capacitor was

calculated. The calculated capacitance provides theoretical values not considering any parasitic or fringe effects. These effects can only be measured from the experimental testing of the prototype. It can be added as an external constant capacitance parallel with the calculated variable capacitor when simulated in Simulink (Torres et al. 2006).

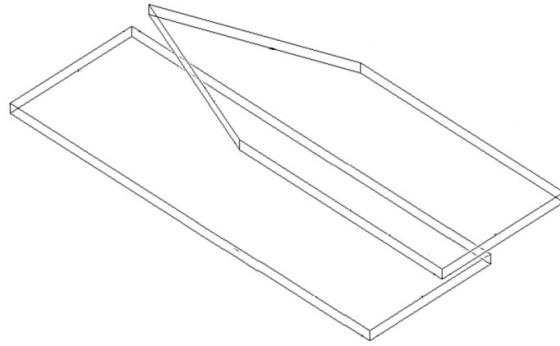


Figure 6.28: Arrow shaped capacitor plate for the first prototype.

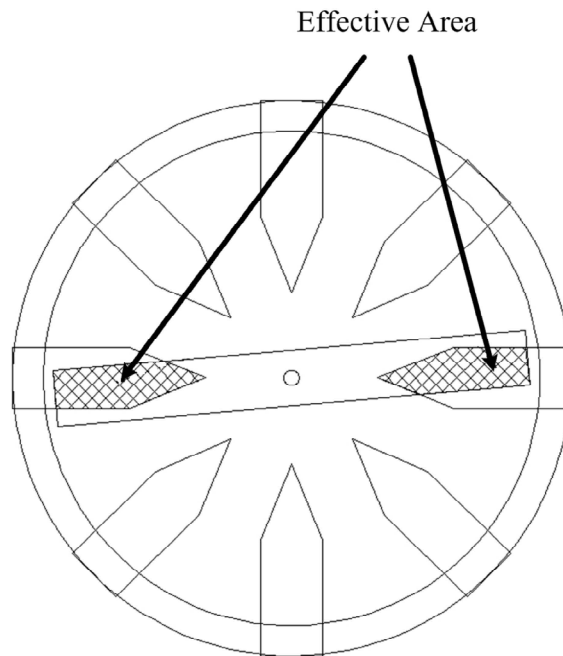


Figure 6.29: Sample of AutoCAD process at an angle of 5°

6.3.2 Experimental setup

Two experiments were conducted to test the variable capacitor prototype and to validate the AutoCAD simulation results. The experiment setups are shown in Figure 6.30. The first experiment used a GW-INSTEK 816 LCR meter and an angular measurement disk to measure the total capacitance at every 5 °of rotation. In order to rotate the rotor, a motor was connected to it to provide a stable rotational motion. To verify the rotor position, a measurement disk was attached to the stator. The LCR was then set to the fast automatic mode to be able to measure the variation of capacitance values at every 5 °of rotation. The second experiment uses a digital storage oscilloscope GWINSTEK GDS 2102 and a pulse generator to test the transient response of the variable capacitor.

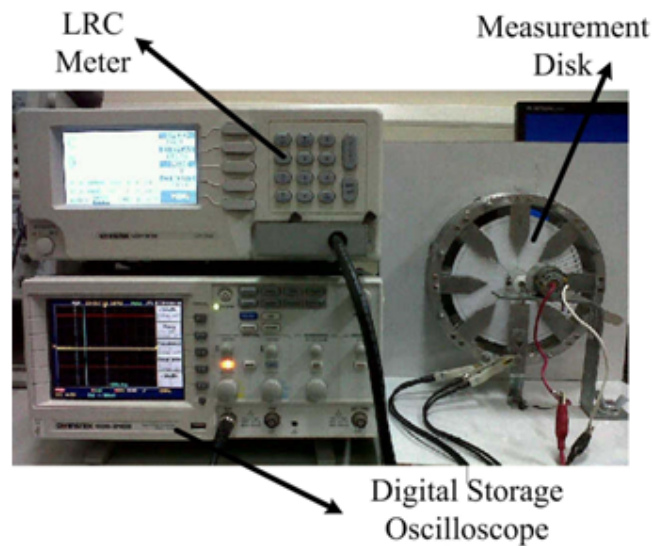


Figure 6.30: Experimental setup for capacitance measurement for the first prototype

Results of capacitance measurement indicated a sinusoidal relation between the angular position and the capacitance as shown in Figure 6.31. Moreover, the experimental result showed a higher capacitance than obtained using AutoCAD with a maximum difference of 39 pF. To get the mathematical expression of the capacitance in terms of the angular position, the simulation and experimental data points were processed using a Matlab mathematical curve fitting tool. The most suitable type of fit for the data points found to be a

Fourier polynomial of degree 1. The resultant capacitance Fourier polynomials for both the AutoCAD capacitance C_{cad} and the experiment C_{exp} are given by (Abdulmunam et al. 2013):

$$C_{cad} = 37.19 + 40.92 \cos(0.1385 x) - 2.08 \sin(0.1385 x) \quad (6.8)$$

$$C_{exp} = 75.91 + 34.96 \cos(0.1386 x) - 2.03 \sin(0.1386 x) \quad (6.9)$$

From (6.8) and (6.9) the difference C_{diff} can be written as follows:

$$C_{diff} = C_{exp} - C_{cad} \quad (6.10)$$

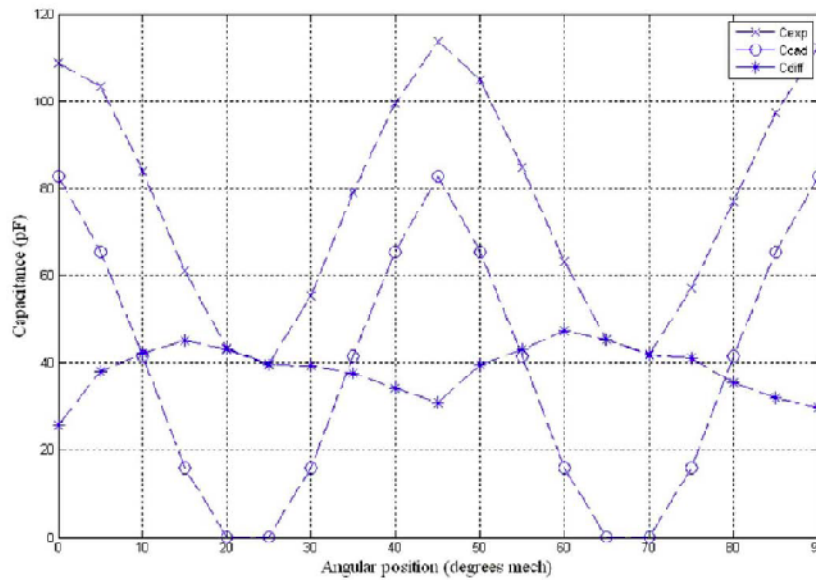


Figure 6.31: Results for the prototype capacitance variations

The prototype capacitor was connected to a pulse generator of 2.5 V and a resistor of 10 k Ω to test the capacitance charging and discharging transient time. Results of the experiment were plotted as shown in Figure 6.32 and 6.33 accordingly. Experimental results indicated that the settling time is 8.8 μ sec at C_{max} and 5.5 μ sec at C_{min} . While the theoretical calculations indicated that the settling time is 5.5 μ sec at C_{max} and 2 μ sec at C_{min} . The small difference in the transient time might be due to the tolerance of the devices and the system parasitic capacitance.

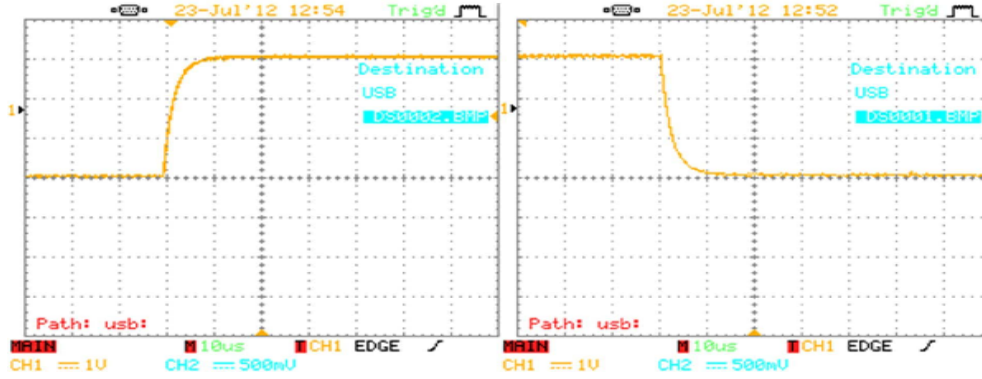


Figure 6.32: Experimental result of the transient response when C is at C_{\max}

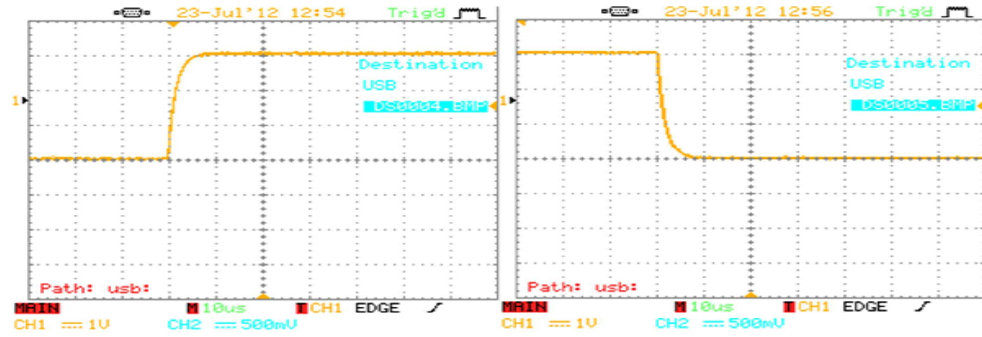


Figure 6.33: Experimental result of the transient response when C is at C_{\min}

As the results indicated, there are slight differences between the simulation and the experiment results. This is due to the manufacturing tolerances, the fringe capacitance and the system parasitic capacitance. The parasitic capacitance is an additional capacitance formed between the capacitor poles and any close by conductors (Wu et al. 2009). This causes a considerable increase in the capacitance value at different angular positions (Torres et al. 2010). The fringe effect is caused by the sharp edges of the multi-pole variable capacitor plates which cause bending of the electric field lines at the edges of the plates. As a result, the flux is not properly linked with the second plate as it is moving in rotational motion which leads to additional small fringe capacitance to be added in parallel to the variable capacitor (Hammer 2010). The parasitic capacitance of the prototype was caused by the lack of isolation of the devices from the physical surrounding while taking the measurements. Moreover the test leads of the LCR meter added a capacitance of around 30

pF although it was shielded cables. The capacitance of the prototype was compared with five different types of variable capacitors used for energy harvesting from previous studies. The result of the comparison was found to be consistent indicating that the variable capacitor performance was satisfactory in terms of capacitance variation and the maximum energy which could be harvested. A summary of the results is given in Table 6.6. However the main drawback of this prototype is that the number and the shape of rectangular rotor plates are not completely matching with the stator plates thus the maximum capacitance variation ΔC_{var} are not achieved within a single rotation. As mentioned previously in Chapter 5, the ΔC_{var} is one of the main parameters that affect the amount of harvested energy during the harvesting cycle. Therefore, an optimised capacitor structure was proposed in Chapter 5.

Table 6.6: Comparison of various types of variable capacitor used in electrostatic harvesters
(Abdulmunam et al. 2013)

This item has been removed due to 3rd Party Copyright. The unabridged version of the thesis can be viewed in the Lanchester Library Coventry University.

6.3.3 Test setup of electrostatic harvester with the RF transmitter

Figure 6.34 shows the schematic diagram of the electrostatic based wind energy harvester. The circuit consists of variable capacitor, an LC to LC energy transfer circuit, PIC microcontroller, RF transmitter circuit and a storage device. The variable capacitor is moved by either applying wind to the attached micro wind turbine or by using a DC motor to confirm the presence of a constant rotational speed for experimental testing purposes. The capacitor is then pre-charged from a lithium-ion battery pack of 4.2 V through the LC to LC circuit. Next energy is harvested and sent to the battery. Before the start and the end of the harvesting cycle, a signal is sent to the RF transmitter as described previously in Chapter 5.

The experiment setup is to show the basic operation of the harvester which is controlled by the PIC microcontroller. The variable capacitor was connected permanently to the digital storage oscilloscope to capture the charging and the discharging of the capacitor during the harvesting cycle. The RF transmitter used is AM-RT4-433FR connected to the 16F82A PIC microcontroller through 2N7000 transistor.

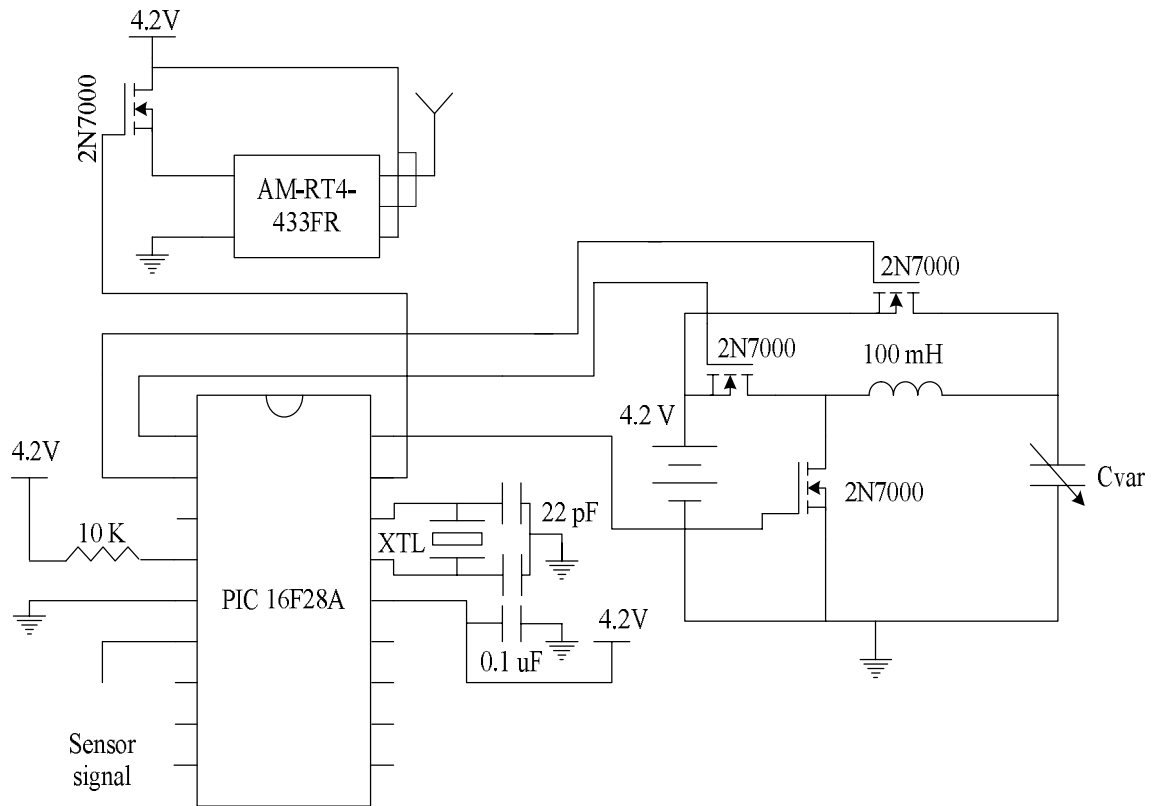
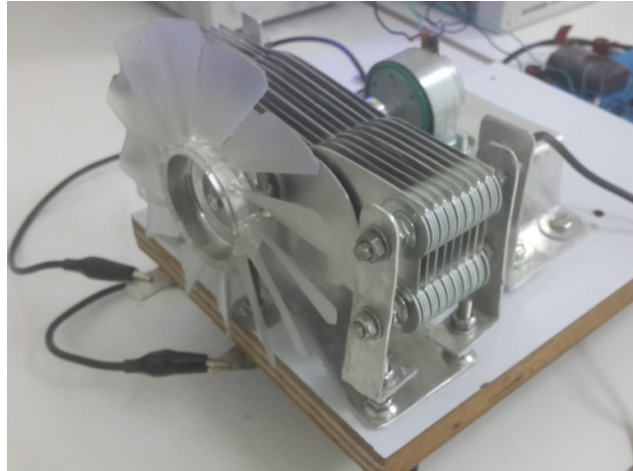
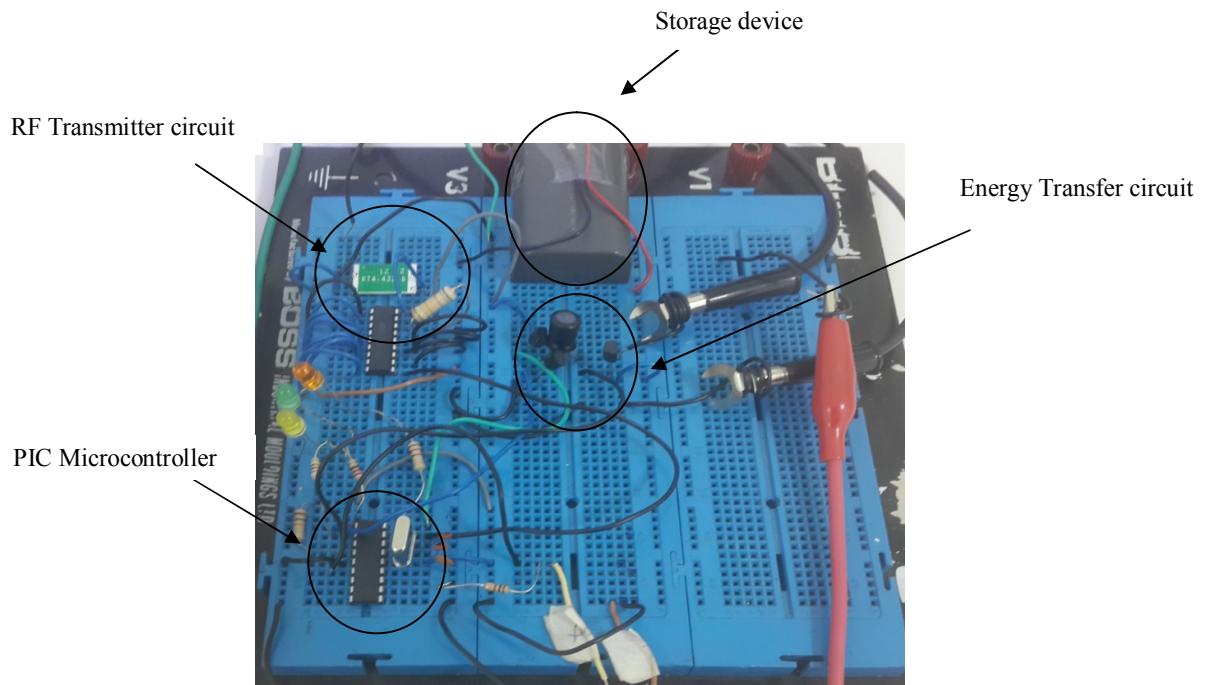


Figure 6.34: Experimental setup of the electrical part of the harvester

A photograph of the electrostatic harvester experimental setup in the electronics laboratory is shown in Figure 6.35 (a) and (b). The physical dimension of the capacitor is $85 \text{ mm} \times 145 \text{ mm} \times 85 \text{ mm}$. When wind blows at the harvester, DC current is generated and directed into the Lithium ion battery by the LC to LC energy transfer circuit.



(a)



(b)

Figure 6.35: Photograph of the electrostatic based wind energy harvester (a) Second prototype of the variable capacitor and (b) the electrical circuit of the harvester

The capacitance was measured using the GW-INSTEK 816 LCR meter as shown in Figure 6.36. The minimum and maximum capacitances of the variable capacitor were measured as

168 pF and 430 pF. The capacitor second prototype used is a two pole capacitor capable of harvesting energy twice within a single rotation. The results of the capacitance measurement are shown in Figure 6.37.



Figure 6.36: LCR meter and the variable capacitor prototype

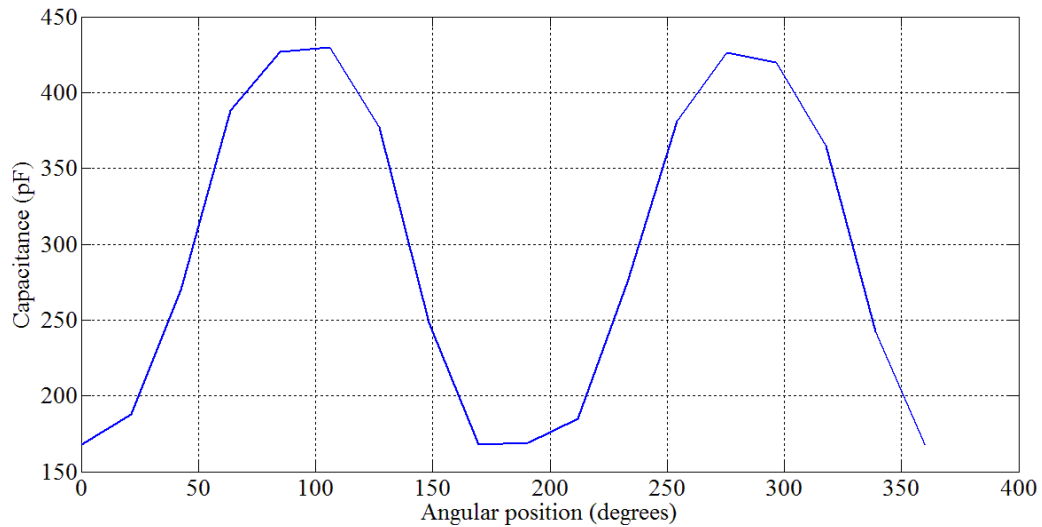


Figure 6.37: Capacitance variation with angular position for the prototype device

The sensor used for monitoring the capacitance in this setup is an inductive proximity switch. Whenever the sensor detects the maximum capacitance C_{\max} , a signal is sent to the

controller to start the pre-charge phase followed by the harvesting and the reset phases. Before the start and the end of the harvesting cycle, the PIC sends signals to the RF transmitter. The data is then displayed on the digital storage oscilloscope to calculate the wind speed that would be detected by the receiver.

Referring to Figure 6.38 (a), the voltage across the capacitor was captured for many harvesting cycles. The time of the pre-charge phase was set in micro seconds while the time of the harvesting phase was measured in msec according to the speed of rotation. As soon as the capacitor reaches the maximum voltage, the harvesting phase starts and then the voltage across the capacitor starts to decrease to the minimum voltage of 1.32 V in 355 msec. After that, the cycle starts again. The capacitor voltage was measured using the digital storage oscilloscope. The experimental results compared with the simulation results as shown in Figure 6.38 (b).

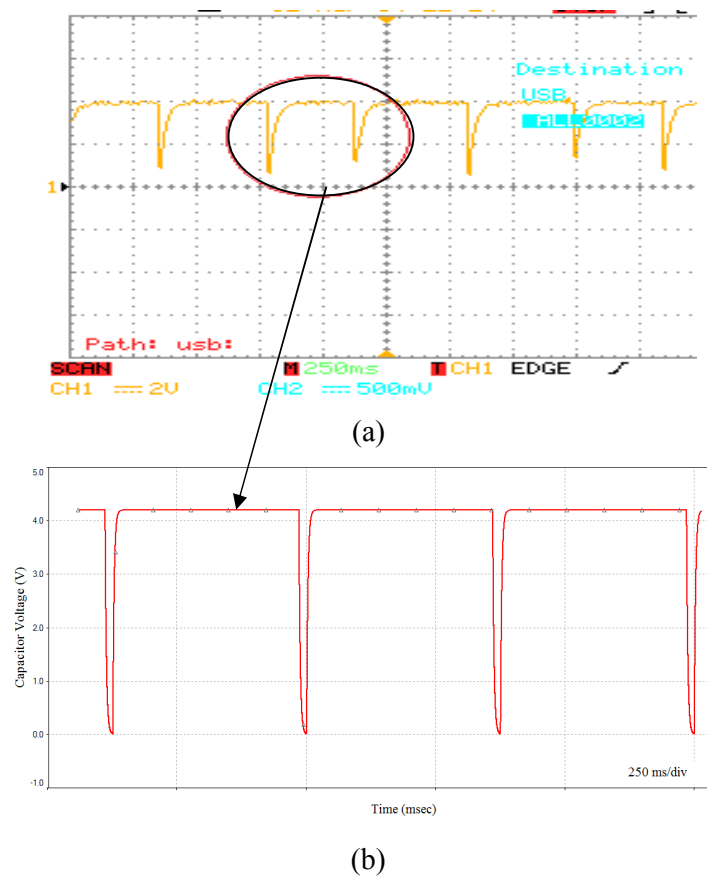


Figure 6.38: Waveform of the capacitor voltage (a) experimental results (b) simulation results

The amount of harvested current measured was 0.068 μA which was calculated to be 0.0755 μA (percentage error of 9.9%) while in simulation it was measured as 0.0740 μA (percentage error of 8.1%). The similar results of the calculated, simulated and measured data give confidence in the accuracy of the experiment.

The energy required by the RF transmitter depends on the data being transmitted. As mentioned earlier the transmission time required for 12 bits of data is around 20 msec. For the purpose of this experiment, the active time of transmission is set to 1 msec therefore the power consumed by the RF transmitter during this time will only be considered. The trigger signal for 1 msec sent by the controller is an indication of the starting point of the harvesting cycle as illustrated in Figure 6.39 which shows the waveform of the data at the RF transmitter end. The data would be used to calculate the wind speed by measuring the time between two consecutive pulses. The experimental results have verified that the RF transmitter is able to successfully transmit data. However, the energy required for the transmission is higher than the harvested energy during one cycle. Thus the harvested energy must be stored in a storage capacitor before being used to perform transmission functions as soon as enough energy is available. Moreover, further improvements to the capacitor structure, the control mechanism and the battery type are essential to be able to use energy harvested by the electrostatic harvester efficiently to transmit data in a wireless manner.

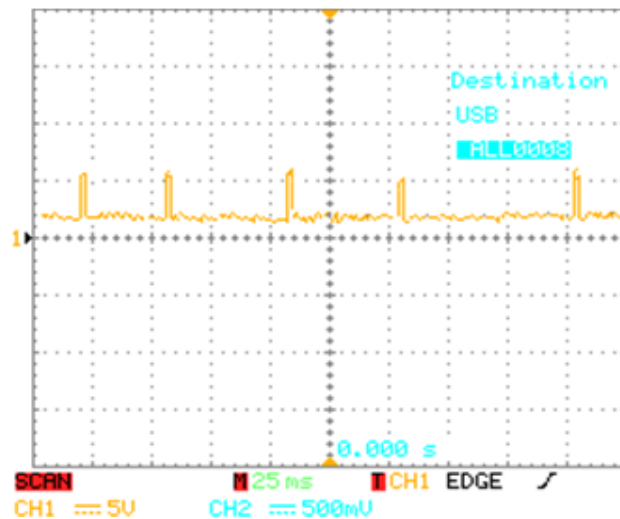


Figure 6.39: Waveform collected at the RF transmitter output

6.4 SUMMARY

This chapter described the various simulation and experiments necessary to test the wind harvester. The simulation involved the testing of the pre-charge, harvest and the rest phase, the testing of one, two, four and eight multi pole capacitors, the energy harvested using the various capacitors, the capacitance and volume optimisation, the testing of the MPCA and finally the energy optimisation. Results from the simulation were discussed and compared.

The experiments involved the testing of two capacitor prototypes and the testing of basic operation of a complete harvester with the RF transmitter. The first prototype of the variable capacitor was tested using the LCR meter. An AutoCAD model was used to calculate the effective area between the stator and the rotor. After that, the total capacitance variation with angular position was determined using Matlab. Simulation results showed a capacitance variation between 83 pF to 0 pF while the experimental measurements show that the capacitance of the device varies from 110 pF to 39 pF due to the presence of parasitic capacitance. The simulation transient response test showed that the settling time for the capacitor at maximum is 5.5 μ sec and at minimum it is 2 μ sec while the experimental transient response showed that the settling time for the capacitor at maximum is 8.8 μ sec and at minimum it is 5.5 μ sec. The second prototype was attached to a gear box and a micro wind turbine to convert mechanical energy to electrical energy. The variable capacitor was then connected to the electronic circuit that consist of the energy transfer circuit, the PIC microcontroller, the RF transmitter circuit and the storage device. The harvested energy measured can be increased if a better prototype is constructed, perhaps using the MPCA model. A better controlling mechanism is required such as the XLP microcontroller with sleep mode could be used to successfully transmit the data in a wireless manner and a better storage is required by using a small capacitor between the harvester and the RF transmitter.

CHAPTER 7

CONCLUSION AND FURTHER WORK

This thesis has been concerned with the design of an electrostatic-based wind energy harvester. The wind harvester consists of two main sub-systems (the wind-capturing device and the electrostatic converter). In order to design an optimised harvester system, it is necessary to understand how each subsystem operates individually and the relationship between them. This chapter describes the technical contributions and achievements of the work presented in this thesis.

7.1 CONCLUSION

This thesis focused on wind energy harvesting using an electrostatic converter. First, it introduced energy harvesting systems and reviewed three main types of mechanical energy converters to determine the most suitable converter for wind energy harvesting. The electrostatic converters were selected based on the advantages of these converters over the other types; they are compact, sensitive to low level mechanical energy, easier to integrate in small scale systems, not requiring smart materials, simple to fabricate, inexpensive and simply structured using less circuitry.

A literature review of the electrostatic energy harvesters was presented for various types of variable capacitor structures and energy conversion mechanisms. This review of previous work helped in establishing general design considerations, including all the factors affecting the design of the harvester. These design factors also helped in developing the design procedure to be used in designing an electrostatic device for wind energy harvesting. The thesis then discussed the operating principles of an electrostatic-based wind energy harvester by providing the theoretical background for the capturing device, variable capacitor, energy transfer circuits, capacitance sensing circuits and controlling systems.

Novel electrostatic energy harvesters were then designed and simulated using Simulink / Matlab software. The main challenge in designing the energy harvester was to achieve

maximum power output from wind energy using the capacitive converter. The choice of capacitor structure depends on the optimum design to harvest maximum energy from the wind. This study found that a multi-pole variable capacitor was the optimum model since it can operate with rotational mechanical energy, produces the greatest net energy gain, and can be modified by adding more poles or using an array of capacitors. As a result, this study was able to propose a novel design of multi-pole capacitor array that can produce more energy than a single variable capacitor. The proposed capacitors were simulated to determine the amount of energy harvested under various wind speed conditions. The simulation results were within very low margin of error compared to theoretical calculations. The complete harvester system was then evaluated in order to offer recommendations to improve the overall system's performance and efficiency.

This work makes several major contributions to the literature concerning wind energy harvesting. First, it developed general design considerations and a design procedure for producing an electrostatic energy harvester. It revealed five factors that influence the design of the harvester: type of mechanical energy, variable capacitor structure, variable capacitor material, energy transfer strategy and type of storage device. The design procedure was developed based on these factors. The type of mechanical energy was first selected according to the energy source and type of capturing devices. After that, a variable area capacitor structure was chosen. Aluminium was preferred for the capacitor plate material based on cost and precision factors. With regard to the energy transfer strategy, this study found that the decision depends on the mode of operation, with either a voltage-constrained or charge-constrained system, inductive energy transfer circuits were found most suitable for the harvester. Finally, the lithium ion battery or super capacitor could be selected as the storage device due to the short charging time, relatively low self-discharge rates and low maintenance requirements.

This study's second main contribution is that it investigated the possibility of harvesting wind energy using the electrostatic approach. Based on the design factors and design procedure, it was possible to develop a novel electrostatic-based wind energy harvester, providing detailed explanation and mathematical analysis of the block diagram and operation cycle. In this design, the harvesting cycle starts by converting wind energy into rotational energy using a micro wind turbine. This energy is then fed into a multi-pole variable capacitor. This is made of aluminium as it is inexpensive, highly conductive and can be

easily formed into sector-shaped capacitor plates. The capacitor is then connected to an inductive LC to LC energy transfer circuit that conducts the additional harvested energy into a Li-Ion battery. The energy produced can be stored in the battery to power small permanently operational devices, located in relatively inaccessible places, while consuming just a few milli or micro watts. For the purposes of this research, the selected application was a low power independent wind speed sensor that sent wind speed data to an RF transmitter proposed and demonstrated with an experimental setup.

The third contribution of this thesis was to determine the optimal design for the electrostatic harvester. First, various inductive energy transfer circuits were compared to identify the most efficient energy transfer strategy. The optimized circuit was found to be the LC to LC circuit. Second, capacitance optimisation was carried out. The optimised capacitor chosen was a multi-pole variable capacitor that improves the capability of energy harvesting during one cycle. A multi-pole capacitor array MPCA was proposed and demonstrated. Such an array has many valuable characteristics for improving the amount of harvested energy. The results from this study indicated that energy harvesting could be increased by modifying the number of poles, the number of capacitors in the array or the battery voltage. Energy optimisation was then used to determine the optimum effective energy and corresponding device parameters. These results also helped to identify the amount of wind speed data that could be transmitted via the RF transmitter. The energy estimates provide enough power to operate an RF transmitter to transmit information using wireless technology. A typical RF transmitter consumes 132 μJ to transmit data in 10 msec (13.2 mW). For example, if the harvested energy is 1,320 μJ at certain values of A_{eff} , d , N_{Pole} , N_{SR} and V_{Bat} then the energy would be enough to transmit data for 100 msec.

7.2 SUGGESTIONS FOR FURTHER WORK

This thesis suggests several possible avenues of research that remain open for further exploration. These will now be discussed.

This study focused on the design of an optimised electrostatic harvester using a multi-pole variable capacitor array (MPCA). However, experimental testing was not performed using the optimised capacitor model. Although the prototypes developed in this work successfully

converted wind into electrical energy, there are certainly many parameters and design factors that could be manipulated to improve the efficiency of wind energy harvesting. For example, an array of small micro wind turbine connected to the MPCA could be used in various applications for battery charging purposes. Once the device is placed in a windy location, the micro turbines would rotate to allow the MPCA to convert mechanical into electrical power. Thus future research could move towards building and testing a harvester that follows the optimisation results of this study, using micro wind turbines linked to an MPCA that can be used to power sophisticated wireless sensor nodes to send various types of data.

This study tested the electrical component of the harvester system on a vero-board using off-the-shelf components and a programmable controller. The performance of the converter circuit could be improved in the future by fabricating the semiconductor switches, inductors and the capacitance sensing components onto silicon chip with a super capacitor as storage device. This would be another major research project that could increase the efficiency of the overall system.

This study restricted the simulation and experimental testing of the harvester to certain wind conditions under the assumption that wind speed is constant during the harvesting cycles. However, in real life, wind speed is variable so the harvester proposed here needs to be tested in a wind tunnel to provide more accurate and realistic results. Furthermore, interfacing the harvester system with the storage devices of various applications should be investigated in order to identify the appropriate interface circuit and charging periods of various applications.

7.3 PUBLICATIONS ARISING FROM THIS WORK

7.3.1 Peer reviewed Journals

Abdulmunam, RT, Taha, LY & Ivey, PC 2013, 'Simulation and Experimental Modelling of a Multi-Pole Variable Capacitor for Electrostatic Wind Energy Harvester', *Turkish journal of electrical engineering and computer sciences*, Turkey.

Abdulmunam, RT, Taha, LY & Ivey, PC 2011, 'Design Consideration for Electrostatic Energy Harvester', *Journal of Applied Mechanics and Materials*, pp.110-116.

7.3.2 Conferences

Abdulmunam, RT, Taha, LY & Ivey, PC 2014, 'Wind Energy Harvesting using Electrostatic Converter for Wireless Sensor Networks', *Optimization of Electrical and Electronic Equipment (OPTIM), 14th International Conference*, Romania, accepted for publication.

Abdulmunam, RT, Taha, LY & Ivey, PC 2012, 'Simulation and Experimental Study of a Multi-Pole Variable Capacitor for Electrostatic Wind Energy Harvester', *International conference on electronics, computer and computation (ICECCO)*, Turkey.

Abdulmunam, RT, Taha, LY & Ivey, PC 2012, 'Modelling of Low Power Electrostatic Wind Energy Harvester for Macro Scale Applications', *International conference of information and electronics engineering (ICIEE)*, Singapore.

Abdulmunam, RT, Taha, LY & Ivey, PC 2012, 'Simulink Model of an Integrated Rotary Electrostatic Energy Harvester', *Optimization of Electrical and Electronic Equipment (OPTIM), 13th International Conference*, Romania, pp. 1006–1011.

Abdulmunam, RT, Taha, LY & Ivey, PC 2011, 'Design Consideration for Electrostatic Energy Harvester', *International conference of power and energy engineering (ICPEE)*, Thailand, pp.110-116.

APPENDIX A

ENERGY TRANSFER CIRCUITS

LC to LC energy transfer circuit mathematical analysis

Stage 1

$$V_s = V_R + V_L + V_C$$

$$V_s = iR + L \frac{di}{dt} + \frac{1}{C} \int i dt \quad (A.1)$$

$$V_s = iR + L \frac{di}{dt} + V_C \quad (A.2)$$

$$i = C \frac{dV_C}{dt} \quad (A.3)$$

From (A.2) and (A.3):

$$V_s = LC \frac{d^2 V_C}{dt^2} + RC \frac{dV_C}{dt} + V_C$$

or :

$$\ddot{V}_C + \frac{R}{L} \dot{V}_C + \frac{1}{LC} V_C = \frac{1}{LC} V_s$$

Taking Laplace transform of (A.4) for V_C :

$$V_C(s) = \frac{\frac{1}{LC}}{s\left(s^2 + \frac{R}{L}s + \frac{1}{LC}\right)} \cdot V_{Bat} \quad (A.4)$$

$$\text{Let } \omega_n = \frac{1}{\sqrt{LC}} \text{ and } 2\zeta\omega_n = \frac{R}{L}$$

$$\zeta = 0.5 R \frac{\sqrt{C}}{\sqrt{L}}$$

$$V_C(t) = V_{Bat} \left[1 - \frac{1}{\sqrt{1-\zeta^2}} e^{-\zeta \omega_n t} \sin(\omega_n \sqrt{1-\zeta^2} t + \phi) \right] \quad (A.5)$$

where: $\emptyset = \cos^{-1}\zeta$

From (A.3) and (A.5):

$$i(t) = C \frac{dV_c}{dt} = C \cdot V_{Bat} \left[\frac{-1}{\sqrt{1-\zeta^2}} \right] \left[\omega_n \sqrt{1-\zeta^2} \cos(\omega_n \sqrt{1-\zeta^2} t + \emptyset) e^{-\zeta \omega_n t} - \zeta \omega_n \sin(\omega_n \sqrt{1-\zeta^2} t + \emptyset) e^{-\zeta \omega_n t} \right]$$

$$\cos \emptyset = \frac{\zeta \omega_n}{\omega_n} = \zeta$$

$$\sin \emptyset = \frac{\omega_n \sqrt{1-\zeta^2}}{\omega_n} = \sqrt{1-\zeta^2}$$

$$\text{Let } \omega_n \sqrt{1-\zeta^2} = \omega_d$$

$$\therefore i(t) = C V_{Bat} \left[\frac{\omega_n}{\sqrt{1-\zeta^2}} \right] \left[e^{-\zeta \omega_n t} \right] [\sin(\omega_d t + \emptyset) \cos \emptyset - \cos(\omega_d t + \emptyset) \sin \emptyset]$$

$$\therefore i(t) = \frac{C V_{Bat} \omega_n}{\sqrt{1-\zeta^2}} \cdot e^{-\zeta \omega_n t} \cdot \sin(\omega_d t + \emptyset - \emptyset)$$

$$\therefore i(t) = \frac{C V_{Bat} \omega_n}{\sqrt{1-\zeta^2}} \cdot e^{-\zeta \omega_n t} \cdot \sin(\omega_n \sqrt{1-\zeta^2} t) \quad (\text{A.6})$$

Note:

For small damping: $\zeta \ll 1 \quad \therefore \zeta^2 \approx 0$

Thus equation (A.6) can be simplified to:

$$i(t) \approx C V_{Bat} \omega_n \sin(\omega_n t) \quad (\text{A.7})$$

Using (A.9):

$$E_c = \int_0^t P_c(t) dt = \int_0^t i(t) V_c(t) dt$$

$$E_c = \int_0^t C \frac{dV_c}{dt} V_c(t) dt = \frac{1}{2} C V_c^2(t)$$

$$E_c \cong \frac{1}{2} CV_{Bat}^2 [1 - \sin(\omega_n t + \emptyset)] \Rightarrow \text{assuming } \sqrt{1 - \zeta^2} \approx 1 \text{ then } e^{-\zeta \omega_n t} \cong 1$$

$$E_c = \frac{1}{2} CV_{Bat}^2 [1 - \cos(\omega_n t)]^2 \quad (\text{A.8})$$

$$E_L = \int_0^t P_L(t) dt = \int_0^t i(t) V_L(t) dt$$

$$E_L = \int_0^t i(t) \frac{di}{dt} dt = \frac{1}{2} Li(t)^2$$

$$E_L \approx \frac{1}{2} L(CV_{Bat} + \omega)^2 \sin^2(\omega_n t) \quad (\text{A.9})$$

$$E_L = \frac{1}{2} CV_{Bat}^2 \sin^2 \omega_n t$$

$$E_R = \int_0^t i^2 \cdot R dt \approx R \int_0^t (CV_{Bat} + \omega_n)^2 \sin^2 \omega_n t dt$$

$$\text{since } \cos 2\omega_n t = 1 - 2 \sin^2 \omega_n t$$

$$\therefore \sin^2 \omega_n t = \frac{1}{2} - \frac{1}{2} \cos 2\omega_n t$$

$$E_R \cong R(CV_{Bat} + \omega_n)^2 \int_0^t \left(\frac{1}{2} - \frac{1}{2} \cos 2\omega_n t\right) dt$$

$$E_R \cong \frac{R}{2} (CV_{Bat} + \omega_n)^2 \left[t - \frac{1}{2\omega_n} \sin 2\omega_n t \right] \quad (\text{A.10})$$

From (A.8) and (A.9):

$$E_c + E_L = \frac{1}{2} CV_{Bat}^2 [1 - \cos \omega_n t]^2 + \frac{1}{2} LC^2 V_{Bat}^2 \omega_n^2 \sin^2 \omega_n t$$

$$E_c + E_L = \frac{1}{2} CV_{Bat}^2 [(1 - \cos \omega_n t)^2 + \sin^2 \omega_n t]$$

$$E_c + E_L = \frac{1}{2} CV_{Bat}^2 [1 + \cos^2 \omega_n t - 2 \cos \omega_n t + \sin^2 \omega_n t]$$

$$E_c + E_L = \frac{1}{2} CV_{Bat}^2 [2 - 2 \cos \omega_n t]$$

$$E_c + E_L = CV_{Bat}^2 [1 - \cos \omega_n t]$$

$$\text{At } t = \frac{2\pi}{\omega_n}, \quad E_c + E_L = CV_{Bat}^2 \left[1 - \cos \frac{\omega_n 2\pi}{\omega_n} \right] = \frac{1}{2} CV_{Bat}^2 \quad (\text{A.11})$$

Summary of assumptions:

- 1) Negligible damping, i.e., $\zeta \cong 0$ Thus $\cos^{-1} \zeta = \cos^{-1} 0 = 90^\circ$
- 2) $e^{-\zeta \omega_n t} \approx 1$
- 3) $\sqrt{1 - \zeta^2} \approx 1$
- 4) $\sin(\omega_n \sqrt{1 - \zeta^2} t + \phi) \cong \sin(\omega_n t + 90^\circ)$
- 5) If $t = \frac{2\pi}{\omega_n}$ $E_c + E_L = \frac{1}{2} CV_{Bat}^2$

Stage 2

$$V_R + V_L + V_C = 0$$

$$iR + L \frac{di}{dt} + V_C = 0 \quad (\text{A.12})$$

$$i = C \frac{dV_C}{dt} \quad (\text{A.13})$$

$$RC \frac{dV_C}{dt} + LC \frac{d^2 V_C}{dt^2} + V_C = 0$$

or:

$$\ddot{V}_C + \frac{R}{L} \dot{V}_C + \frac{1}{LC} V_C = 0$$

Solution using the Laplace transform:

$$s^2 v_c(s) - s v_c(0) - v_c(0) + \frac{R}{L} (s v_c(s) - v_c(0)) + \frac{1}{LC} v_c(s) = 0$$

$$\left(s^2 + \frac{R}{L} s + \frac{1}{LC} \right) v_c(s) = s v_c(0) + v_c(0) + \frac{R}{L} v_c(0)$$

$$\text{Let } v_c(0) = a \text{ and } v_c(0) + \frac{R}{L} v_c(0) = b$$

$$\therefore V_c(s) = \frac{as + b}{s^2 + \frac{R}{L}s + \frac{1}{LC}}$$

From Laplace inverse table :

$$\mathcal{L}^{-1} \frac{s + \alpha}{(s + \alpha)^2 + w^2} = e^{-\alpha t} \cos wt$$

$$\mathcal{L}^{-1} \frac{w}{(s + \alpha)^2 + w^2} = e^{-\alpha t} \sin wt$$

Solving for V_C :

$$V_c(s) = \frac{SV_C(0) + V_c(0) + \frac{R}{L}V_C(0)}{s^2 + \frac{R}{L}s + \frac{1}{LC}} \quad (A.14)$$

$$V_c(s) = V_C(0) \cdot \frac{SV_C(0) + \frac{V_c(0)}{V_C(0)} + \frac{R}{L}}{s^2 + \frac{R}{L}s + \frac{1}{LC}}$$

$$V_c(s) = V_C(0) \cdot \frac{S + \frac{V_c(0)}{V_C(0)} + \frac{R}{L}}{s + \frac{R}{L}s + \frac{R^2}{4L^2} + \frac{1}{LC} - \frac{R^2}{4L^2}}$$

$$V_c(s) = V_C(0) \cdot \frac{S + \frac{R}{L} + \frac{V_c(0)}{V_C(0)}}{(s + \frac{R}{2L})^2 + \frac{1}{LC} - \frac{R^2}{4L^2}}$$

$$V_c(s) = V_C(0) \left[\frac{S + \frac{R}{L}}{(s + \frac{R}{2L})^2 + \frac{1}{LC} - \frac{R^2}{4L^2}} + \frac{\frac{R}{2L} + \frac{V_c(0)}{V_C(0)}}{(s + \frac{R}{2L})^2 + \frac{1}{LC} - \frac{R^2}{4L^2}} \right]$$

where:

$$\beta = \frac{R}{2L} + \frac{v_c(0)}{V_C(0)}$$

Assuming:

$$V_C(0) = V_{C(Final)} \text{ of Stage1} = \frac{V_{Bat}}{2}$$

$$V_C(t) = V_{Bat}(1 - \cos \omega_n t)$$

$$v_c(t) = \omega_n V_{Bat} \sin \omega_n t$$

Assume:

$$\alpha = \frac{R}{2L}$$

$$\omega = \sqrt{\frac{1}{LC} - \frac{R^2}{4L^2}}$$

$$\therefore V_C(t) = V_C(0) \left[e^{-\alpha t} \cos \omega t + \frac{\beta}{\omega} e^{-\alpha t} \sin \omega t \right]$$

Note that:

$$\omega = \sqrt{\frac{1}{LC} - \frac{R^2}{4L^2}}$$

$$s^2 + \frac{R}{L}s + \frac{1}{LC} = s^2 + 2\zeta\omega_n s + \omega_n^2$$

$$\omega_n = \frac{1}{\sqrt{LC}}$$

$$\zeta = \frac{1}{2} \frac{R}{\omega_n L}$$

$$\zeta = \frac{LC}{2} \frac{R}{L}$$

$$\zeta = \frac{R}{L} \sqrt{\frac{C}{L}}$$

$$\omega = \sqrt{\frac{1}{LC} - \frac{4\omega_n^2 L^2 \zeta^2}{4L^2}}$$

$$\omega = \sqrt{\omega_n^2 - \omega_n^2 \zeta^2}$$

$$\omega = \omega_n \sqrt{1 - \zeta^2}$$

For low ζ , $\zeta \approx 0$, $\omega \cong \omega_n$

$$\therefore V_C(t) = V_C(0) \left[e^{-\alpha t} \cos \omega_n t + \frac{\beta}{\omega_n} e^{-\alpha t} \sin \omega_n t \right]$$

$$\beta = \frac{R}{2L} + \frac{V_C(0)}{V_C(0)}$$

$$\frac{\beta}{\omega_n} = \frac{1}{\omega_n} \left[\frac{R}{2L} + \frac{\omega_n V_{Bat} \sin \pi/3}{V_{Bat} (1 - \cos \pi/3)} \right]$$

$$\frac{\beta}{\omega_n} = \frac{1}{\omega_n} \left[\omega_n \zeta + \frac{\omega_n \sin \pi/3}{(1 - \cos \pi/3)} \right] = \zeta + \frac{\sqrt{3}}{2(1 - 0.5)} = \zeta + \sqrt{3} \approx \sqrt{3}$$

$$V_C(t) = V_C(0) [\cos \omega_n t + \sqrt{3} \sin \omega_n t]$$

$$\therefore i(t) = C \frac{dV_C}{dt}$$

$$V_C(t) = CV_C(0) [\sqrt{3} \omega_n \cos \omega_n t - \omega_n \sin \omega_n t]$$

$$i(t) = V_C(0) \sqrt{\frac{C}{L}} [\sqrt{3} \cos \omega_n t - \sin \omega_n t]$$

Substituting $V_C(0)$ by $V_{C\text{Final}}$ of Stage1 which is equal to $\frac{1}{2} V_{Bat}$:

$$V_C(t) = V_{Bat} \sin(\omega_n t + 30^\circ) \tag{A.15}$$

$$i(t) = \sqrt{\frac{C}{L}} V_{Bat} \cos(\omega_n t + 30^\circ) \tag{A.16}$$

For energy study:

$$E_C = \int_0^t i(t) V_C(t) dt = \int_0^t C \frac{dV_C}{dt} V_C dt$$

$$E_C = \frac{1}{2} C V_C^2(t)$$

$$E_C = \frac{1}{2} C V_{Bat}^2 \sin^2(\omega_n t + 30^\circ) \tag{A.17}$$

$$E_L = \int_0^t i(t)V_L(t) = \int_0^t i(t)L \frac{di}{dt} dt$$

$$E_L = \frac{1}{2}Li(t)^2$$

$$E_L = \frac{1}{2}L \cdot \frac{C}{L} V_{Bat}^2 \cos^2(\omega_n t + 30^\circ)$$

$$E_L = \frac{1}{2}C V_{Bat}^2 \cos^2(\omega_n t + 30^\circ) \quad (A.18)$$

$$E_R = \int_0^t Ri(t)^2 dt = R \frac{C}{L} V_{Bat}^2 \int_0^t \cos^2(\omega_n t + 30^\circ) dt$$

$$E_R = \frac{RC}{L} V_{Bat}^2 \int_0^t \frac{1}{2} dt + \frac{1}{2} \cos(2\omega_n t + \frac{\pi}{6}) dt$$

$$E_R = \frac{RC}{L} V_{Bat}^2 \left[\frac{t}{2} + \frac{\sin(2\omega_n t + \frac{\pi}{6})}{4\omega_n} \right]$$

$$E_R = \frac{RC}{L} V_{Bat}^2 \left[\frac{1}{2}t + \frac{\sin(2\omega_n t + 30^\circ) - \sin(30^\circ)}{4\omega_n} \right] \approx 0 \quad (A.19)$$

Energy losses in the resistor is approximately 0 because $\frac{RC}{L} \approx 0$

$$V_L(t) = L \frac{di}{dt} = L \sqrt{\frac{C}{L}} V_{Bat} (-\omega_n) \sin(\omega_n t + 30^\circ)$$

$$V_L(t) = -V_{Bat} \sin(\omega_n t + 30^\circ)$$

$$V_R(t) = iR$$

$$V_R(t) = R \sqrt{\frac{C}{L}} V_{Bat} \cos(\omega_n t + 30^\circ)$$

$$\frac{V_C(t)}{V_L(t)} = \frac{V_{Bat} \sin(\omega_n t + 30^\circ)}{-V_{Bat} \sin(\omega_n t + 30^\circ)} = -1$$

$$V_C(t) + V_L(t) = 0$$

For:

$$V_R(t) = R \sqrt{\frac{C}{L}} V_{Bat} \cos(\omega_n t + 30^\circ)$$

$$\zeta = 0.5R \sqrt{\frac{C}{L}}$$

$$V_R(t) = 2\zeta V_{Bat} \cos(\omega_n t + 30^\circ) \approx 0 \text{ because } \zeta \ll 1 \quad (\text{A.20})$$

L to LC energy transfer circuit mathematical analysis

Stage 1

$$I_o = \frac{V_{Bat}}{R}$$

$$i = \frac{V_{Bat}}{R} (1 - e^{-\frac{R}{L}t}) \quad (\text{A.21})$$

$$i = I_o (1 - e^{-\frac{t}{\tau}})$$

where: $\tau = \frac{L}{R} \Rightarrow \text{Time constant}$

$$\text{at } t = 0, \quad V_L = \frac{LI_o}{\tau} = L \frac{\frac{V_{Bat}}{R}}{\frac{L}{R}} = V_{Bat}$$

$$V_R = iR = V_{Bat} (1 - e^{-\frac{R}{L}t}) \quad (\text{A.22})$$

$$V_L = V_{Bat} - V_R = V_{Bat} e^{-\frac{R}{L}t} \quad (\text{A.23})$$

$$V_{Bat} = i.R + V_L$$

$$V_L = L \frac{di}{dt}$$

$$\therefore i = \frac{1}{L} \int V_L dt$$

$$\therefore V_{Bat} = \frac{R}{L} \int V_L dt + V_L$$

$$\frac{dV_L}{dt} + \frac{R}{L} V_L = \frac{dV_{Bat}}{dt}$$

Alternative method :

$$\left(S + \frac{R}{L}\right) V_L(s) = s \cdot V_{Bat}(s)$$

$$\therefore V_L(s) = \frac{S}{S + \frac{R}{L}} \cdot \frac{V_{Bat}}{S}$$

$$\therefore V_L(t) = V_{Bat} e^{-\frac{R}{L}t}$$

$$E_L = \frac{1}{2} L i^2 \tag{A.24}$$

$$E_L = \frac{1}{2} L \left(\frac{V_{Bat}}{R}\right)^2 \left(1 - e^{-\frac{t}{\tau}}\right)^2$$

At $t = t_{\text{Final}}$ the energy in the inductor must be equal to the energy of the capacitor when $C = C_{\text{max}}$

$$\therefore E_L = \frac{1}{2} C_{\text{max}} \cdot V_{Bat}^2 = \frac{1}{2} L \left(\frac{V_{Bat}}{R}\right)^2 [1 - e^{-\frac{t}{\tau}}]^2$$

$$\therefore \frac{R^2 C_{\text{max}}}{L} = [1 - e^{-\frac{t}{\tau}}]^2$$

$$\frac{R\sqrt{C_{\text{max}}}}{\sqrt{L}} = 1 - e^{-\frac{t}{\tau}}$$

$$e^{-\frac{t}{\tau}} = 1 - \frac{R\sqrt{C_{\text{max}}}}{\sqrt{L}} = \frac{\sqrt{L} - R\sqrt{C_{\text{max}}}}{\sqrt{L}}$$

$$\frac{-t}{\tau} = \ln \frac{\sqrt{L} - R\sqrt{C_{\text{max}}}}{\sqrt{L}}$$

$$\therefore t = \frac{L}{R} \ln \frac{\sqrt{L}}{\sqrt{L} - R\sqrt{C_{\text{max}}}} \tag{A.25}$$

Approximation using Taylor series:

Since Taylor series is $1 - \left[1 - \frac{t}{\tau} + \frac{t^2}{2\tau^2} - \frac{t^3}{6\tau^3} \dots\right] \approx 1 - \left(1 - \frac{t}{\tau}\right) = \frac{t}{\tau} = \frac{t}{L} \cdot R$

Thus $\frac{R}{\sqrt{L}} \sqrt{C_{max}} = 1 - e^{\frac{-t}{\tau}}$

$$\frac{R\sqrt{C_{max}}}{\sqrt{L}} = \frac{t}{L} R$$

$$t = \sqrt{LC_{max}} \quad (\text{A.26})$$

Stage 2

$$I_{Final} = \frac{V_{Bat}}{R} (1 - e^{\frac{-\sqrt{CL}}{\tau}})$$

$$I_{Final} = \frac{V_{Bat}}{R} \left[1 - e^{\frac{\sqrt{CL}}{L} \cdot R}\right]$$

$$I_{Final} \approx \frac{V_{Bat}}{R} \left[1 - \left(1 - \frac{R\sqrt{C}}{\sqrt{L}}\right)\right] \quad (\text{A.27})$$

$$I_{Final} \approx \frac{V_{Bat}}{R} \cdot \frac{R\sqrt{C}}{\sqrt{L}} = \sqrt{\frac{C}{L}} V_{Bat}$$

$$\text{For Stage1 } i(t) = \frac{V_{Bat}}{R} \left(1 - e^{\frac{-t}{\tau}}\right)$$

$$\text{When } (t = t_{Final}) \quad \frac{di}{dt} = \frac{V_{Bat}}{R} \cdot \frac{1}{\tau} \cdot e^{\frac{-t}{\tau}} \approx \frac{V_{Bat}}{R} \cdot \frac{1}{L} \cdot R \cdot \left[1 - \frac{\sqrt{CL}}{L} \cdot R\right]$$

$$\frac{di}{dt} = \frac{V_{Bat}}{R} \left[1 - R \frac{\sqrt{C}}{\sqrt{L}}\right]$$

Note:

$$\text{When } (t = t_{Final}) \quad \frac{di}{dt} = \frac{V_{Bat}}{R} \cdot \frac{R}{L} e^{\frac{-\sqrt{CL}}{L} R} = \frac{V_{Bat}}{L} \cdot e^{-R \sqrt{\frac{C}{L}}}$$

Also:

$$i(t = t_{Final}) = C \frac{dV_C}{dt}$$

$$\therefore \frac{dV_C}{dt} = \frac{1}{C} \cdot \sqrt{\frac{C}{L}} V_{Bat} = \frac{V_{Bat}}{\sqrt{LC}} = \omega_n V_{Bat}$$

From previous analysis :

$$V_C(s) = \frac{sV_C(0) + V_C(0) + \frac{R}{L}V_C(0)}{s^2 + \frac{R}{L}s + \frac{1}{LC}} \quad (A.28)$$

$$V_C(s) = \frac{\omega_n}{\left(s + \frac{R}{2L}\right)^2 + \omega_n^2}$$

Since the Laplace inverse of $\frac{w}{(s+\alpha)^2+w^2} = e^{-\alpha t} \cdot \sin \omega t$

$$\therefore V_C(t) = V_{Bat} \cdot e^{-\alpha t} \sin \omega t \quad (A.29)$$

$$V_C(t) \approx V_{Bat} \sin \omega t \text{ for } \alpha \ll 1 \quad (A.30)$$

$$i = C \frac{dV_C}{dt} = C\omega V_{Bat} \cos \omega t \quad (A.31)$$

$$E_c(t) = \frac{1}{2} C V_C(t)$$

$$E_c(t) = \frac{1}{2} C V_{Bat}^2 \cdot e^{-\alpha t} \cdot \sin^2 \omega t$$

$$E_c(t) = \frac{1}{2} C V_{Bat}^2 \left[\frac{1}{2} - \frac{1}{2} \cos 2\omega_n t \right] \quad (A.32)$$

$$\cos 2\omega_n t = -1$$

$$\therefore 2\omega_n t = \pi$$

$$t = \frac{\pi}{2\omega_n} = \frac{2\pi}{4\omega_n}$$

$$V_L(t) = L \frac{d_i}{d_t} = L [C\omega_n V_{Bat}] [-\omega] \sin \omega_n t$$

$$V_L(t) = -C\omega^2 L V_{Bat} \cdot \sin \omega_n t = -V_{Bat} \cdot \sin \omega_n t$$

$$E_L = \frac{1}{2} Li^2 = \frac{1}{2} \cdot L \cdot C^2 \cdot \omega^2 \cdot V_{Bat}^2 \cdot (\cos \omega_n t)^2$$

$$E_L = \frac{1}{2} CV_{Bat}^2 \cos^2 \omega t \quad (A.33)$$

$$\text{If } t = \frac{2\pi}{4 \cdot n}$$

$$\therefore E_L = \frac{1}{2} CV_{Bat}^2 \cos^2 \frac{\pi}{2} = 0$$

$$E_C + E_L = \frac{1}{2} CV_{Bat}^2 \sin^2 \omega t + \frac{1}{2} CV_{Bat}^2 \cos^2 \omega t = \frac{1}{2} CV_{Bat}^2 \quad (A.34)$$

Alternative method:

$$E_C(t) = \int_0^t P_C(t) dt = \int_0^t V_{Bat} \cdot \sin \omega_n t \cdot C \omega V_{Bat} \cos \omega_n t dt$$

$$E_C(t) = C \omega V_{Bat}^2 \int_0^t \sin \omega_n t \cos \omega_n t dt$$

$$E_C(t) = \frac{1}{2} C \omega V_{Bat}^2 \int_0^t \sin 2 \omega_n t dt$$

$$E_C(t) = \frac{1}{2} C \omega V_{Bat}^2 \left(-\frac{\cos 2 \omega_n t}{2 \omega} \right)$$

$$E_C(t) = \frac{1}{2} CV_{Bat}^2 \left[\frac{1 - \cos 2 \omega_n t}{2} \right]$$

If:

$$2 \omega_n t = \pi, t = \frac{\pi}{2 \omega_n} = \frac{2\pi}{4 \omega_n}$$

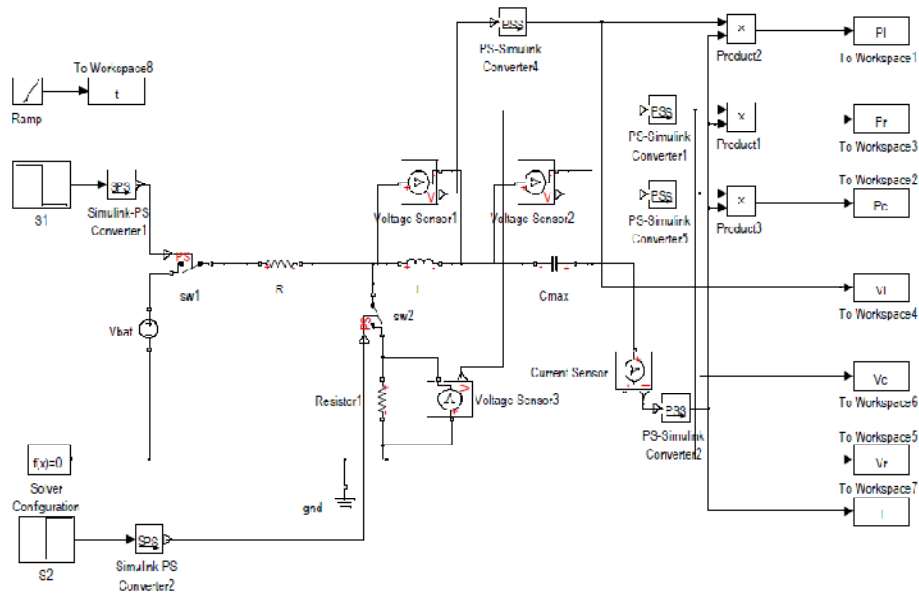
Then:

$$E_C(t) = \frac{1}{2} CV_{Bat}^2 \left[\frac{1 - (-1)}{2} \right] = \frac{1}{2} CV_{Bat}^2$$

APPENDIX B

MATLAB/ SIMULINK PROGRAM TO TEST THE PRE-CHARGE, HARVESTING AND RESET PHASES

Pre-charge phase



```
col=['r' 'b' 'g' 'y'];
Vb=7.4
L=100e-3
C=2.5e-9
wn=1/sqrt(L*C)
Tmax=(2*pi)/(6*wn)
Tsim= 2*Tmax
```

```
WC=cumtrapz(t,Pc);
WL=cumtrapz(t,Pl);
WR=cumtrapz(t,Pr);
```

```
Emax=(0.5*C*Vb^2)/1e-9
Emaxsim=max(WC)/1e-9
```

```
subplot(4,3,1);
plot(t,I,'LineWidth',2,'MarkerSize',10);title('I','FontWeight','Normal','FontSize',14,'FontName','times');grid;
subplot(4,3,4);
plot(t,Vc,'LineWidth',2,'MarkerSize',10);title('VC','FontWeight','Normal','FontSize',14,'FontName','times');grid;
```

```

subplot(4,3,7);
plot(t,Vl,'LineWidth',2,'MarkerSize',10);title('VL','FontWeight','Normal',
'FontSize',14,'FontName','times');grid;
subplot(4,3,10);
plot(t,Vr,'LineWidth',2,'MarkerSize',10);title('VR','FontWeight','Normal',
'FontSize',14,'FontName','times');grid;

subplot(4,3,2);
plot(t,(Pc+Pl+Pr),'LineWidth',2,'MarkerSize',10);title('Pin','FontWeight',
'Normal','FontSize',14,'FontName','times');grid;
subplot(4,3,5);
plot(t,Pc,'LineWidth',2,'MarkerSize',10);title('PC','FontWeight','Normal',
'FontSize',14,'FontName','times');grid;
subplot(4,3,8);
plot(t,Pl,'LineWidth',2,'MarkerSize',10);title('PL','FontWeight','Normal',
'FontSize',14,'FontName','times');grid;
subplot(4,3,11);
plot(t,Pr,'LineWidth',2,'MarkerSize',10);title('PR','FontWeight','Normal',
'FontSize',14,'FontName','times');grid;

subplot(4,3,3);    plot(t,WC+WL,'LineWidth',2,'MarkerSize',10);title('WC  +
WL','FontWeight','Normal','FontSize',14,'FontName','times');grid;
subplot(4,3,6);
plot(t,WC,'LineWidth',2,'MarkerSize',10);title('WC','FontWeight','Normal',
'FontSize',14,'FontName','times');grid;
subplot(4,3,9);
plot(t,WL,'LineWidth',2,'MarkerSize',10);title('WL','FontWeight','Normal',
'FontSize',14,'FontName','times');grid;
subplot(4,3,12);
plot(t,WR,'LineWidth',2,'MarkerSize',10);title('WR','FontWeight','Normal',
'FontSize',14,'FontName','times');grid;

figure

subplot(2,2,1);
plot(t,I/1e-3,'LineWidth',2,'MarkerSize',10);title('Current
(I)','FontWeight','Normal','FontSize',20,'FontName','times');grid;
ylabel('Current
(mA)','FontWeight','Normal','FontSize',20,'FontName','times')
xlabel('Time
(Sec)','FontWeight','Normal','FontSize',20,'FontName','times')
subplot(2,2,2); plot(t,Vc,'LineWidth',2,'MarkerSize',10);title('Capacitor
Voltage
(Vc)','FontWeight','Normal','FontSize',20,'FontName','times');grid;
ylabel('Voltage
(V)','FontWeight','Normal','FontSize',20,'FontName','times')
xlabel('Time
(Sec)','FontWeight','Normal','FontSize',20,'FontName','times')
subplot(2,2,3);                                plot(t,Pc/1e-
3,'LineWidth',2,'MarkerSize',10);title('Capacitor                    Power
(Pc)','FontWeight','Normal','FontSize',20,'FontName','times');grid;
ylabel('Power
(mW)','FontWeight','Normal','FontSize',20,'FontName','times')
xlabel('Time
(Sec)','FontWeight','Normal','FontSize',20,'FontName','times')
subplot(2,2,4);                                plot(t,WC/1e-
9,'LineWidth',2,'MarkerSize',10);title('Capacitor                    Energy
(Ec)','FontWeight','Normal','FontSize',20,'FontName','times');grid;
ylabel('Energy
(nJ)','FontWeight','Normal','FontSize',20,'FontName','times')

```

```

xlabel('Time
(Sec) ','FontWeight','Normal','FontSize',20,'FontName','times')

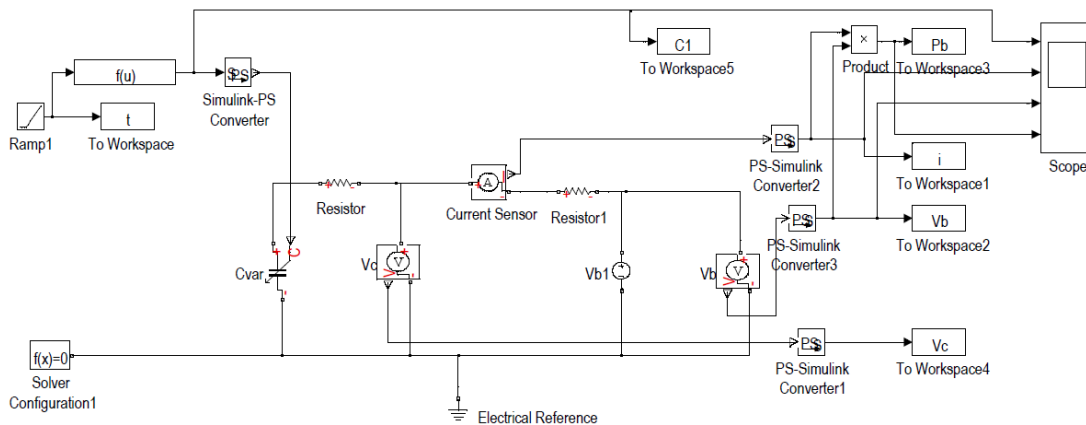
figure

plot(t/1e-3,WC/1e-9,col(1),'LineWidth',2,'MarkerSize',10);title('      Energy
','FontWeight','Normal','FontSize',12,'FontName','times');grid;
hold on
plot(t/1e-3,WL/1e-9,col(2),'LineWidth',2,'MarkerSize',10);title('      Energy
','FontWeight','Normal','FontSize',12,'FontName','times');grid;
hold on
plot(t/1e-3,WR/1e-9,col(3),'LineWidth',2,'MarkerSize',10);title('      Energy
','FontWeight','Normal','FontSize',12,'FontName','times');grid;
ylabel('Energy
(nJ) ','FontWeight','Normal','FontSize',20,'FontName','times')
xlabel('Time
(mSec) ','FontWeight','Normal','FontSize',20,'FontName','times')

legend('Capacitance energy ','Inductance Energy','Resistences Energy')

```

Harvesting phase



```

n=length(t)-3;
x1 =t(3:n)/1e-3
x2=t(3:n)/1e-3
y1 = C1(3:n)/1e-9;
y2 = E(3:n)/1e-9;

[AX,H1,H2] = plotyy(x1,y1,x2,y2,'plot');
set(get(AX(1),'Ylabel'),'String','Capacitance'                                nF
','FontWeight','Normal','FontSize',14,'FontName','times')
set(get(AX(2),'Ylabel'),'String','Harvested Energy'                            nJ
','FontWeight','Normal','FontSize',14,'FontName','times')
xlabel('Time
(msec) ','FontWeight','Normal','FontSize',14,'FontName','times')
set(H1,'LineStyle','--','LineWidth',2,'MarkerSize',12)
set(H2,'LineStyle',':','LineWidth',2,'MarkerSize',12)
grid

```



```

Cmax=2.5e-9
Cmin=0.6e-9
Vbat=7.4

n=length(t)-2;

V=Vb(1:n);
I=i(1:n);
P=Pb(1:n);
tt=t(1:n);

E=cumtrapz(tt,P);
Isim= mean(i(3:n))/1e-9
II=Vbat*diff(C1)./diff(t);
Ical=(Vbat*(Cmax-Cmin))/tt(n)/1e-9
Esim=max(E)/1e-9
Ecal= (Cmax-Cmin)*Vbat^2/1e-9
subplot(4,1,1); semilogy(tt,I*1e9);title('current I');grid;
subplot(4,1,2); plot(tt,V);title('Vbat');grid;
subplot(4,1,3); semilogy(tt,P*1e9);title('Pbat');grid;
subplot(4,1,4); plot(tt,E*1e9);title('Ebat');grid;

Y1=C1(3:n);
Y2=I(2:n);
figure

subplot(3,1,1)
plot(t(3:n),Y1)
title('C(t)')
grid on

subplot(3,1,2)
plot(t(2:n),Y2)
title('Current')
grid on

subplot(3,1,3)
plot(t(3:n-1),diff(C1(3:n))./diff(t(3:n)))
title('dC/dt')
grid on

figure
subplot(2,1,1);
plot(t(2:n),Y2/1e-6,'LineWidth',2,'MarkerSize',10)
ylabel('Harvested Current (uA)','FontWeight','Normal','FontSize',14,'FontName','times')
grid on
subplot(2,1,2); plot(tt,E/1e-9,'LineWidth',2,'MarkerSize',10);
ylabel('Harvested Energy (nJ)','FontWeight','Normal','FontSize',14,'FontName','times');grid;
xlabel('T (Sec)','FontWeight','Normal','FontSize',14,'FontName','times')

figure

subplot(2,2,1); plot(t(3:n),I(3:n)/1e-9,'LineWidth',2,'MarkerSize',10);title('Harvested Current (I)','FontWeight','Normal','FontSize',12,'FontName','times');grid;
ylabel('Current (nA)','FontWeight','Normal','FontSize',12,'FontName','times')

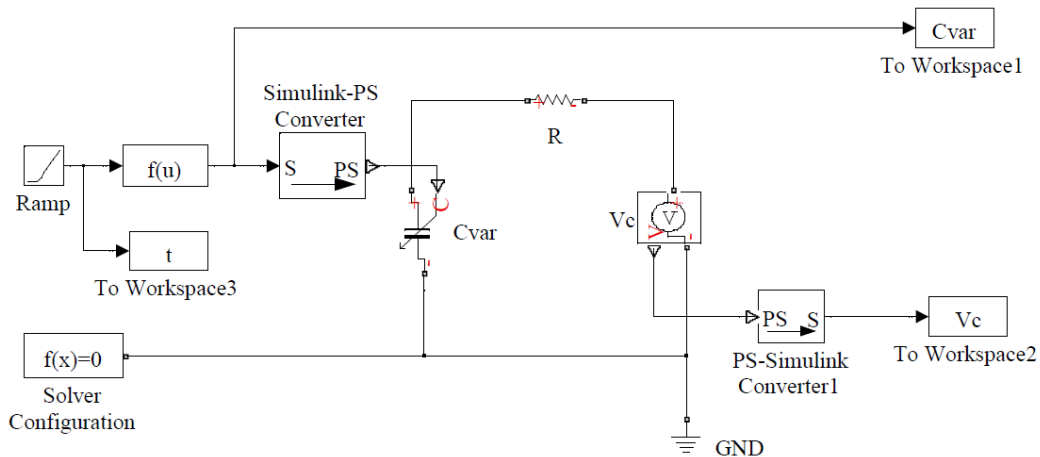
```

```

xlabel('Time
(Sec)', 'FontWeight', 'Normal', 'FontSize', 12, 'FontName', 'times')
subplot(2,2,2); plot(tt,V, 'LineWidth', 2, 'MarkerSize', 10); title('Battery
Voltage
(Vbat)', 'FontWeight', 'Normal', 'FontSize', 12, 'FontName', 'times'); grid;
ylabel('Voltage
(V)', 'FontWeight', 'Normal', 'FontSize', 12, 'FontName', 'times')
xlabel('Time
(Sec)', 'FontWeight', 'Normal', 'FontSize', 12, 'FontName', 'times')
subplot(2,2,3); plot(t(3:n), Pb(3:n)/1e-3, 'LineWidth', 2, 'MarkerSize', 10); title('Battery
Power
(Pbat)', 'FontWeight', 'Normal', 'FontSize', 12, 'FontName', 'times'); grid;
ylabel('Power
(mW)', 'FontWeight', 'Normal', 'FontSize', 12, 'FontName', 'times')
xlabel('Time
(Sec)', 'FontWeight', 'Normal', 'FontSize', 12, 'FontName', 'times')
subplot(2,2,4); plot(tt,E/1e-9, 'LineWidth', 2, 'MarkerSize', 10); title('Harvested
Energy
(Eharv)', 'FontWeight', 'Normal', 'FontSize', 12, 'FontName', 'times'); grid;
ylabel('Energy
(nJ)', 'FontWeight', 'Normal', 'FontSize', 12, 'FontName', 'times')
xlabel('Time
(Sec)', 'FontWeight', 'Normal', 'FontSize', 12, 'FontName', 'times')

```

Reset phase



```

n=length(t)-3;
x1 =t(1:n)/1e-3
x2=t(1:n)/1e-3
y1 = Cvar(1:n)/1e-9;
y2 = Vc(1:n);
[AX,H1,H2] = plotyy(x1,y1,x2,y2,'plot');
set(get(AX(1), 'Ylabel'), 'String', 'Capacitance', 'FontSize', 20, 'FontName', 'times')
set(get(AX(2), 'Ylabel'), 'String', 'Capacitor Voltage', 'FontSize', 20, 'FontName', 'times')
xlabel('Time
(msec)', 'FontWeight', 'Normal', 'FontSize', 20, 'FontName', 'times')
set(H1, 'LineStyle', '--', 'LineWidth', 2, 'MarkerSize', 12)
set(H2, 'LineStyle', ':', 'LineWidth', 2, 'MarkerSize', 12)
grid

```

APPENDIX C

MATLAB PROGRAM TO CALCULATE THE CAPACITANCE AND ENERGY OF THE MULTI POLE CAPACITORS

```
close all; clear all; clc
r1=0.01
r2=0.04
r3=0.045
Np=1 % No of Poles

theta1 = [180 160 140 120 100 80 60 40 20 0]./Np
theta2 = [0 20 40 60 80 100 120 140 160 180]./Np

a1= 0.5*(theta1.*(pi/180))*r1^2
a2= 0.5*(theta1.*(pi/180))*r2^2
a3= 0.5*(theta1.*(pi/180))*r3^2

a11= 0.5*(theta2.*(pi/180))*r1^2
a21= 0.5*(theta2.*(pi/180))*r2^2
a31= 0.5*(theta2.*(pi/180))*r3^2

Amax1=a3-a1
Amin1=a31-a21
Ax=Amax1+Amin1

aly= 0.5*(theta2.*(pi/180))*r1^2
a2y= 0.5*(theta2.*(pi/180))*r2^2
a3y= 0.5*(theta2.*(pi/180))*r3^2

a11y= 0.5*(theta1.*(pi/180))*r1^2
a21y= 0.5*(theta1.*(pi/180))*r2^2
a31y= 0.5*(theta1.*(pi/180))*r3^2

Amax2=a3y-aly
Amin2=a31y-a21y
Ay=Amax2+Amin2

eo= 8.85*1e-12
er=1

Ns=50 % No of slices
d=0.001 % distance between plates

Cx =(eo*er*(2*Ns-1)*Ax*Np)/d
Cy =(eo*er*(2*Ns-1)*Ay*Np)/d
C =[ Cy Cx]
theta =[0:360/19:360]
Cc= [ C]

plot (theta,Cc/1e-9,'LineWidth',2,'MarkerSize',10)
```

```

ylabel('Capacitance','FontWeight','Normal','FontSize',20,'FontName','times')
xlabel('Angular position
(degrees)','FontWeight','Normal','FontSize',20,'FontName','times')
grid on

ws= [2 4 6 8 10 ]
c =2*pi*r3
T= c./ws
Tc=T./Np
Th=Tc./2
%Time vectors for wind speeds
t2 =[0 :Th(1)/9:Th(1)]
t4 =[0 :Th(2)/9:Th(2)]
t6 =[0 :Th(3)/9:Th(3)]
t8 =[0 :Th(4)/9:Th(4)]
t10 =[0 :Th(5)/9:Th(5)]

Tws = [ max(t2) max(t4) max(t6) max(t8) max(t10)]

figure
E =[ 0 0 0 0 0 0 0 0 0 0:104/10:104]
x1 =theta
x2=theta
y1 = Cc/1e-9;
y2 = E ;

[AX,H1,H2] = plotyy(x1,y1,x2,y2,'plot');
set(get(AX(1),'Ylabel'),'String','Capacitance (nF)
','FontWeight','Normal','FontSize',20,'FontName','times')
set(get(AX(2),'Ylabel'),'String','Harvested Energy( nJ
)','FontWeight','Normal','FontSize',20,'FontName','times')
xlabel('Angular Position
(degrees)','FontWeight','Normal','FontSize',20,'FontName','times')
set(H1,'LineStyle','--','LineWidth',2,'MarkerSize',12)
set(H2,'LineStyle',':','LineWidth',2,'MarkerSize',12)
grid

```

Energy calculation of the multi poles capacitors

```

close all;clear all;clc
col=['r' 'b' 'g' 'm' 'y'];

ws = [2 4 6 8 10]
Cmax=2.5e-9
Cmin=0.6e-9
Vbat=7.4
r3=0.045
Np=1

c =2*pi*r3
T= c./ws
Tc=T./Np
Th=Tc./2

```

```

%Time vectors for wind speeds
t2 =[0 :Th(1)/9:Th(1)]
t4 =[0 :Th(2)/9:Th(2)]
t6 =[0 :Th(3)/9:Th(3)]
t8 =[0 :Th(4)/9:Th(4)]
t10 =[0 :Th(5)/9:Th(5)]

Tws = [ max(t2) max(t4) max(t6) max(t8) max(t10)]
Vec =[ 1 1 1 1 1]
Ical= (Vbat*(Cmax-Cmin))./Tws/1e-9
Ecal= (Cmax-Cmin)*Vbat^2/1e-6 .* Vec

Isim = [ 193.5991 387.8194 580.0144 773.5849 971.6973]
Esim = [100.2982 100.2810 100.2638 100.2466 100.2294].*1e-3

EsimS = Esim./T
EcalS = Ecal./T

subplot(2,1,1)
plot(ws,Isim,col(1),'LineWidth',2,'MarkerSize',10)
hold on
plot(ws,Ical,col(2),'LineWidth',2,'MarkerSize',10)
ylabel('Harvesting Current ( nA
'),'FontWeight','Normal','FontSize',20,'FontName','times')
xlabel('Wind speed ( m/sec
'),'FontWeight','Normal','FontSize',20,'FontName','times')
grid
legend ('I_ Simulation','I_ Calculation')

subplot(2,1,2)
plot(ws,EsimS(1:length(T)),col(1),'LineWidth',2,'MarkerSize',10)
hold on
plot(ws,EcalS(1:length(T)),col(2),'LineWidth',2,'MarkerSize',10)
ylabel('Energy Gain( \mu J
)/sec','FontWeight','Normal','FontSize',20,'FontName','times')
xlabel('Wind speed ( m/sec
'),'FontWeight','Normal','FontSize',20,'FontName','times')
grid
legend ('E_ Simulation','E_ Calculation')

figure

plot(ws,EcalS(1:length(T)),col(1),'LineWidth',2,'MarkerSize',10)
hold on
plot(ws,2.*EcalS(1:length(T)),col(2),'LineWidth',2,'MarkerSize',10)
hold on
plot(ws,4.*EcalS(1:length(T)),col(3),'LineWidth',2,'MarkerSize',10)
hold on
plot(ws,8.*EcalS(1:length(T)),col(4),'LineWidth',2,'MarkerSize',10)

ylabel('Energy Gain ( \mu J
)/sec','FontWeight','Normal','FontSize',20,'FontName','times')
xlabel('Wind speed ( m/sec
'),'FontWeight','Normal','FontSize',20,'FontName','times')
grid
legend ('One pole','Two poles', 'Four poles' , 'Eight poles')

```

```

figure

Ecal1= 1*(Cmax-Cmin)*Vbat^2/1e-6
Ecal2= 2*(Cmax-Cmin)*Vbat^2/1e-6
Ecal4= 4*(Cmax-Cmin)*Vbat^2/1e-6
Ecal8= 8*(Cmax-Cmin)*Vbat^2/1e-6

ws = [2 4 6 8 10]
T= c./ws

E1=Ecal1./T
E2=Ecal2./T
E4=Ecal4./T
E8=Ecal8./T

plot (ws,E1,col(1),'LineWidth',2,'MarkerSize',10)
hold on
plot (ws,E2,col(2),'LineWidth',2,'MarkerSize',10)
hold on
plot (ws,E4,col(3),'LineWidth',2,'MarkerSize',10)
hold on
plot (ws,E8,col(4),'LineWidth',2,'MarkerSize',10)

ylabel('Energy Gain ( \mu J /sec','FontWeight','Normal','FontSize',20,'FontName','times')
xlabel('Wind speed ( m/sec','FontWeight','Normal','FontSize',20,'FontName','times')
grid
legend ('One pole','Two poles', 'Four poles' , 'Eight poles')

```

APPENDIX D

MATLAB PROGRAM FOR CAPACITANCE, VOLUME AND ENERGY OPTIMIZATION

Capacitance and volume optimization

```
close all;clear all;clc
%Factors affecting the total capacitance
%Area, Distance, Number of parallel plates

r1=1e-3.*[5 7.5 10 12.5 15 17.5]
r2=1e-3.*[20 30 40 50 60 70]
r3=1e-3.*[25 35 45 55 65 75]
Np=8 % No of Poles
a1=(pi*r1.^2)/(2*Np)
a2=(pi*r2.^2)/(2*Np)
a3=(pi*r3.^2)/(2*Np)
Amax=(a3-a1).*Np
Amin=(a3-a2).*Np
eo= 8.85*1e-12;
er=1;
N =[30 40 50 60 70 80]
d=1e-3.*[0.25 0.5 1 2 3 4]
w=(1*1e-3);

for i = 1:6;
    for j= 1:6;
        for k=1:6;

C1(i,j,k)= ((2.*N(i)-1)* eo*er.*Amax(j)./d(k)./1e-9);
C2(i,j,k)= ((2.*N(i)-1)* eo*er.*Amin(j)./d(k)./1e-9);
Cd(i,j,k)= C1(i,j,k) - C2(i,j,k);

        end
    end
end

for m= 1:6;

subplot(3,2,m)

plot(N,Cd(:,1,m),
N,Cd(:,2,m),N,Cd(:,3,m),N,Cd(:,4,m),N,Cd(:,5,m),N,Cd(:,6,m))
legend('Minimum Amax - Amin')
ylabel('Capacitance
(nF)','FontWeight','Normal','FontSize',16,'FontName','times')
xlabel('Number of stator-rotor
sets','FontWeight','Normal','FontSize',16,'FontName','times')
```

```

Title ([' Variation of Cmax - Cmin at d = ' num2str(d(m)*1000),' mm
'],'FontWeight','Normal','FontSize',16,'FontName','times')
grid on
end

figure

for n=1:6;
    for o=1:6;
        for p=1:6;

Vol1(n,o,p)= 1e9*((pi*r3(n)^2)*(2*N(o)*w+ (N(o)-1)*d(p)));

            end
        end
    end

r =r3/1e-3

for m= 1:6;

subplot(3,2,m)

plot(r,Vol1(:,1,m),r,Vol1(:,2,m),r,Vol1(:,3,m),r,Vol1(:,4,m),r,Vol1(:,5,m)
,r,Vol1(:,6,m))
legend(' Minimum number of SR sets ')
ylabel('Volume(                                     mm^3
'),'FontWeight','Normal','FontSize',16,'FontName','times')
xlabel('Radius          of          the          capacitor          (          mm
'),'FontWeight','Normal','FontSize',16,'FontName','times')
Title (['          d          =          '          num2str(d(m)*1000),'          mm
'],'FontWeight','Normal','FontSize',16,'FontName','times')
grid on
end
figure
for m= 1:6;

subplot(2,2,m)
plot(N,Cd(:,1,m),
N,Cd(:,2,m),N,Cd(:,3,m),N,Cd(:,4,m),N,Cd(:,5,m),N,Cd(:,6,m))
legend('Minimum Amax - Amin')
ylabel('Capacitance
(nF)','FontWeight','Normal','FontSize',16,'FontName','times')
xlabel('Number          of          stator-rotor
sets','FontWeight','Normal','FontSize',16,'FontName','times')
Title ([' Variation of Cmax - Cmin at d = ' num2str(d(m)*1000),' mm
'],'FontWeight','Normal','FontSize',16,'FontName','times')
grid on
end

```


Energy optimization

```

close all; clear all; clc ;
r1=0.01
r2=0.040
r3=0.045
Np=8 % No of Poles
Cmax=2.5e-9
Cmin=0.6e-9
Vb=7.4
Eb= (Cmax-Cmin)*Vb^2.*Np
Nc= [ 1 2 4 8 10]
Es=(Cmax-Cmin)*Vb^2.*Np
ws= [2 4 6 8 10 ]
c =2*pi*r3
T= c./ws
Tc=T./Np
Th=Tc./2
%Time vectors for wind speeds
t2 =[0 :Th(1)/4:Th(1)]
t4 =[0 :Th(2)/4:Th(2)]
t6 =[0 :Th(3)/4:Th(3)]
t8 =[0 :Th(4)/4:Th(4)]
t10 =[0 :Th(5)/4:Th(5)]
T= [ max(t2) max(t4) max(t6) max(t8) max(t10)]
Tx=c/10
Ty =c/2
[Np1,Nc1] = meshgrid(linspace(1,20,21),linspace(1,20,21))
E=1e6*(Cmax-Cmin)*Vb^2.*Np1./(Tx./Nc1)
surface(Np1,Nc1,E) ; % Plot a surface such that : X= r, Y = d , Z = EV
xlabel('No.of poles in the capacitor','FontWeight','Normal','FontSize',20,'FontName','times')
ylabel('No.of Capacitors in the Array','FontWeight','Normal','FontSize',20,'FontName','times')
zlabel('Harvested Energy (\mu J)','FontWeight','Normal','FontSize',20,'FontName','times')
grid on
figure
[Tcy,Nc1] = meshgrid(linspace(Tx,Ty,21),linspace(1,20,21))
E=1e6*(Cmax-Cmin)*Vb^2.*Np./(Tcy./Nc1)
surface(Np1,Nc1,E) ; % Plot a surface such that : X= r, Y = d , Z = EV
xlabel('The harvesting cycle time (msec)','FontWeight','Normal','FontSize',20,'FontName','times')
ylabel('No.of Capacitors in the Array','FontWeight','Normal','FontSize',20,'FontName','times')
zlabel('Harvested Energy (\mu J)','FontWeight','Normal','FontSize',20,'FontName','times')
grid on
figure
[Vb1,Nc1] = meshgrid(linspace(3,10,21),linspace(1,20,21))
E=1e6*(Cmax-Cmin)*Vb1.^2.*Np./(Tx./Nc1)
surface(Vb1,Nc1,E) ; % Plot a surface such that : X= r, Y = d , Z = EV
xlabel('Battery Voltage (V)','FontWeight','Normal','FontSize',20,'FontName','times')
ylabel('No.of Capacitors in the Array','FontWeight','Normal','FontSize',20,'FontName','times')
zlabel('Harvested Energy (\mu J)','FontWeight','Normal','FontSize',20,'FontName','times')
grid on

```

APPENDIX E

PIC BASIC CODE FOR TESTING THE ENERGY HARVESTER

Harvester testing – without interrupt

```
TRISA = %00000      ' set A to OUTPUT port
TRISB = %11111111    ' set B to INPUT port

Start:

IF PORTB.0=0 THEN RF1 ' C max is detected
IF PORTB.0=1 THEN RESET ' C min is detected

goto start

RF1:  \ Send signal to the RF Transmitter

HIGH PORTA.0

PAUSE 1

LOW PORTA.0

GOTO CHARGE1

CHARGE1: \ Send signal to the SW1

HIGH PORTA.1

PAUSEUS 5

low PORTA.1

GOTO CHARGE2

CHARGE2: \Send signal to the SW2

HIGH PORTA.2

PAUSEUS 5

LOW PORTA.2

goto HARVEST

HARVEST: \ Send signal to the SW3

HIGH PORTA.3

IF PORTB.0 = 0 THEN HARVEST
```

```

GOTO RF2

RF2: ` Send signal to the transmitter

HIGH PORTA.0

PAUSE 1

LOW PORTA.0

GOTO RESET

RESET: ` start reset mode all switches are off

LOW PORTA

GOTO START

```

Harvester testing – with interrupt

```

START :

symbol in=portb.7 'button connected to this pin
TRISB=%10000000 'set portb.7 AND 0 as input
TRISA = %000000    ' set A to OUTPUT port
OPTION_REG=%11000000

on interrupt goto isr

intcon=%10001001 'i enabled the global and the portb 4-7 interrupt

main:

SLEEP 1

goto main

disable

isr: 'interrupt handler starts here


intcon.0=0

RF1:

HIGH PORTA.0

PAUSE 1

LOW PORTA.0

GOTO CHARGE1

CHARGE1:

```

```
HIGH PORTA.1
PAUSEUS 5
low PORTA.1
GOTO CHARGE2
CHARGE2:
HIGH PORTA.2
PAUSEUS 5
LOW PORTA.2
goto HARVEST
HARVEST:
HIGH PORTA.3
IF PORTB.0 = 0 THEN HARVEST
GOTO RF2
RF2:
HIGH PORTA.0
PAUSE 1
LOW PORTA.0
GOTO RESET
RESET:
LOW PORTA
resume
enable
GOTO START
```

APPENDIX F

LOW RISK RESEARCH ETHICS APPROVAL CHECKLIST

Applicant Details

Name	Rita Tareq	E-mail	rita.abdulmunam@emirates.com
Department	Engineering -EAC	Date	16 Feb 2011
Course	PhD	Title of Project:	Electrostatic Generator

Project Details

Research Objectives

3.5 Set up the design consideration for an electrostatic energy harvester and evaluate the previous work related to the different available electrostatic energy harvester approaches.

3.6 Develop new ways to extract energy from the environment using macro scale electrostatic energy harvester.

3.7 Produce an alternative outline design to develop a new electrostatic energy harvester

3.8 Improve the efficiency of the electrostatic generator by designing a novel power conditioning circuit to extract the maximum power from the electrostatic generator.

Research Design

Researches will be conducted adopting an experimental and literature approach. First and foremost, a preparation phase will involve a study through literature of the history and evolution of the electrostatic power generators. This initial phase will build an essential basis for the rest of my work, as it will provide an overview of the different types of micro power generator, as well as the different basic rules and conventions that have been set in this domain. A study of the problems and solutions raised by previous research will also be conducted to complete and narrow down the orientation that will be taken for the following steps of my project.

Prototypes will be elaborated combining software and hardware using the communication toolbox of MatLab/ Simulink and Multisim software. Every prototype will be evaluated; the evaluations will aim at revealing new concepts and reorienting the research to another analysis phase and so starting a new cycle. Thus, this process will be iterated along my thesis (analysis – prototypes – evaluations), each iteration aiming at focusing on the interesting ideas, developing new ones, and finally refining and enhancing the different prototypes.

Methods of Data Collection

All practical experiments and software testing will be completed at the Emirates Aviation

College electrical & electronics workshops and /or other workshops as per the requirements.

Participants in your research

Will the project involve human participants?		No
--	--	----

If you answered **Yes** to this questions, this may **not** be a low risk project. Please discuss your project with your Supervisor.

Risk to Participants

Will the project involve human patients/clients, health professionals, and/or patient (client) data and/or health professional data?		No
Will any invasive physical procedure, including collecting tissue or other samples, be used in the research?		No
Is there a risk of physical discomfort to those taking part?		No
Is there a risk of psychological or emotional distress to those taking part?		No
Is there a risk of challenging the deeply held beliefs of those taking part?		No
Is there a risk that previous, current or proposed criminal or illegal acts will be revealed by those taking part?		No
Will the project involve giving any form of professional, medical or legal advice, either directly or indirectly to those taking part?		No

If you answered **Yes** to **any** of these questions, this may **not** be a low risk project. Please discuss your project with your Supervisor.

Risk to Researcher

Will this project put you or others at risk of physical harm, injury or death?		No
Will project put you or others at risk of abduction, physical, mental or sexual abuse?		No
Will this project involve participating in acts that may cause psychological or emotional distress to you or to others?		No
Will this project involve observing acts which may cause psychological or emotional distress to you or to others?		No
Will this project involve reading about, listening to or viewing materials that may cause psychological or emotional distress to you or to others?		No
Will this project involve you disclosing personal data to the participants other than your name and EAC as your contact and e-mail address?		No
Will this project involve you in unsupervised private discussion with people who are not already known to you?		No

Will this project potentially place you in the situation where you may receive unwelcome media attention?		No
Could the topic or results of this project be seen as illegal or attract the attention of the security services or other agencies?		No
Could the topic or results of this project be viewed as controversial by anyone?		No

If you answered **Yes** to **any** of these questions, this is **not** a low risk project. Please discuss your project with your Supervisor.

Informed Consent of the Participant

Are any of the participants under the age of 18?		No
Are any of the participants unable mentally or physically to give consent?		No
Do you intend to observe the activities of individuals or groups without their knowledge and/or informed consent from each participant (or from his or her parent or guardian)?		No

If you answered **Yes** to **any** of these questions, this may **not** be a low risk project. Please discuss your project with your Supervisor.

Participant Confidentiality and Data Protection

Will the project involve collecting data and information from human participants who will be identifiable in the final report?		No
Will information not already in the public domain about specific individuals or institutions be identifiable through data published or otherwise made available?		No
Do you intend to record, photograph or film individuals or groups without their knowledge or informed consent?		No
Do you intend to use the confidential information, knowledge or trade secrets gathered for any purpose other than this research project?		No

If you answered **Yes** to **any** of these questions, this may **not** be a low risk project. Please discuss your project with your Supervisor.

Gatekeeper Risk

Will this project involve collecting data outside EAC buildings?		No
Do you intend to collect data in shopping centres or other public places?		No
Do you intend to gather data within nurseries, schools or colleges?		No

Do you intend to gather data within healthcare premises?		No
--	--	----

If you answered **Yes** to **any** of these questions, this is **not** a low risk project. Please discuss your project with your Supervisor.

Other Ethical Issues

Is there any other risk or issue not covered above that may pose a risk to you or any of the participants?		No
Will any activity associated with this project put you or the participants at an ethical, moral or legal risk?		No

If you answered **Yes** to these questions, this may **not** be a low risk project. Please discuss your project with your Supervisor

Principal Investigator Certification

If you answered **No** to **all** of the above questions, then you have described a low risk project. Please complete the following declaration to certify your project and keep a copy for your record as you may be asked for this at any time.

Agreed restrictions to project to allow Principal Investigator Certification

Please identify any restrictions to the project, agreed with your Supervisor or the Dean of Postgraduate Studies to allow you to sign the Principal Investigator Certification declaration.

Participant Information Leaflet attached.
Informed Consent Forms attached.

Principal Investigator's Declaration

Please ensure that you:

Tick all the boxes below and sign this checklist.

Students must get their Supervisor to countersign this declaration.

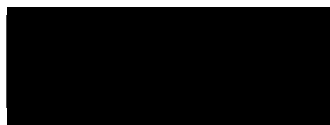
I believe that this project does not require research ethics approval . I have completed the checklist and kept a copy for my own records. I realise I may be asked to provide a copy of this checklist at any time.	√
I confirm that I have answered all relevant questions in this checklist honestly.	√
I confirm that I will carry out the project in the ways described in this checklist. I will immediately suspend research and request a new ethical approval if the project subsequently changes the information I have given in this checklist.	√

Signatures

If you submit this checklist and any attachments by e-mail, you should type your name in the signature space. An email attachment sent from your EAC inbox will be assumed to have been signed electronically.

Principal Investigator : Rita Tareq Aljadiri

Signed



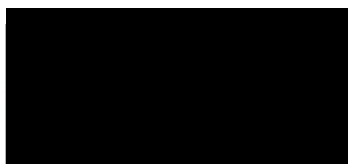
(Principal Investigator or Student)

Date: 16/02/2011

Students storing this checklist electronically must append to it an email from your Supervisor confirming that they are prepared to make the declaration above and to countersign this checklist. This-email will be taken as an electronic countersignature.

Student's Supervisor: Dr. Luay Yassin Taha

Countersigned



(Supervisor)

Date: 16/02/2011

I have read this checklist and confirm that it covers all the ethical issues raised by this project fully and frankly. I also confirm that these issues have been discussed with the student and will continue to be reviewed in the course of supervision.

REFERENCES

1. Ab.com, Inductive Proximity Sensors, n.d., viewed 3 January 2014, <<http://www.ab.com/en/epub/catalogs/12772/6543185/12041221/12041227/print.html>>.
2. Abdulmunam, RT, Taha, LY, Ivey, PC 2012, 'Modelling of Low Power Electrostatic Wind Energy Harvester for Macro Scale Applications', *International conference of information and electronics engineering (ICIEE)*, Singapore.
3. Abdulmunam, RT, Taha, LY, Ivey, PC 2013, 'Simulation and Experimental Modelling of a Multi-Pole Variable Capacitor for Electrostatic Wind Energy Harvester', *Turkish journal of electrical engineering and computer sciences*, Ankara, Turkey.
4. Almouahed, S, Gouriou, M, Hamitouche, C, Stindel, E & Roux, C 2010, 'Self-powered instrumented knee implant for early detection of postoperative complications', IEEE engineering in medicine and biology society.
5. Altena, G, Renaud, M, Elfrink, R, Goedbloed, MH, Nooijer, CD & Schaijk, RV 2013, 'Design improvements for an electret-based MEMS vibrational electrostatic energy harvester', *Journal of Physics: Conference Series*, vol. 476, no.1.
6. Ambokar, M 2011, Design of a Novel Electrostatic Micro Energy Harvester, MSc Thesis, University of Texas at Arlington.
7. Atbatt.com, 2014, Digital camera Batteries, viewed 5 August 2014,<<http://www.atbatt.com/digital-camera-batteries.asp>>.
8. Beeby, SP, Torah, RN & Tudor, MJ 2008, 'Kinetic Energy Harvesting', *Act Workshop on Innovative Concepts. Esa-Estec*, pp. 1-10.
9. Boisseau, S, Despesse, G & Seddik, AB 2012, 'Electrostatic Conversion for Vibration Energy Harvesting', *Small-Scale Energy Harvesting*.
10. Boisseau, S, Despesse, G 2012, 'Energy harvesting, wireless sensor networks & opportunities for industrial applications', *EE Times*, viewed 15 February 2013, <<http://www.eetimes.com/design/smart-energy-design/4237022/Energy-harvesting-wireless-sensor-networks-opportunities-for-industrial-applications>>.
11. Boland, JS, Lo, HW, Messenger, JDM & Tai, YC 2005, 'Arrayed liquid rotor electric power generator system', *Proc. of The 18th IEEE International Conference on MEMS*, pp. 618 – 621.
12. Bowen, CR, Lopez-Prieto, M, Mahon, S & Lowrie, F 2000,' Impedance spectroscopy of piezoelectric actuators', *Scripta Mater*, pp. 813–818.

13. Boylestad, R & Nashelsky, 2011, *Introductory Circuit Analysis*, Prentice Hall, USA.
14. Bu, L, Wu, X & Liu, L 2010, 'Collision Based Capacitive Vibration Energy Harvesting', *Solid-State and Integrated Circuit Technology (ICSICT) 10th IEEE International Conference*, pp. 1955 – 1957.
15. Bu, L, Wu, X & Liu, L 2010, 'Collision Based Capacitive Vibration Energy Harvesting', *Solid-State and Integrated Circuit Technology (ICSICT) 10th IEEE International Conference*, pp. 1955 – 1957.
16. Carbonanotubebattery.com, 2009, MIT Carbon Nanotube Research, viewed 12 April 2011, <<http://carbonanotubebattery.com/mit-carbon-nanotube-research/>>.
17. Cellphoneshop.com, 2014, Cell Phone Batteries, viewed 5 August 2014,<<http://www.cellphoneshop.net/celphonbat.html>>.
18. Cotia, YA, V Bhatt, V 2012, 'Design and Simulation of Micro-Cantilever Beams for variable capacitor, *Proceedings of the International Journal of Computer Applications (IJCA)*, pp. 28-32.
19. Csgnetwork.com, 2011, Battery Charge Time Calculator, viewed 5 August 2014, <<http://www.csgnetwork.com/batterychgcalc.html>>.
20. D'hulst, R, Sterken, T, Puers, R & Driesen, J n.d., 'Requirements for Power Electronics used for Energy Harvesting Devices', viewed 14 January 2012, <http://www.researchgate.net/publication/242096692_Requirements_for_Power_Electronics_used_for_Energy_Harvesting_Devices>.
21. Das, R 2010, Wind energy harvester from Humdinger, viewed 30 August 2014, <<http://www.energyharvestingjournal.com/articles/wind-energy-harvester-from-humdinger-00002146.asp?sessionid=1>>.
22. Dbp.idebate.org 2010, Argument: Abundant wind energy can displace fossil fuels and slash emissions, viewed 10 June 2013, <http://dbp.idebate.org/en/index.php/Argument:_Abundant_wind_energy_can_displace_fossil_fuels_and_slash_emissions>.
23. Despesse, G, Jager, T, Condemine, C & Berger PD 2008, 'Mechanical Vibrations Energy Harvesting and Power Management', *IEEE Sensors Conference*, pp. 29 -32.
24. Docs.autodesk.com, 2010, AutoCAD 2010 User Documentation, viewed 4 August 2014, <<http://docs.autodesk.com/ACD/2010/ENU/AutoCAD%202010%20User%20Documentation/index.html?url=WS1a9193826455f5ffa23ce210c4a30acaf-4a2c.htm,topicNumber=d0e262122>>.

25. Dudka, A, Galayko, D, Basset, P 2009, 'VHDL-AMS modeling of adaptive electrostatic harvester of vibration energy with dual-output DC-DC converter', *Behavioral Modeling and Simulation Workshop*, pp.13-18.
26. Edamoto, M, Suzuki, Y, Kasagii, N, Kashiwagi, K, Morizawa, Y, Yokoyama, T, Seki, T & Oba M 2009, 'Low-Resonant-Frequency Micro Electret Generator for Energy Harvesting Application', *Micro Electro Mechanical Systems IEEE 22nd International Conference*, pp 1059–1062.
27. Farnell.com, 2006, AM Hybrid Transmitter, viewed 6 June 2013, <<http://www.farnell.com/datasheets/56733.pdf>>.
28. Firebox.com, 1998, HY Mini Wind Turbine, viewed 5 March 2012 <<http://www.firebox.com/product/2111/HY-Mini-Wind-Turbine>>.
29. Florentino, HR, Freire, RCS, Florentino, CS 2010, 'Optimization of Control Switch for Energy Harvest Circuit Using Electrostatic Charges', *Circuits and Systems (APCCAS), 2010 IEEE Asia Pacific Conference*, pp. 668 -671.
30. Floyd, 1984, *Electronic Devices*, 6th edn, Prentice Hall, New Jersey, USA.
31. Floyd, 2007, *Principle of Electric Circuits*, Prentice Hall, New Jersey, USA.
32. Galayko, D, Basset, P, Paracha, AM 2008, 'Optimization and AMS Modeling for Design of an Electrostatic Vibration Energy Harvester's Conditioning Circuit with an Auto-Adaptive Process to the External Vibration Changes' , *Symposium on Design, Test, Integration and Packaging of MEMS/MOEMS - DTIP*.
33. Gilbert, JM, Balouchi, F 2008, 'Comparison of Energy Harvesting Systems for Wireless Sensor Networks', *International Journal of Automation and Computing*, pp 334-347.
34. Grogg, K 2005, 'Harvesting the Wind: The Physics of Wind Turbines', *Physics and Astronomy Comps Papers*, viewed 7 March 2013, <<https://dspace.lasrworks.org/bitstream/handle/10349/145/fulltext.pdf>>.
35. Guillemet, R, Basset, P, D. Galayko, D, Marty, F & Bourouina, T 2012, 'Efficient In-plane Gap closing MEMS Electrostatic Vibration Energy Harvester', *Power MEMS 2012*, Atlanta, GA, USA, pp. 137-140.
36. Guillemet, R, Basset, P, Galayko, D, Bourouina, T 2010, 'Combined optimization of electrical and mechanical parameters of an out-of-plane gap-closing electrostatic Vibration Energy Harvester (VEH)', *Design Test Integration and Packaging of MEMS/MOEMS (DTIP), 2010 Symposium*, pp. 73-78.

37. Haas, CH & Kraft, M 2004, 'Modelling and analysis of a MEMS approach to DC voltage step-up conversion', *Journal of Micromechanics and Micro-engineering*, pp.114-122.
38. Halvorsen, E, Blystad, LCJ, Husa, S & Eskill Westby, E 2007, 'Simulation Of Electromechanical Systems Driven By large Random Vibrations' , *MEMS tech*, Lviv-Polyana, Ukraine .
39. Halvorsen, E, Westby, ER, Husa, S, Vog, A, Østbø, NP, Leonov,V, Sterken, T & Kvisterøy, T 2009, 'An Electrostatic Energy Harvester with Electret Bias', *Solid-State Sensors, Actuators and Microsystems Conference*, pp. 1381 -1384.
40. Hammer, H 2010, 'Analytical model for comb-capacitance fringe fields', *Micro electromechanical systems*, vol. 19, pp. 175 – 182.
41. Hku.hk, 2007, '*HKU and Motorwave Limited Jointly Developed Micro-Wind Turbine Technology for Crowded Cities*', University of Hong Kong , viewed online 4 March 2012, <https://www.hku.hk/press/news_detail_5535.html>.
42. Hodge, N 2012, *The Truth about Energy Taking Sides is Costing you Money*, Energy and Capital, viewed 20 December 2013, <<http://www.energyandcapital.com/articles/the-truth-about-energy/2535>>.
43. Ivey, B 2009, 'nano Watt and nano XLP Technologies: an introduction to Microchips low power devices', Microchip Technology Inc., viewed 5 January 2014, <<http://ww1.microchip.com/downloads/en/AppNotes/01267a.pdf>>.
44. Janicek,V & Husak, M 2013, '3D Energy Harvester Evaluation', *Radio Engineering*, vol. 22, no. 1,pp. 251-258
45. Kempitiya, A, Borca-Tasciuc, DA, Member & Hella, MM 2011, 'Analysis and Optimization of Asynchronously Controlled Electrostatic Energy Harvesters', *Industrial Electronics, IEEE Transactions*, vol. 59, no. 1, pp. 456 – 463.
46. Kennnedey, G & Davis, B 1992, *Electronic Communication Systems*, 4th edn, Mc-graw hill international editions, Singapore.
47. Kim, SH, Ji, CH, , Galle, P, Herrault, F, Wu, X, Lee, JH , Choi, CA & Allen MG 2008, 'An Electromagnetic Energy Scavenger From Direct Airflow', *Proceedings of Power MEMS 2008 and micro EMS 2008*, Sendai, Japan, pp. 133 -136.
48. Kiziroglou, ME, He, C & Yeatman, EM 2009, 'Rolling Rod Electrostatic Microgenerator', *IEEE Transactions On Industrial Electronics*, vol. 56, no. 4, pp. 1101-1108.

49. Kompis, C & Aliwell, S 2008, 'Energy harvesting technologies to enable remote and wireless sensing', *Sensors and Instrumentation*, viewed 2 December 2011, <https://connect.innovateuk.org/c/document_library/get_file?groupId=430051&folderId=3927636&title=Energy+Harvesting+Technologies+to+Enable+Remote+%26+Wireless+Sensing.pdf>.
50. Krishnan, R & Srivatsa, SK 2007, 'Mathematical modeling of wind energy systems', *Information Technology*, vol. 6, pp. 1160-1166.
51. Kwon, D, Gabriel, A, Mora, R & Torres, EO 2010, 'Harvesting Kinetic Energy with Switched-Inductor DC-DC Converters', *Georgia Tech Analog, Power, and Energy IC Research*.
52. Le, CP & Halvorsen, E 2009, 'Electrostatic Modeling of In-Plane Overlap Energy Harvesters', *Power MEMS*, Washington DC, USA, pp. 336-339.
53. Leung, DY, Deng, Y & Leung, MKH 2010, 'Design Optimization of a Cost-Effective Micro Wind Turbine', *Proceedings of the World Congress on Engineering 2010*, vol. 2, London, U.K, pp. 2078-0958.
54. Lim, YM, Yang, B, Kotlanka, R.K, Heng, CH, Xie, J, Tang, M, Han, H, Feng, H & Lee, C, 2008, 'Theoretical Study of the Output Energy for Various MEMS Based Electrostatic Mechanisms', *Sustainable Energy Technologies, ICSET*, pp. 552 – 557.
55. Lu, F, Lee, HP & Lim, SP 2004, 'Modeling and analysis of micro piezoelectric power generators for micro-electromechanical-systems applications', *Smart Materials and Structure*, pp. 57–63.
56. Manuell, JF, McGowan, JG & Roger, LG 2009, *Wind Energy Explained*, 2nd edn, John Wiley and sons, Sussex, United Kingdom.
57. Masters, GM 2004, *Renewable and Efficient Electric Power Systems*, John Wiley & Sons, viewed on 5 June 2012, <<http://edge.rit.edu/content/P12401/public/WIND%20POWER%20SYSTEM.pdf>>.
58. Mathworks.com, n.d., *Getting started with Simscape*, viewed 2 August 2011, <<http://www.mathworks.com/help/physmod/simscape/getting-started-with-simscape.html>>.
59. Mearian, L 2014, 'Micro-wind turbines can recharge cell phones', viewed 5 February 2014, <Micro-wind turbines can recharge cell phones>.
60. Meninger, S, Miranda, JM, Chandrakasan, JLA, Slocum, A, Schmidt, M & Amirtharajah, R 2001, 'Vibration to electric energy conversion', *IEEE Transactions Very Large Scale Integration (VLSI) Systems*, vol. 9, pp. 64-76.

61. Meninger, S, Miranda, JOM, Amirtharajah, R, Chandrakasan, A & Lang, J 1999, 'Vibration-to-Electric Energy Conversion', *Low Power Electronics and Design Proceedings. 1999 International Symposium*, pp. 48 – 53.
62. Miao, P, Holmes, AS, Yeatman, EM, Green, TC & Mitcheson, PD 2003 'Micro-Machined Variable Capacitors for Power Generation', *Electrostatics*, vol. 178, pp. 53-58.
63. Michler, A 2011, *Vibro-Wind Piezoelectric Pads Harness Wind Energy without Turbines*, viewed 15 March 2011, <<http://inhabitat.com/vibro-wind-piezoelectric-pads-harness-wind-energy-without-turbines/>>.
64. Microchip.com, n.d., 'eXtreme Low Power PIC Microcontrollers', viewed 5 January 2014, <<http://www.microchip.com/pagehandler/en-us/technology/xlp/>>.
65. Miki, D, Suzuki,Y & Kasagi, N 2009, 'Effect of Nonlinear External Circuit on Electrostatic Damping Force of Micro Electret Generator' , *Solid-State Sensors, Actuators and Microsystems Conference*, pp. 636-639.
66. Miranda, JOM 2004, 'Electrostatic Vibration -to- Electric Energy Conversion', PhD Thesis, Massachusetts institute of Technology, Massachusetts ,USA.
67. Mitcheson, PD, 2005, 'Analysis and Optimisation of Energy-Harvesting Micro-Generator Systems', PhD Thesis, University of London.
68. Mitcheson, PD, Green, TC & Yeatman EM , 2004, 'Power processing circuits for electromagnetic, electrostatic and piezoelectric inertial energy scavengers', *Microsyst Technol*, pp. 1629–1635.
69. Mitcheson, PD, Green, TC & Yeatman, EM 2006, 'Power Processing Circuits for MEMS Inertial Energy Scavengers', *Symposium on Design, Test, Integration and Packaging of MEMS/MOEM.S*
70. Mitcheson, PD, Sterken, T, He, C, Kiziroglou, M, Yeatman, EM & Puers, R 2008, 'Electrostatic Micro-generators', viewed 3 February 2013, <<https://biblio.ugent.be/input/download?func=downloadFile&recordId=1847718&fileId=1847733>>.
71. Mitcheson, PD, Yeatman, EM, Rao, GK, Holmes, AS & Green,TC 2008 'Energy Harvesting From Human and Machine Motion for Wireless Electronic Devices', *Proceedings of the IEEE*, vol. 96, no. 9, pp. 1457-1486.
72. Mizuno, S, Ishihara, M, Wickramanayaka, S & Miyazaki, N 2003, *Electrostatic chuck device* , JUSTIA Patent.

73. Naruse, Y, Matsubara, N, Mabuchi, K, Izumi, M, Honma, K 2008, 'Electrostatic Micro Power Generator From Low Frequency Vibration Such As Human Motion', *Proceedings of Power MEMS*, pp. 19 -22.
74. Nguyen, H, Hah, D, Patterson, PR, Piywattanametha, W & Wu, MC 2002, 'A Novel MEMS Tunable Capacitor Based on Angular Vertical Comb Drive Actuators', *Solid-State Sensor, Actuator and Microsystems Workshop*, pp. 277 -280.
75. Npl.co.uk 2012, Vibrational energy harvesting, viewed 4 January 2013,<<http://www.npl.co.uk/science-technology/functional-materials/research/vibrational-energy-harvesting>>.
76. O'Donnell, R, Schofield, N, Smith, AC & Cullen, J 2009, 'Design Concepts for High-Voltage Variable-Capacitance DC Generators', *Industry Applications, IEEE Transactions*, vol. 45 , no .5, pp. 1778-1784.
77. Pallas-Areny, R & Webster, JG 2001, *Sensors And Signal Conditioning*, 2nd edn, John Wiley and sons, USA.
78. Paracha, AM, Basset, P, Galayko, D, Marty, F & Bourouina, T 2009, 'A Bidirectional Vibration Powered Electric Energy Generator Based on Electrostatic Transduction using In-Plane Overlap Plate (IPOP) Mechanism', *Design, Test, Integration & Packaging of MEMS/MOEMS*, pp. 300 – 303.
79. Park, JK, Kim ,KM, Kwon ,SD & Law, KH n.d., 'An aero-elastic flutter based electromagnetic energy harvester with wind speed augmenting funnel', viewed 3 January 2014,<http://eil.stanford.edu/publications/jinkyoo_park/AWAS12.pdf>.
80. Pasquale, GD & Somà, A 2008, 'Investigations on Energy Scavenging Methods using MEMS Devices', *Proceedings of the Semiconductor Conference*, Torino, Italy, pp. 163-166.
81. Pasquale, GD, Brusa, E & Somà, A 2009, 'Capacitive Vibration Energy Harvesting with Resonance Tuning', *Proceedings of the Design, Test, Integration & Packaging of MEMS/MOEMS Symposium*, Torino, Italy, pp. 280 - 285
82. Pentland, AP, 1998, Wearable Intelligence, *Scientific American*, pp. 90-95
83. People.bu.edu n.d., *Types of Wind Turbines*, Boston University, viewed 14 December 2013, <<http://people.bu.edu/dew11/turbinetypes.html>>.
84. Philp, SF, 1977, 'The Vacuum-Insulated, Varying Capacitance Machine', *IEEE transactions on electrical insulation*, vol.12, no. 2, pp 130 -136.
85. Platt, SR 2003, 'Electric power generation within Orthopaedic implants using piezoelectric ceramics', M.Sc Thesis, University Nebraska- Lincoln.

86. Priya, S, Chen, CT, Fye, D & Zahnd, J 2005, 'Piezoelectric Windmill: A Novel Solution To Remote Sensing', *Japanese Journal Of Applied Physics*, vol. 44, no. 3, pp. L104 – L107.
87. Radio-electronics.com, 2012, *Tantalum Capacitors*, viewed 5 June 2012, <<http://www.radio-electronics.com/info/data/capacitor/tantalum-capacitor.php>> .
88. Raffat, I, Ragie, H & Galayko, D 2009, 'Modeling of Self Initialized Electrostatic Energy Scavenger', *International Conference on Micro-Electronics*, pp. 406 – 409.
89. Rahman, T, Sakir, SR & Onna, SD 2012, 'Design Of An Efficient Energy Harvester from Ambient Vibration', MSc Thesis, Brac University.
90. Reznikov, M 2010, 'Electrostatic Swing Energy Harvester', *Proceedings of ESA Annual Meeting on Electrostatics*, viewed 7 December 2011, <http://www.electrostatics.org/images/ESA2010_G3_Reznikov.pdf>.
91. Rocha, JG, Gonçalves, LM, Rocha, PF, Silva, MP & Lanceros-Méndez, S 2010, 'Energy Harvesting from Piezoelectric Materials Fully Integrated in Footwear', *IEEE Transactions on Industrial Electronics*, vol. 57,no. 3, pp. 813 -819.
92. Romanblack.com, 2013, *High res cap meter with PIC16F628*, viewed 5 January, 2014, <<http://www.romanblack.com/onesec/CapMeter.htm>>.
93. Roundy, S 2003, 'Energy Scavenging for Wireless Sensor Nodes with a Focus on Vibration to Electricity Conversion', PhD Thesis, University of California, Berkeley.
94. Roundy, S, Wright, PK & Rabaey, JM 2004, 'Energy Scavenging for Wireless Sensor Networks with Special Focus on Vibrations', *Massachusetts Kluwer Academic Publishers*.
95. Roundy, S, Wright, PK, Kristofer, S & Pister, J 2002, 'Micro-Electrostatic Vibration-to-Electricity Converters,' *ASME International Mechanical Engineering Congress*.
96. Salem, M, Salem, M, Andra, D, Tasciuc, B & Hella MM 2007, 'Electrostatic MEMS Converters with a Switchable Dielectric Constant for Micro-Scale Power Generation', *Proceedings of the IEEE Microelectronics conference*, pp. 205 – 208.
97. Serway, RA, Beichner, RJ & Jewett, JW 1996, *Physics for Scientists and Engineers*, Michigan.
98. Sterken, T, Baert, K, Borghs, G, Fiorini, P & Puers, R 2003, 'An electret-based electrostatic μ -generator'. *Proceedings of the 12th International Conference on Solid State Sensors, Actuators and Microsystems*, pp. 1291-1294.

99. Sterken, T, Fiorinil, P, Altena, G, Hoof, CV, & Puers, R 2007, 'Harvesting Energy From Vibrations by a Micro machined Electret Generator', *International Conference On Solid State Sensor*, France.
100. Suzuki, T, Nagasawa, S, Okamoto, H & Kuwano, H 2010, 'Novel Vibration-Driven Micro-Electrostatic Induction Energy Harvester With Asymmetric Multi-Resonant Spring', *IEEE sensors 2010 conference*, pp. 1161-1164
101. Taha, LY, 2009, 'Design and Modelling of a MEMS Piezoelectric Microgenerator', PhD thesis, Universiti Kebangsaan Malaysia.
102. Talal, R, 2008, Transpiration as a Mechanism for Mechanical and Electrical Energy Conversion, PhD Thesis, University of Michigan.
103. Tan, YK & Panda, SK 2007, 'A Novel Piezoelectric Based Wind Energy Harvester for Low-power Autonomous Wind Speed Sensor', *Proceedings of the 33rd Annual Conference of the IEEE Industrial Electronics Society (IECON)*, Taipei, Taiwan, pp. 2175- 2180.
104. Tavares, J, Velez, FJ & Ferro, JM 2008, 'Application of Wireless Sensor Networks to Automobiles', *Measurement science review*, pp. 65 -70.
105. Torres, EO & Rincón-Mora, GA 2010, 'Self-Tuning Electrostatic Energy-Harvester IC', *IEEE Transactions on Circuits and Systems*, vol. 57, no. 10, pp. 808- 812.
106. Torres, EO & Rincon-Mora, GA 2005, 'Long lasting self sustaining and energy harvesting system in Package (SiP) wireless micro sensor solution', *International conference on energy, environment and disasters (INCEED 2005)*, USA, Charlotte, NC.
107. Torres, EO, Gabriel, A & Mora, R 2006, 'Electrostatic Energy Harvester and Li-Ion Charger Circuit for Micro-Scale Applications', *Circuits and Systems 49th IEEE International Midwest Symposium*, pp. 65 – 69.
108. Torres, EO, Gabriel, A & Mora, R 2009a, 'Energy budget and high gain strategies for voltage constrained electrostatic harvesters", *IEEE transactions on Power and energy*.
109. Torres, EO, Gabriel, A & Mora, R 2009b, 'Electrostatic Energy-Harvesting And Battery-Charging CMOS System Prototype', *IEEE transactions on circuits and systems: regular papers*, vol. 56, no. 9.
110. Torres, EO, Gabriel, A & Mora, R 2010, '0.7- μ m BiCMOS Electrostatic Energy-Harvesting System IC', *Solid-State Circuits, IEEE Journal*, vol. 45, pp 483 – 496.
111. Tsutsumino, T, Suzuki, Y & Kasagi, N 2007, 'Electromechanical Modeling of Micro Electret Generator for Energy Harvesting', *The 14th international conference on Solid state sensors, actuator and micro systems*, Lyon, France, pp. 863-866.

112. Tsutsumino, TS, Suzuki, Y, Kasagi, N & Sakane, Y 2006, 'Seismic power generator using high-performance polymer electret', *Micro Electro Mechanical Systems*, pp. 98 – 101.
113. Tsutsumino, TS, Suzuki, Y, Kasagi, N, Kashiwagi, K & Morizawa, Y 2006, 'Efficiency Evaluation of Micro Seismic Electret Power Generator', *Proceedings of the 23rd Sensor Symposium*, pp. 521-524.
114. Tvedt, LGW, Blystad, LCJ & Halvorsen, E 2008, 'Simulation of an Electrostatic Energy Harvester at Large Amplitude Narrow and Wide Band Vibrations', *Proceedings of the DTIP MEMS and MOEMS*, pp. 296-301.
115. UCSUSA.org 2013, Environmental Impacts of Wind Power, viewed 10 June 2013, <http://www.ucsusa.org/clean_energy/our-energy-choices/renewable-energy/environmental-impacts-wind-power.html>.
116. Vullers, RJM, Schaijk, RV, Doms, I, Van Hoof, C & Mertens, R 2009, 'Micropower energy harvesting', *Solid-State Electronics*, vol. 53, pp. 684–693.
117. Weatherspark.com, 2012, Average Weather for Dubai, United Arab Emirates, viewed 10 March 2013, <<http://weatherspark.com/averages/32855/Dubai-United-Arab-Emirates>>.
118. Webster, JG 1999, *The Measurement, Instrumentation, and Sensors: Handbook*, CRC Press LLC, IEEE Press, USA.
119. Weiser, M, 1991, 'The Computer for the Twenty First Century', *Scientific American*, pp. 66 -75.
120. Williams, CB & Yates, RB 1995, 'Analysis of a micro-electric generator for Microsystems', *Proceedings of the 8th International Conference on Solid-State Sensors and Actuators and Eurosensors*, pp. 369-372.
121. Wu, JM, Lo, CW, Huang, BY, Yang, NK & Li, SC 2009, 'PCB ground-parasitic effects on a WIMAX low-noise amplifier RFIC wireless communications', *Networking and Mobile Computing*, pp.1-3.
122. Yedavalli, RK & Belapurkar, RK 2011, 'Application of wireless sensor networks to aircraft control and health management systems', *Journal of control theory applications*, pp. 28-32.
123. Yen, CB & Lang, JH 2005, 'A Variable-Capacitance Vibration-to-Electric Energy Harvester', *IEEE Transactions on Circuits and Systems-I: Fundamental Theory and Applications*, pp.1- 8.

124. Zhang, Y, Hui, F, Xingbing, W, Lizhen, W ,Aiqin Zhang, A, Tongchi, Huichao, Zhang, XLL 2009, 'Progress of electrochemical capacitor electrode materials', *International Journal of Hydrogen Energy*, vol. 34, no.11, pp.4889–4899.
125. Zhu, D, Beeby, SP, Tudor, MJ, White, NM & Harris, NR 2013, 'Novel Miniature Airflow Energy Harvester for Wireless Sensing Applications in Buildings', *IEEE sensors journal*, pp 691 – 700.
126. Zipp, K 2010, 'The plus side of large two-blade turbines', viewed 7 March 2013, <<http://www.windpowerengineering.com/featured/the-plus-side-of-large-two-blade-turbines-2/>>.